USING SILICONE COATINGS TO CREATE BIOREPELLENT SURFACES

PRODUCING FLOURINE-FREE POLYSILOXANE HIERARCHICAL STRUCTURES AS HIGHLY BIOREPELLENT SURFACES

By LIANE LADOUCEUR, B.SC., B. ENG.

A Thesis Submitted to the School of Graduate Studies in Partial Fulfillment

of the Requirements for the Degree Master of Applied Science

MASTER OF APPLIED SCIENCE (2021) Biomedical Engineering, McMaster University

Hamilton, Ontario

TITLE: Using Polysiloxane Nanostructures for Hierarchical Structure to Create Repellent Surfaces

AUTHOR: Liane Ladouceur, B. Sc., B. Eng.

SUPERVISOR: Dr. Tohid Didar

PAGES: xiv, 135

Lay Abstract

The goal of creating a surface capable of repelling biological samples continues to present challenges due to surface stability, scalability, and cost of manufacturing techniques. Beyond this, many of the existing solutions use fluorine-based chemicals that present a risk to the environment due to the difficulty in breaking down these molecules. This thesis aims to understand the current state of repellent surfaces used for biological applications, including prevention of surface contamination by bacteria and viruses, then investigates the use of more environmentally friendly methods to produce repellent surfaces. Using a silicone-based coating combined with heat induced shrinking of shape memory polymers (SMPs), we have created a flexible surface with multiscale roughness that demonstrates repellency to bacteria and whole blood.

Abstract

Though the past two decades have seen a dramatic increase in research toward self-cleaning repellent surfaces, multiple challenges exist in the creation of biorepellent surfaces for everyday use. Environmental concerns persist with many of the chemicals utilized in this field and the need for scalable, low-cost alternatives remains. Spread of pathogens including bacteria and viruses in healthcare and public settings also presents a need for stable surfaces. In the work presented here, we report on the current status of antimicrobial nanomaterials and coatings toward virus repellency, followed by an investigation into the application of polysiloxane nanostructures in creation of flexible hierarchical surfaces. Using n-propyltrichlorosilane (n-PTCS) coated on activated polyolefin (PO) we were able to demonstrate superhydrophobicity, reporting water contact angles above 153° paired with <1° sliding angles on hierarchical surfaces. A transfer assay, that closely mimics contact with high-touch surfaces, using *Escherichia coli* K-12 transfected with green fluorescent protein (GFP) reported a 1.6-log (97.5%) reduction in fluorescence on surfaces compared to planar PO controls, paired with a 1.2-log (93%) reduction in CFU/mL in comparison to control groups. Additionally, surfaces demonstrated a contact angle of 140.8° with citrated whole blood. Droplets of blood incubated on our surfaces for 15 min showed a 93% reduction in visible staining, while submersion in citrated whole blood for 20 minutes revealed an 87% reduction in blood adhered to the surfaces. The applications for these biorepellent surfaces have widespread potential, including the demonstrated need for prevention of surface contamination to minimize spread of hospital acquired infections (HAIs) within the healthcare system.

Acknowledgements

I would first like to thank my supervisor, Dr. Tohid Didar, for inspiring me to pursue graduate studies and for his constant guidance and support throughout this degree. His approach to research changed my perspective on the field and has taught me invaluable lessons I will certainly carry with me throughout my career. He has challenged me to grow as a researcher and encouraged me to exceed my own expectations.

Next, I would like to thank Dr. Leyla Soleymani, who has provided invaluable advice and direction throughout this degree and whose collaboration has allowed me opportunities I would not have otherwise had access to. I will be graduating with a set of skills far beyond the scope contained in these pages thanks to her support. I would also like to thank Dr. Natalia Nikolova and Dr. Carlos Filipe for their respective roles in the development and completion of this degree.

Furthermore, I would like to thank Dr. Jeffrey Weitz for kindly allowing me to spend countless hours in his lab for collaboration, and his team at TaARI for their continued support. In particular, a thank you to Jim Fredenburgh and Rida Malik for never hesitating to answer my countless questions.

I would also like to thank all my colleagues in the Didar and Soleymani labs for their support and collaboration, especially Dr. Amid Shakeri, Roderick MacLachlan, Sara Imani, Shadman Khan, Noor Abu Jarad, Martin Villegas, and Dr. Maryam Badv.

Finally, I wish to express my deepest gratitude to my family and friends who have supported me through this wild ride. To my family, Tim and Carolyn, Ian and Mel, I could not have made it this far without your endless love and support, especially on the most challenging days. Levi, thank you for supporting me through the roughest days and always finding a way to make me smile. To Cam and Taylor, thank you for putting up with my ungodly hours and always being my sounding board for engineering ideas. There are so many more that deserve thanks, but I could not possibly fit each of you here, so I will simply say you know who you are.

Table of Contents

List of Figures

List of Tables

List of Abbreviations

CFU	Colony-forming units
cSt	Centi-Stoke (equivalent to $1mm^2/s$)
CVD	Chemical Vapor Deposition
E. coli	Escherichia coli
GFP	Green fluorescent protein
HAI	Healthcare acquired infection
LIS	Liquid-infused surface
LPD	Liquid phase deposition
n-PTCS	n-propyltrichlorosilane
PO	Polyolefin
SARS-CoV-2	Severe acute respiratory syndrome coronavirus 2
SEM	Scanning Electron Microscope
SFE	Surface Free Energy
SMP	Shape memory polymer
TCES	Trichloro(ethyl)silane
TCMS	Trichloro(methyl)silane

Declaration of Academic Achievement

- Chapter 1, “Introduction”, was drafted by Liane Ladouceur and revised by Dr. Tohid Didar.
- For Chapter 2, “Antimicrobial Nanomaterials and Coatings: Current Mechanisms and Future Perspectives to Control the Spread of Viruses Including SARS-CoV-2”, literature review was performed by Liane Ladouceur and Sara M. Imani, who collaborated to write the initial review paper draft with input from Terrel Marshall and Roderick MacLachlan on specific sections, under the supervision of Dr. Tohid Didar and Dr. Leyla Soleymani. The manuscript was revised for final publication by Dr. Tohid Didar and Dr. Leyla Soleymani.
- For Chapter 3, “Producing Fluorine-Free and Lubricant-Free Flexible Pathogen and Blood Repellent Surfaces Using Polysiloxane-Based Hierarchical Structures”, Liane Ladouceur was involved in the design and execution of all experiments and data analysis. Dr. Tohid Didar and Dr. Leyla Soleymani designed the experiments and supervised the project. Dr. Amid Shakeri, Shadman Khan and Alejandra Rey Rincon conducted specific bioassays with samples provided by Liane Ladouceur and assisted in data analysis. Liane Ladouceur wrote the manuscript with contributions from Alejandra Rey Rincon and Dr. Tohid Didar.
- Chapter 4, “Conclusion”, was drafted by Liane Ladouceur and revised by Dr. Tohid Didar.

1 Introduction

In March 2020, the world was forever changed by a virus that initiated a global pandemic. Severe acute respiratory syndrome coronavirus-2 (SARS-CoV-2), the cause of coronavirus disease (COVID-19), set in motion a large-scale shutdown and shifted perspectives on public health as well as priorities. The ramifications of this pandemic are still only beginning to be understood in terms of health, economics and international affairs, as the world is still working to control the spread of this highly contagious virus [1]. In the wake of these extraordinary circumstances, however, individuals have been left with a heightened sense of awareness toward the risk associated with pathogen spread and the importance of controlling contamination in everyday life [2]–[4]. Most importantly, this awareness has been reinforced within in our healthcare system.

In 1995, the Canadian Nosocomial Infection Surveillance Program (CNISP) was established to track an increase in what had become known as nosocomial infections or healthcare associated infections (HAIs) [5]. These are infections which present particular risk to patients who are already being treated within the healthcare system, as they are acquired during a patient's care for another condition [6]. Efforts to reduce the impact of HAIs within healthcare settings as well as the impact of harmful bacteria and viruses to all public health can be regarded as requiring two simultaneous strategies: prevention of spread and treatment of disease. Unfortunately, HAIs are particularly problematic due to the antibiotic-resistant nature of the bacteria which cause them. CNISP tracks cases of these HAIs using representative data from hospitals across Canada. Based on their most recent reports, 1 in 217 patients contracted an infection while receiving care at these hospitals [7]. Beyond this, Canadian data for seasonal flus illustrates that risk of transmission through fomites presents regular health risks to the general public, with 48,818 cases of laboratory-

confirmed influenza detections for the 2018-2019 flu season alone [8]. For this reason, it is important to introduce controls at a higher level and focus on the earlier strategy, prevention of pathogen spread.

Surface repellency represents a major area of investigation within nanotechnology, with biorepellency representing a significant portion of the potential applications [9]. A number of diverse settings have the potential to benefit from advances in this area, from healthcare to food industry and from surfaces in public settings all the way down to surfaces of cutting-edge biosensors. However, with all of the potential benefit, there are still many limitations in current technology, including environmental impact, scalability, cost and surface stability [9]. For the purposes of this thesis, prevention of pathogen spread will be the primary focus, particularly through the control of surface contamination. We aim to do this while also addressing the stated limitations.

1.1 Surface Wettability

The study of interactions between liquids and solid surfaces includes examination of surface wettability. Wettability was first described by Young in 1805 [10], and can be expressed through Young's equation,

$$cos\theta = \frac{\gamma_{SV} - \gamma_{SL}}{\gamma_{LV}}$$

Where γ_{SV} represents the surface tension of the solid surface, γ_{LV} is the surface tension of the liquid and γ_{SL} is the liquid-solid interfacial tension [9]. This highlights the importance of surface tensions to the wettability of the surface and introduces the concept of contact angle measurements to understand the interactions between a liquid droplet and solid surface. Contact angle is measured at the point where the liquid-solid interface meets the surrounding gas phase, as visualized in

Figure 1.1a. Based on this relationship between interfacial tensions and surface wettability, contact angle measurements have become a primary quantification method for surface hydrophilicity or hydrophobicity. For hydrophilic surfaces, contact angles are measured below 90°, becoming superhydrophilic below 10°. For hydrophobic surfaces, contact angles measure above 90°, characterized as superhydrophobic beyond 150° [9].

Inspired by self-cleaning and repellent species in nature, manipulation of surface wettability has been the target of extensive research. There are two main pathways used to increase hydrophobicity: decrease of surface free energy (SFE) through surface chemistry or increase in surface roughness through alteration of the surface architecture. To alter the chemical structure of a surface, fluoropolymeric coatings or silane layers such as (1H,1H,2H,2H-perfluorooctyl) silane or 1H,1H,2H,2H-perfluorooctyltriethoxysilane (PTES) are commonly used based on their low SFE. Unfortunately, manipulation of surface chemistry alone has not proven sufficient to create superhydrophobic surfaces to date, typically achieving contact angles around 120° [11]. In order to achieve superhydrophobic characteristics, research instead uses a combination of low SFE and surface roughness, such as roughening a low SFE poly(tetrafluoroethylene) (PTFE) film by stretching and revealing fibrous crystals [12]. Most recently, research has begun to create surface roughness using hierarchical surfaces, which will be considered more in-depth in section 1.3.

Understanding of wetting characteristics for textured hydrophobic surfaces was first established in 1936 by Wenzel, with his research into repellency on textiles leading to the initial model of water droplet behaviour on rough surfaces [13]. The manner in which a water droplet will infiltrate the texture is illustrated in **Figure 1.1b**. Wenzel also introduced the concept that a smooth surface with repellent properties will become more repellent if it is artificially roughened. Continuing work on repellency for textiles, in 1944 Cassie and Baxter established the wetting

model for what was called porous surfaces, illustrating the creation of a heterogeneous interface by air pockets trapped within the textured solid surface, altering the surface effectively seen by liquid droplets when applied to the surface [14]. This can be visualized in **Figure 1.1c**. The key difference between these wetting models is droplet movement. From **Figure 1.1**, it is easy to understand that in the Wenzel model of wetting, droplets tend to be pinned in place, with high sliding angles. In contrast, Cassie-Baxter tends to model more highly hydrophobic surfaces which also typically demonstrate low sliding angles. These models are used today to predict the wetting behaviour of artificially roughened surfaces, including hierarchical surfaces.

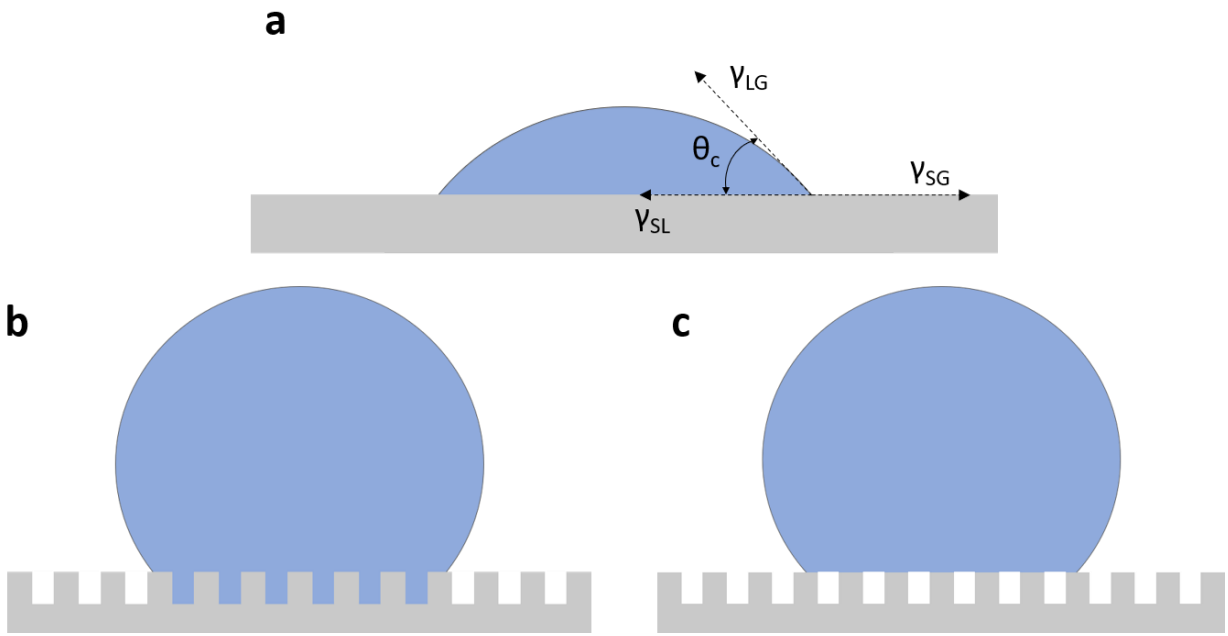

Figure 1.1 a) Contact angle measurement (θ_c) measured at the point where interfacial and surface tensions of all three phases intersect **b)** Wenzel model of wetting **c)** Cassie-Baxter model of wetting.

1.2 Liquid-Infused Surfaces

An additional type of surface modification to induce repellency is liquid-infused surfaces (LIS). While not the focus of this work, lubricated surfaces will act as a competitor to the goal of

this research and hence will be considered briefly here. These surfaces are characterized by their low sliding angles, measured at less than 5° [15]. They demonstrate omniphobic and amphiphobic properties, repelling liquids with high surface tensions, such as water (72.3 mN m^{-1}), and low surface tensions such as hexadecane (27.5 mN m^{-1}). These surfaces are constructed by application of a lubricant layer to a surface with appropriate chemical and often structural modification to capture and retain a thin film. It is worth noting that while the surface must have correct chemistry to be compatible with the lubricant, increased surface roughness through surface selection or structural modification will improve performance but is not required [16], [17]. Commonly used lubricants include perfluorodecalin, Fluorinent (FC70) and Krytox, though many options are available including silicone oils which are more viscous and avoid the volatility that is a main limitation to applications for these surfaces [15]. Unfortunately, due to the liquid nature of these modifications, they are not particularly well-suited for any applications with high-touch probability. This gap is the focus of numerous lines of research, including the present work.

1.3 Hierarchical Surfaces

Based on our understanding of surface wettability including the models put forth by Cassie-Baxter and Wenzel [13], [14], research has used bioinspiration from sources such as the lotus leaf and butterfly wings to produce highly repellent surfaces by increasing roughness [18], [19]. With the advances in nanotechnology over the past two decades however, images using a scanning electron microscope (SEM) have revealed that in fact the lotus leaf demonstrates multi-scale roughness, as seen in **Figure 1.2**. It follows then, that by artificially creating multi-scale roughness, it is also possible to increase hydrophobicity to levels previously unattained. This has been achieved in recent research using combinations of many different methods, including nanoparticle deposition [20], [21], microscale manufacturing techniques such as etching,

lithography and surface micromachining [22]–[24], chemical modification [25], and heat shrinkable shape memory polymers (SMPs) [26].

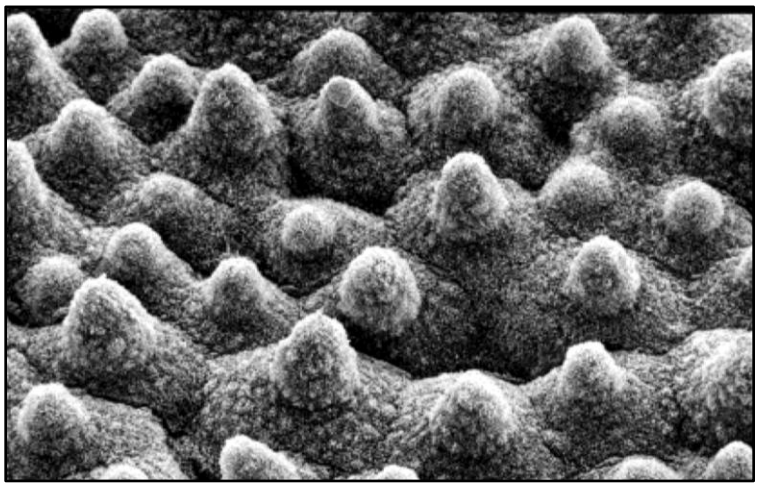

Figure 1.2 Lotus leaf imaged using SEM to demonstrate the hierarchical structure (double roughness) seen on the surface. [19]

A particularly appealing approach to hierarchy is found in heat shrinkable SMPs. With these types of thermoplastics, the polymer is heated, stretched beyond its natural state, then cooled to freeze the altered polymer structure in place [27]. To make use of this alteration for hierarchy, a coating is applied as a skin layer to the surface of these polymers with the intention of causing a mismatch in stiffness between the skin layer and the polymer. In this way, when the temperature of the combined surface is then altered to shrink the SMP back to its original size, the interaction of strain between the skin layer and polymer induces strain on the surface to cause buckling that results in micro- or nanoscale wrinkling [28]. Notably, it is possible to control the amplitudes and wavelengths of the wrinkles, based on the thickness of skin layer applied and the characteristics of the chosen polymer [29].

The introduction of multiscale roughness also begins to address a major problem faced by many superhydrophobic surfaces – low durability [30]. Often, chemical modifications including coatings on a surface can be easily disturbed by mechanical manipulation [31]. In contrast,

hierarchical surfaces have been proven to demonstrate much higher durability, conveyed by the combination of approaches. For example, the combination of a porous epoxy resin coating with embedded SiO_2 nanoparticles presented by Jia *et al.* demonstrated the desired durability from epoxy resin while maintaining superhydrophobicity through rough structure provided by texturing and nanoparticles [32]. An additional benefit to many of these surfaces is the low sliding angles demonstrated without the requirement of introducing a lubricant layer. This is particularly relevant for production of surfaces to be utilized in high-touch or open-air environments.

1.4 Polysiloxane Nanostructures

Investigation of silicon-based polymers, or polysiloxanes, examines chemicals that include the repeating O-Si-O unit. In the case of research involving trichlorosilane precursors, structures formed tend toward crosslinked polymers [33]. The three chlorine functional groups present on these molecules allow for increased reactivity, moving away from the chain polymers that are common to many biomaterials and toward self-assembled layers. Using trichlorosilanes with short hydrocarbon chains has produced a distinctive line of research that forms polysiloxane nanostructures on surfaces subjected to liquid phase deposition (LPD) or chemical vapour deposition (CVD) with these chemicals. Since the inception of this work by Artus *et al.* in 2006 [34], many facets of nanostructure growth have been explored including chemical precursors, substrates to be coated, control of environmental conditions and addition of lubricant.

Much this research utilizes the precursors trichloro(methyl)silane (TCMS) and trichloro(ethyl)silane (TCES) [34]–[36]. Early work in the area tested these chemicals with a number of different substrates, beginning with glass but shifting to aluminum, poly(dimethylsiloxane) (PDMS), SiO_2, textiles and more soon after [34], [37]–[39]. These surfaces invariably demonstrated superhydrophobic properties, with contact angles above 150°, though the

best performing have been hybrid coatings that first dip-coat surfaces with silica nanoparticles then apply silicone nanofilaments through CVD to achieve contact angles of 179.8° and sliding angle of 1.3° [40]. Hierarchy has been introduced using other approaches as well, including introduction of glass beads with TiO_2 nanoparticles [41], and use of polyethylene, an SMP, as a substrate [42]. Various applications have also been considered for these structures, including patterning for study of extreme wetting properties [43] and antibacterial capabilities [44].

An interesting aspect of growth with these chemicals is the variability of nanostructures formed. The control of this characteristic has only recently been closely investigated but highlights the tunability of these structures to various applications. These investigations have primarily utilized TCES and apply both liquid and gas phase reactions to manipulate the resulting structures. Shapes include stars, helices, nanofilaments, volcanoes, rods, chalices and tubes [45], though volcanoes have also been labeled microrings and combinations of these structures are also seen regularly [46]. These shapes can be visualized in **Figure 1.3**. To create the nanofilaments which are most commonly found, as well as volcanos and rods, temperature and relative humidity were controlled for a gas phase reaction. Chalices were primarily found when the precursor was switched to TCMS and low temperatures were paired with high humidity [45]. Generally speaking, it has been seen that increasing relative humidity will increase the diameter of structures formed, moving from nanofilaments to rods and then to volcanoes/rings as humidity is increased at room temperature [46]. Stars and helices were also created in the gas phase using TCMS but were formed on metal soaps rather than glass coverslips. Finally, tube structures have been solely created in liquid phase growth, synthesized in toluene [45].

A final exploration of this work has been the introduction of lubricant to create LIS. By first growing silicone nanofilaments on the surface using TCMS, then coating the modified surface

with PFDTS, and finally applying Krytox, researchers achieved ultra-low sliding angles for liquids including water, n-hexadecane and n-decane [47]. Alternatively, the use of n-propyltrichlorosilane (n-PTCS) as the precursor chemical has been explored for nanostructure growth prior to lubricant application. This chemical demonstrated similar nanofilament growth, though at a slightly higher ideal RH (~55%), with contact angle of 170° after 24-hr growth. Application of a silicone oil lubricant (350 cSt) to n-PTCS treated glass slides resulted in sliding angle measurement of 5° for a 5 µL water droplet [48]. This excellent performance was also transferred to additional substrates, including catheters and nasal splints, and demonstrated decreased bacterial adhesion and thrombosis suppression [49].

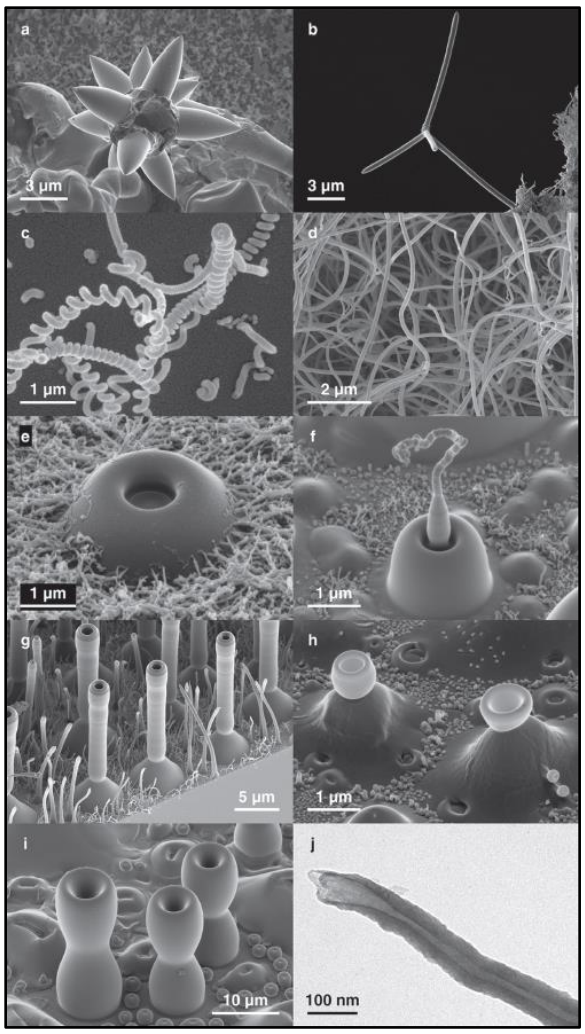

Figure 1.3 Variability of nanostructure formation through growth of polysiloxane on surfaces. **a,b)** stars; **c)** helices; **d)** nanofilaments; **e)** volcanoes/microrings; **f,g,h)** combination of nanofilament, rod, and chalice, respectively, on top of a volcano; **i)** chalice; **j)** tube. [45]

1.5 Environmental Considerations

In all research it is ethically necessary to consider the down-stream impact that work will have, whether this is the implications certain results could have on society or impact the experiment itself will have on the environment. This latter consideration is particularly relevant in the research of surface modification, due to the frequent use of fluorocarbons. Concerns around the use of various fluorocarbons have existed for many years, with the first major article against the use of

chlorofluorocarbons (CFCs) published by Molina & Rowland in 1974, citing concerns of ozone layer destruction [50]. In the years to come, the first concerns with persistence of long-chain fluorocarbons in the environment were raised, specifically for perfluoroalkyl acids (PFAAs), perfluorocarboxylic acids (PFCAs) and their salts and precursors [51], [52]. Unfortunately, the same properties that make these chemicals appealing are the source of the problem. Fully fluorinated hydrocarbons are very stable molecules, however this renders them nearly impossible to degrade biologically [53]. While some forms of fluorocarbons have been integrated into Food and Drug Administration (FDA) compliant substances and devices [54], [55], the risk of using these chemicals in research lies in the improper disposal and potential for unreacted molecules to reach the environment. Indeed, researchers in 2004 were alarmed to find high levels of long-chain perfluorinated acids in the tissues of mammals in the Canadian arctic and in animals across the globe [56], [57]. This led to studies on the toxicology of these molecules. Data from mouse and rat studies shows overwhelming evidence of the negative effects of both PFAAs and PFCAs including hepatoxicity, developmental toxicity and immunotoxicity [52]. Given this evidence and the unclear impact of a number of related fluorocarbons that fall in the mid-range of chain length, such as 8-carbon chains, governments have begun to enforce restrictions on the use of many fluorocarbons [58], [59]. These include trichloro(1H, 1H, 2H, 2H-perfluorooctyl) silane (TPFS) and 1H, 1H, 2H, 2H-perfluorodecyltrichlorosilane (PFDTS), which are commonly used in surface modification.

Efforts to decrease the chain length of fluorocarbons used in both industry and research have been underway for nearly as long as these impact studies and there is reason to believe that short chains are less harmful. A recent study compared the effects of long- and short-chain perfluorinated compounds, comparing perfluoro-octanoic acid (PFOA) and perfluoro-alkyl

sulphonate (PFOS) with perfluorobutane-sulfonic acid (PFBS), perfluorobutanoic acid (PFBA), pentafluoropropionic anhydride (PFPA) and perfluoropentanoic acid (PFPeA) [60]. Researchers found that these short-chain perfluorocarbons (PFCs) demonstrated no acute cytotoxicity in the thyroid cells tested. This is promising since short-chain fluorocarbons appear to allow better clearance in animal tissues [61]. Nonetheless, concerns over long-term impact of these short-chain fluorocarbons in the environment persist [62], making the case for elimination of these chemicals from research altogether.

1.6 Outline of Thesis

The principal goal of this thesis has been the investigation of surface modification techniques to achieve superhydrophobicity and by extension biorepellent surfaces. Established procedures for the growth of polysiloxane nanostructures were optimized for a thermoplastic material in order to combine two scales of roughness, similar to strategies employed in nature. The detailed objectives included in this thesis are as follows:

- Detailed literature review on the production of nanomaterials and coatings designed to provide antimicrobial capabilities (chapter 2),
- Optimize the fabrication of polysiloxane nanostructures on polyolefin surfaces by creating a customized humidity chamber (chapter 3),
- Characterize surfaces with varying levels of polysiloxane growth based on incubation time to define an ideal superhydrophobic surface (chapter 3), and
- Investigate the performance of an ideal hierarchical surface with bacterial adhesion and complex biofluid studies (chapter 3).

1.7 References

[1] G. A. Rossi, O. Sacco, E. Mancino, · Luca Cristiani, and F. Midulla, "Differences and similarities between SARS-CoV and SARS-CoV-2: spike receptor-binding domain recognition and host cell infection with support of cellular serine proteases," *Infection*, vol. 48, pp. 665–669, 2020, doi: 10.1007/s15010-020-01486-5.

[2] W. McKibbin and R. Fernando, "The Global Macroeconomic Impacts of COVID-19: Seven Scenarios," *Asian Econ. Pap.*, pp. 1–30, 2021, doi: 10.1162/asep_a_00796.

[3] S. P. Jun, H. S. Yoo, and J. S. Lee, "The impact of the pandemic declaration on public awareness and behavior: Focusing on COVID-19 google searches," *Technol. Forecast. Soc. Change*, vol. 166, p. 120592, May 2021, doi: 10.1016/j.techfore.2021.120592.

[4] S. Rousseau and N. Deschacht, "Public Awareness of Nature and the Environment During the COVID-19 Crisis," *Environ. Resour. Econ.*, vol. 76, no. 4, pp. 1149–1159, 2020, doi: 10.1007/s10640-020-00445-w.

[5] "CNISP Protocols & Publications | IPAC Canada." https://ipac-canada.org/cnisp-publications.php#About CNISP (accessed Apr. 11, 2021).

[6] World Health Organization, "Prevention of hospital-acquired infections A practical guide 2nd edition." Accessed: Apr. 11, 2021. [Online]. Available: http://www.who.int/emc.

[7] Public Health Agency of Canada, "Healthcare-associated infection rates in Canadian hospitals." https://www.canada.ca/en/public-health/services/publications/science-research-data/healthcare-associated-infection-rates-canadian-hospitals-infographic.html (accessed Mar. 21, 2021).

[8] Public Health Agency of Canada, "FluWatch annual report: 2018-19 influenza season."

[9] S. Parvate, P. Dixit, and S. Chattopadhyay, "Superhydrophobic Surfaces: Insights from

Theory and Experiment," *J. Phys. Chem. B*, vol. 124, no. 8, pp. 1323–1360, 2020, doi: 10.1021/acs.jpcb.9b08567.

[10] Thomas Young, "III. An essay on the cohesion of fluids," *Philos. Trans. R. Soc. London*, vol. 95, pp. 65–87, 1805, doi: 10.1098/rstl.1805.0005.

[11] R. Blossey, "Self-cleaning surfaces - Virtual realities," *Nat. Mater.*, vol. 2, no. 5, pp. 301–306, 2003, doi: 10.1038/nmat856.

[12] J. Zhang, J. Li, and Y. Han, "Superhydrophobic PTFE surfaces by extension," *Macromol. Rapid Commun.*, vol. 25, no. 11, pp. 1105–1108, 2004, doi: 10.1002/marc.200400065.

[13] R. N. Wenzel, "Resistance of solid surfaces to wetting by water," *Ind. Eng. Chem.*, vol. 28, no. 8, 1936, doi: 10.1021/ie50320a024.

[14] A. B. D. Cassie and S. Baxter, "Wettability of porous surfaces," *Trans. Faraday Soc.*, vol. 40, 1944, doi: 10.1039/tf9444000546.

[15] M. Villegas, Y. Zhang, N. Abu Jarad, L. Soleymani, and T. F. Didar, "Liquid-Infused Surfaces: A Review of Theory, Design, and Applications," *ACS Nano*, vol. 13, no. 8, pp. 8517–8536, Aug. 2019, doi: 10.1021/acsnano.9b04129.

[16] D. C. Leslie *et al.*, "A bioinspired omniphobic surface coating on medical devices prevents thrombosis and biofouling," *Nat. Biotechnol.*, 2014, doi: 10.1038/nbt.3020.

[17] K. Y. Law and H. Zhao, *Surface wetting: Characterization, contact angle, and fundamentals*. 2015.

[18] G. Chen, Q. Cong, Y. Feng, and L. Ren, "Study on the wettability and self-cleaning of butterfly wing surfaces," 2004. Accessed: Mar. 26, 2021. [Online]. Available: www.witpress.com,.

[19] N. A. Patankar, "Mimicking the lotus effect: Influence of double roughness structures and

slender pillars," *Langmuir*, vol. 20, no. 19, pp. 8209–8213, 2004, doi: 10.1021/la048629t.

[20] S. M. Imani *et al.*, "Flexible Hierarchical Wraps Repel Drug-Resistant Gram-Negative and Positive Bacteria," *ACS Nano*, vol. 14, no. 1, pp. 454–465, 2020, doi: 10.1021/acsnano.9b06287.

[21] A. Dramé, T. Darmanin, S. Y. Dieng, E. T. De Givenchy, and F. Guittard, "Superhydrophobic and oleophobic surfaces containing wrinkles and nanoparticles of PEDOT with two short fluorinated chains," *RSC Adv.*, vol. 4, no. 21, pp. 10935–10943, 2014, doi: 10.1039/c3ra47479h.

[22] Y. Xiu, L. Zhu, D. W. Hess, and C. P. Wong, "Hierarchical silicon etched structures for controlled hydrophobicity/ superhydrophobicity," *Nano Lett.*, vol. 7, no. 11, pp. 3388–3393, 2007, doi: 10.1021/nl0717457.

[23] M. T. Alameda, M. R. Osorio, J. J. Hernándezhernández, and I. Rodríguez, "Multilevel Hierarchical Topographies by Combined Photolithography and Nanoimprinting Processes To Create Surfaces with Controlled Wetting," 2019, doi: 10.1021/acsanm.9b00338.

[24] Z. Wang, D. Nandyala, C. E. Colosqui, T. Cubaud, and D. J. Hwang, "Glass surface micromachining with simultaneous nanomaterial deposition by picosecond laser for wettability control," *Appl. Surf. Sci.*, vol. 546, p. 149050, Apr. 2021, doi: 10.1016/j.apsusc.2021.149050.

[25] P. Suresh Kumar, J. Sundaramurthy, D. Mangalaraj, D. Nataraj, D. Rajarathnam, and M. P. Srinivasan, "Enhanced super-hydrophobic and switching behavior of ZnO nanostructured surfaces prepared by simple solution - Immersion successive ionic layer adsorption and reaction process," *J. Colloid Interface Sci.*, vol. 363, no. 1, pp. 51–58, Nov. 2011, doi: 10.1016/j.jcis.2011.07.015.

[26] S. Schauer, M. Worgull, and H. Hölscher, "Bio-inspired hierarchical micro- and nano-wrinkles obtained: Via mechanically directed self-assembly on shape-memory polymers," *Soft Matter*, vol. 13, no. 24, pp. 4328–4334, 2017, doi: 10.1039/c7sm00154a.

[27] S. Lin, E. K. Lee, N. Nguyen, and M. Khine, "Thermally-induced miniaturization for micro- and nanofabrication: Progress and updates," *Lab Chip*, vol. 14, no. 18, pp. 3475–3488, 2014, doi: 10.1039/c4lc00528g.

[28] N. Bowden, S. Brittain, A. G. Evans, J. W. Hutchinson, and G. M. Whitesides, "Spontaneous formation of ordered structures in thin filmsofmetals supported on an elastomeric polymer," *Nature*, vol. 393, no. May, pp. 146–149, 1998.

[29] J. Y. Chung, A. J. Nolte, and C. M. Stafford, "Surface wrinkling: A versatile platform for measuring thin-film properties," *Advanced Materials*, vol. 23, no. 3. pp. 349–368, 2011, doi: 10.1002/adma.201001759.

[30] K. Manoharan and S. Bhattacharya, "Superhydrophobic surfaces review: Functional application, fabrication techniques and limitations," *J. Micromanufacturing*, vol. 2, no. 1, pp. 59–78, 2019, doi: 10.1177/2516598419836345.

[31] Y.-Y. Quan, Z. Chen, Y. Lai, Z.-S. Huang, and H. Li, "Recent advances in fabricating durable superhydrophobic surfaces: a review in the aspects of structures and materials," *Mater. Chem. Front*, 2021, doi: 10.1039/d0qm00485e.

[32] S. Jia, X. Lu, S. Luo, Y. Qing, N. Yan, and Y. Wu, "Efficiently texturing hierarchical epoxy layer for smart superhydrophobic surfaces with excellent durability and exceptional stability exposed to fire," *Chem. Eng. J.*, vol. 348, pp. 212–223, Sep. 2018, doi: 10.1016/j.cej.2018.04.195.

[33] M. Zeldin, "Polymers, Inorganic and Organometallic," in *Encyclopedia of Physical Science*

and Technology, Elsevier, 2003, pp. 675–695.

[34] G. R. J. Artus, S. Jung, J. Zimmermann, H. P. Gautschi, K. Marquardt, and S. Seeger, "Silicone nanofilaments and their application as superhydrophobic coatings," *Adv. Mater.*, vol. 18, no. 20, pp. 2758–2762, 2006, doi: 10.1002/adma.200502030.

[35] A. Stojanovic, S. Olveira, M. Fischer, and S. Seeger, "Polysiloxane nanotubes," *Chem. Mater.*, vol. 25, no. 14, pp. 2787–2792, 2013, doi: 10.1021/cm400851k.

[36] E. G. Atici, E. Kasapgil, I. Anac, and H. Y. Erbil, "Methyltrichlorosilane polysiloxane filament growth on glass using low cost solvents and comparison with gas phase reactions," *Thin Solid Films*, vol. 616, pp. 101–110, 2016, doi: 10.1016/j.tsf.2016.07.041.

[37] J. Zimmermann, G. R. J. Artus, and S. Seeger, "Superhydrophobic silicone nanofilament coatings," *J. Adhes. Sci. Technol.*, vol. 22, no. 3–4, pp. 251–263, 2008, doi: 10.1163/156856108X305165.

[38] H. S. Khoo and F. G. Tseng, "Engineering the 3D architecture and hydrophobicity of methyltrichlorosilane nanostructures," *Nanotechnology*, vol. 19, no. 34, 2008, doi: 10.1088/0957-4484/19/34/345603.

[39] J. Zimmermann, F. A. Reifler, G. Fortunato, L. C. Gerhardt, and S. Seeger, "A simple, one-step approach to durable and robust superhydrophobic textiles," *Adv. Funct. Mater.*, vol. 18, no. 22, pp. 3662–3669, 2008, doi: 10.1002/adfm.200800755.

[40] J. Zhang and S. Seeger, "Silica/silicone nanofilament hybrid coatings with almost perfect superhydrophobicity," *ChemPhysChem*, vol. 14, no. 8, pp. 1646–1651, 2013, doi: 10.1002/cphc.201200995.

[41] X. Zhang, S. Liu, A. Salim, and S. Seeger, "Hierarchical Structured Multifunctional Self-Cleaning Material with Durable Superhydrophobicity and Photocatalytic Functionalities,"

Small, vol. 15, no. 34, 2019, doi: 10.1002/smll.201901822.

[42] S. Liu, X. Zhang, and S. Seeger, "Solvent-Free Fabrication of Flexible and Robust Superhydrophobic Composite Films with Hierarchical Micro/Nanostructures and Durable Self-Cleaning Functionality," *ACS Appl. Mater. Interfaces*, vol. 11, no. 47, pp. 44691–44699, 2019, doi: 10.1021/acsami.9b15318.

[43] J. Zimmermann, M. Rabe, G. R. J. Artus, and S. Seeger, "Patterned superfunctional surfaces based on a silicone nanofilament coating," *Soft Matter*, vol. 4, no. 3, pp. 450–452, 2008, doi: 10.1039/b717734h.

[44] M. Meier, V. Dubois, and S. Seeger, "Reduced bacterial colonisation on surfaces coated with silicone nanostructures," *Appl. Surf. Sci.*, vol. 459, no. July, pp. 505–511, 2018, doi: 10.1016/j.apsusc.2018.08.003.

[45] G. R. J. Artus, S. Olveira, D. Patra, and S. Seeger, "Directed In Situ Shaping of Complex Nano- and Microstructures during Chemical Synthesis," *Macromol. Rapid Commun.*, vol. 38, no. 4, pp. 1–9, 2017, doi: 10.1002/marc.201600558.

[46] S. Olveira, A. Stojanovic, and S. Seeger, "Systematic parametric investigation on the CVD process of polysiloxane nano- and microstructures," *J. Nanoparticle Res.*, vol. 20, no. 11, 2018, doi: 10.1007/s11051-018-4394-0.

[47] J. Zhang, A. Wang, and S. Seeger, "Nepenthes pitcher inspired anti-wetting silicone nanofilaments coatings: Preparation, unique anti-wetting and self-cleaning behaviors," *Adv. Funct. Mater.*, vol. 24, no. 8, pp. 1074–1080, 2014, doi: 10.1002/adfm.201301481.

[48] E. Kasapgil, I. Anac, and H. Y. Erbil, "Transparent, fluorine-free, heat-resistant, water repellent coating by infusing slippery silicone oil on polysiloxane nanofilament layers prepared by gas phase reaction of n-propyltrichlorosilane and methyltrichlorosilane,"

Colloids Surfaces A Physicochem. Eng. Asp., vol. 560, no. September 2018, pp. 223–232, 2019, doi: 10.1016/j.colsurfa.2018.09.064.

[49] E. Kasapgil *et al.*, "Polysiloxane nanofilaments infused with silicone oil prevent bacterial adhesion and suppress thrombosis on intranasal splints," *ACS Biomater. Sci. Eng.*, vol. 7, no. 2, pp. 541–552, 2021, doi: 10.1021/acsbiomaterials.0c01487.

[50] M. J. Molina and F. S. Rowland, "Stratospheric sink for chlorofluoromethanes : chlorine atomc-atalysed destruction of ozone," *Nature*, vol. 249, pp. 810–812, 1974.

[51] Environment Canada, "Environment and Climate Change Canada - Ecological Screening Assessment Report on Long-Chain (C9–C20) Perfluorocarboxylic Acids, their Salts and their Precursors," Sep. 09, 2013. http://ec.gc.ca/ese-ees/default.asp?lang=En&n=CA29B043-1 (accessed Apr. 10, 2021).

[52] C. Lau, K. Anitole, C. Hodes, D. Lai, A. Pfahles-Hutchens, and J. Seed, "Perfluoroalkyl acids: A review of monitoring and toxicological findings," *Toxicological Sciences*, vol. 99, no. 2. Oxford Academic, pp. 366–394, Oct. 01, 2007, doi: 10.1093/toxsci/kfm128.

[53] B. D. Key, R. D. Howell, and C. S. Criddle, "Fluorinated organics in the biosphere," *Environmental Science and Technology*, vol. 31, no. 9. pp. 2445–2454, 1997, doi: 10.1021/es961007c.

[54] CFR, "CFR - Code of Federal Regulations Title 21 - Chapter I - Subchapter H." https://www.accessdata.fda.gov/scripts/cdrh/cfdocs/cfcfr/cfrsearch.cfm?fr=872.3680 (accessed Apr. 10, 2021).

[55] CFR, "CFR - Code of Federal Regulations Title 21 - Chapter I - Subchapter B." https://www.accessdata.fda.gov/scripts/cdrh/cfdocs/cfcfr/cfrsearch.cfm?fr=177.1550 (accessed Apr. 10, 2021).

[56] J. W. Martin, M. M. Smithwick, B. M. Braune, P. F. Hoekstra, D. C. G. Muir, and S. A. Mabury, "Identification of Long-Chain Perfluorinated Acids in Biota from the Canadian Arctic," *Environ. Sci. Technol.*, vol. 38, no. 2, pp. 373–380, 2004, doi: 10.1021/es034727+.

[57] L. Ahrens, "Polyfluoroalkyl compounds in the aquatic environment: A review of their occurrence and fate," *J. Environ. Monit.*, vol. 13, no. 1, pp. 20–31, Jan. 2011, doi: 10.1039/c0em00373e.

[58] Government of Canada, "Substance prohibition summary for PFOA, long-chain PFCAs and related substances," *Government of Canada*, 2018. https://www.canada.ca/en/environment-climate-change/services/canadian-environmental-protection-act-registry/substance-prohibition-summary-perfluorooctanoic-acid.html (accessed Apr. 10, 2021).

[59] EPA, "PFAS Laws and Regulations: Clean Air Act." https://www.epa.gov/pfas/pfas-laws-and-regulations (accessed Apr. 10, 2021).

[60] L. Croce, F. Coperchini, M. Tonacchera, M. Imbriani, M. Rotondi, and L. Chiovato, "Effect of long- and short-chain perfluorinated compounds on cultured thyroid cells viability and response to TSH," *J. Endocrinol. Invest.*, vol. 42, no. 11, pp. 1329–1335, Nov. 2019, doi: 10.1007/s40618-019-01062-1.

[61] J. W. Martin, S. A. Mabury, K. R. Solomon, and D. C. G. Muir, "Dietary accumulation of perfluorinated acids in juvenile rainbow trout (Oncorhynchus mykiss)," *Environ. Toxicol. Chem.*, vol. 22, no. 1, pp. 189–195, Jan. 2003, doi: 10.1002/etc.5620220125.

[62] S. Brendel, É. Fetter, C. Staude, L. Vierke, and A. Biegel-Engler, "Short-chain perfluoroalkyl acids: environmental concerns and a regulatory strategy under REACH," *Environ. Sci. Eur.*, vol. 30, no. 1, 2018, doi: 10.1186/s12302-018-0134-4.

2 Antimicrobial Nanomaterials and Coatings: Current Mechanisms and Future Perspectives to Control the Spread of Viruses Including SARS-CoV-2

Sara M. Imani [a,Ψ], Liane Ladouceur [a,Ψ], Terrel Marshall [b], Roderick Maclachlan [b], Leyla Soleymani* [a,b], Tohid F. Didar* [a,c,d]

[a] McMaster University, School of Biomedical Engineering, 1280 Main Street West, Hamilton, L8S 4L7, Canada

[b] McMaster University, Department of Engineering Physics, 1280 Main Street West, Hamilton, L8S 4L7, Canada

[c] McMaster University, Department of Mechanical Engineering, 1280 Main Street West, Hamilton, L8S 4L7, Canada.

[d] Michael G. DeGroote Institute of Infectious Disease Research, McMaster University, Hamilton, ON L8N 3Z5, Canada

Ψ These authors contributed equally to this work.

This article was published by ACS Nano on October 9, 2020.

https://pubs.acs.org/doi/10.1021/acsnano.0c05937

Author contributions: T.F.D. and L.S. supervised and conceived the research. S.M.I. and L.L. designed and wrote the main manuscript text with help from T.F.D and L.S. T.M. and R.M. contributed to specific sections. All authors contributed to editing the manuscript.

2.1 Abstract

The global COVID-19 pandemic has attracted considerable attention toward innovative methods and technologies for suppressing the spread of viruses. Transmission *via* contaminated surfaces has been recognized as an important route for spreading SARS-CoV-2. While significant efforts have been made to develop antibacterial surface coatings, the literature remains scarce for a systematic study on broad-range antiviral coatings. Here, we aim to provide a comprehensive overview of the antiviral materials and coatings that could be implemented for suppressing the spread of SARS-CoV-2 *via* contaminated surfaces. We discuss the mechanism of operation and effectivity of several types of inorganic and organic materials, in the bulk and nanomaterial form, and assess the possibility of implementing these as antiviral coatings. Toxicity and environmental concerns are also discussed for the presented approaches. Finally, we present future perspectives with regards to emerging antimicrobial technologies such as omniphobic surfaces and assess their potential in suppressing surface-mediated virus transfer. Although some of these emerging technologies have not yet been tested directly as antiviral coatings, they hold great potential for designing the next generation of antiviral surfaces.

Keywords: antiviral surfaces, antimicrobial coatings, pathogen-repellent surfaces, nanocoatings, photoactive materials, engineered surfaces, COVID-19, virus inactivation, virus repellent

2.2 Introduction

The COVID-19 pandemic has intensified the world's attention toward the spread of contamination facilitated by *high touch* surfaces. In response, surfaces and coatings capable of minimizing the presence of active viral pathogens are being explored for application in a variety of settings such as healthcare centres, long-term care facilities, public transport, schools, and various businesses, to reduce human exposure and mitigate the spread of infectious pathogens.

One area of particular significance in the transmission of infectious diseases is the ability of microbes to survive on surfaces, both in healthcare settings and on common surfaces. Considerable research has been conducted to investigate solutions that prevent bacterial transmission and biofilm formation by killing and/or reducing attachment of microbes. These have been realized through surface-bound active antimicrobials and biocidal coatings [1] or passive pathogen-repellent surfaces [2] developed using nanomaterials, chemical modifications, and micro- and nanostructuring.[2–5]

Many of the previously-reported antimicrobial coatings have focused on antibacterial capabilities; however, there has been much less focus on antiviral surfaces and coatings. Persistence of active viruses on surfaces varies dramatically based on the type of the surface and the virus.[6] For example, the viability of coronaviruses on surfaces ranges from 2 hours to 9 days.[6] Lack of host cells, immediate inactivation of some viruses on surfaces (*e.g.* Rinderpest virus),[7] and incapability of some viruses to spread outside the body (*e.g.* Human Immunodeficiency Virus-HIV),[8] have attracted less attention to the transmission of viruses *via* surfaces. However, infectious viruses such as SARS-CoV-2 that remain viable on surfaces pose a great risk for transmission *via* the surface route, highlighting the urgent need for effective solutions that prevent the survival of viruses on surfaces.[6,9] In order to highlight antimicrobial research which has definitively

demonstrated antiviral capabilities, throughout this review we will use the term antiviral to refer to nanomaterials and coatings which have proven antiviral capabilities, whereas the term antimicrobial will be used as a more general term to characterize nanomaterials and coatings that demonstrate effectiveness against other microorganisms, such as bacteria, but to date have no proven antiviral capability.

A challenge encountered in reviewing the antiviral surface literature is related to the wide range of viruses used in testing. It is common to find tests conducted using bacteriophages, influenza, or HIV, however, there is often no systematic study that allows for the precise understanding of virucidal behaviour. Viruses have a multitude of architectures – enveloped or non-enveloped, RNA-based or DNA-based – and can be further classified as positive- or negative-sense, or single- or double-stranded, respectively. This is only the high-level variation witnessed in viruses, which illustrates the clear need for more robust testing when claiming antiviral capabilities.

Despite these caveats related to the lack of standardized evaluation methods, this review aims to provide a comprehensive summary of the current state of research toward antiviral materials and surfaces (**Figure 2.1**), using antimicrobial research as a starting point, whereas other review papers regarding reducing the spread of COVID-19 have focused on therapeutics and tools that inactivate SARS-CoV-2.[10,11] First, we present a comprehensive review of metal and inorganic materials, with a focus on nanomaterials, with antiviral properties namely, copper, silver, zinc, and titanium dioxide. We then discuss polymeric and organic surface coatings such as polyelectrolytes and photosensitizer materials that inactivate viruses (**Figure 2.1**). The toxicity and environmental concerns considered for each of these approaches will also be discussed. We finally present and propose emerging technologies that have not yet been used for antiviral purposes but hold great

promise and potential for the future engineering of antiviral surfaces as they have been tested for their antimicrobial properties.

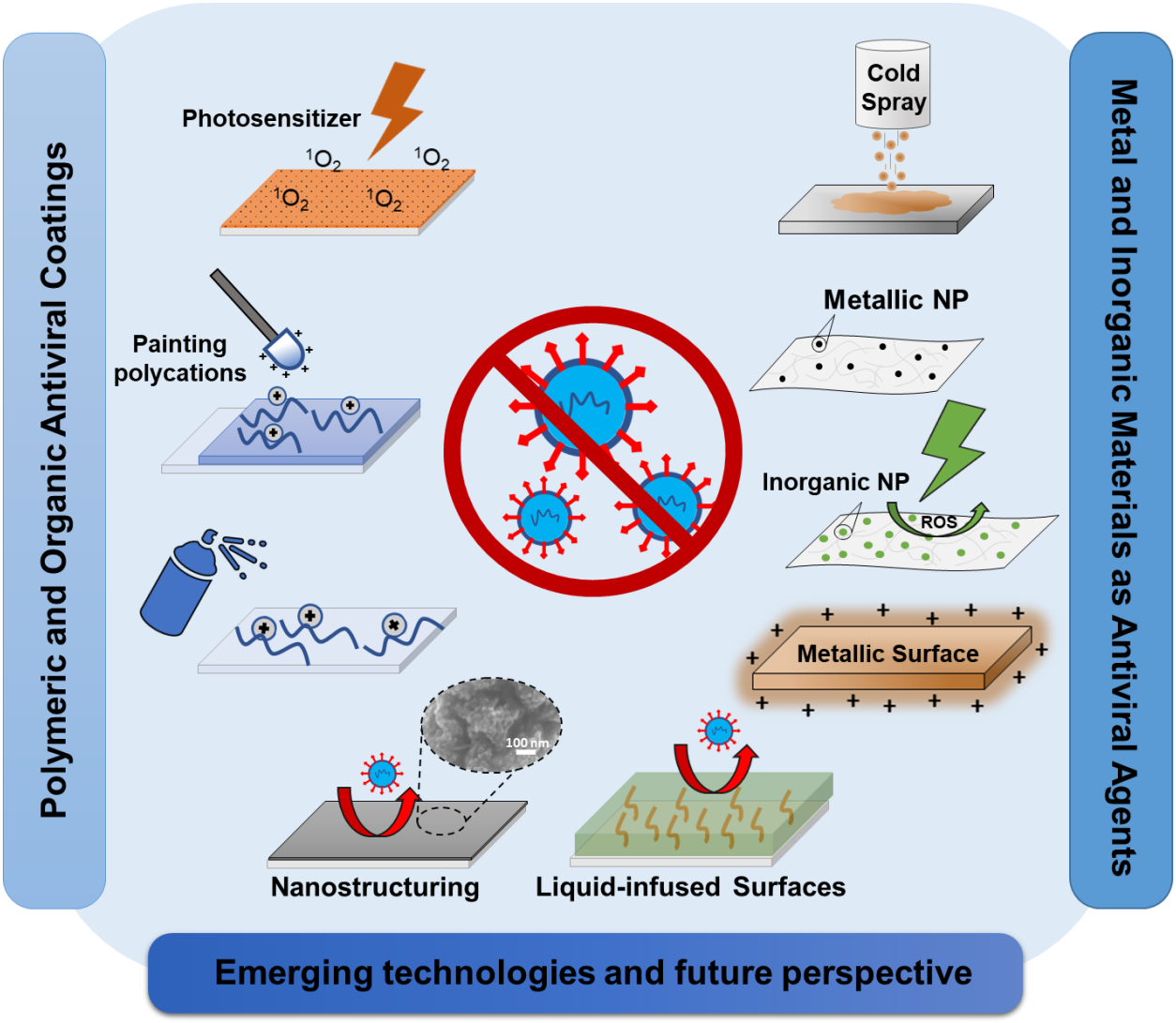

Figure 2.1 – Schematic diagram of the current research and emerging antiviral coatings and surfaces, including metal and inorganic nanomaterials, polymeric and organic coatings and emerging technologies such as omniphobic pathogen-repellent coatings.

2.3 Metal and Inorganic Materials as Antiviral Agents

2.3.1 Copper

Copper is perhaps the most widely-recognized and well-characterized antimicrobial metal used to date.[12] Use of copper in medicine, as an antiseptic and anti-inflammatory agent, dates back millennia.[13] Through bacterial investigations, modern research has identified multiple antimicrobial mechanisms for copper such as: (1) plasma membrane permeabilization, (2) membrane lipid peroxidation, (3) alteration of proteins, (4) inhibition of protein assembly and activity, or (5) denaturation of nucleic acids.[14] Membrane disruption can occur due to the electrostatic forces exerted by copper ions on the outer plasma membrane of cells.[15] Damage to proteins occurs *via* the displacement of essential metals from their native binding sites on proteins or direct interactions with the proteins.[16] Copper-binding sites on nucleic acids also enable protein denaturation.[17] Additionally, cyclic redox reactions between Cu^{+} and Cu^{2+} are known to produce highly reactive hydroxyl radicals. Reactive oxygen species (ROS) are either responsible for or contribute to cell death by interaction with the cell membrane.[18]

While some hypotheses have been made into the virucidal action of copper, the majority of antimicrobial copper research is focused on its antibacterial properties.[12] Research has demonstrated that copper targets the viral genome, particularly encoding genes that are essential for viral infectivity (**Figure 2.2a**).[19] It has been demonstrated that the primary effectors of inactivation for viruses such as murine norovirus are Cu(II) and Cu(I).[20] Additionally, many researchers have postulated that the same ROS mechanism found in antibacterial activity can act on the viral envelope or capsid.[12] Notably, viruses are susceptible to the damage induced by copper since they do not possess the repair mechanisms found in bacteria or fungi.[14]

Mechanisms that result in the immediate deactivation of microbes upon contact are commonly referred to as "contact killing".[21] Researchers have taken advantage of this functionality to create copper-based antiviral surfaces (**Table 2.1**). Inactivation of influenza A was demonstrated to be significantly higher on planar copper in comparison to stainless steel, leaving only 500 infectious virus particles after 6 hours from the 2×10^6 virus particles inoculated, while stainless steel retained 500,000 infectious virus particles after 24 hours.[22] Influenza A and *Escherichia* bacteriophage (Qβ) were also tested on solid-state copper compounds and compared to solid-state silver compounds, with efficient inactivation achieved using cuprous oxide in solid-state but not cupric oxide or silver sulfide solid-states.[23] This difference between cuprous oxide solid-state copper and cupric compounds was in line with work by Sunada *et al.* using bacteriophage Qβ, which revealed a 6-log reduction for cuprous oxide (Cu_2O) in 30 minutes but a less than 1-log reduction on cupric oxide (CuO) in the same duration.[18] In tests on copper coupons, a copper-mediated inactivation was illustrated for a range of bacteriophages by Li and Dennehy.[24] This study included a range of double-stranded DNA, single-stranded DNA, and single-stranded RNA bacteriophages, with lipid-containing bacteriophages demonstrating the most susceptibility to copper in solution, such as *Pseudomonas* bacteriophage (bacteriophage Φ6) showing a 2-log reduction in the first hour.[24] Studies using copper have also demonstrated significant reduction to orthopoxviruses, with monkeypox virus and vaccinia virus being inactivated within three minutes of contact with copper surfaces.[21] Warnes and Keevil have highlighted the effectiveness of copper alloys, with 60% or higher copper component, in completely inactivating dry touch murine norovirus as fast as 5 minutes and showing significant reductions to wet fomite infectivity, up to complete inactivation within 60 minutes.[20] Of particular interest for the current COVID-19 pandemic, in 2015 Warnes *et al.* investigated the use of copper alloys for the inactivation of human

coronavirus 229E and showed that complete inactivation of 10^3 PFU applied to a 1 cm^2 coupon occurred in less than 60 minutes on a range of alloys, with Cu/Zn brasses being very effective at 70% or higher copper concentrations.[25]

Researchers have also investigated the incorporation of copper ions into other materials to invoke antiviral capabilities. The research in this area was pioneered by Karlstrom and Levine in 1991 when the inhibition of proteases, proteins essential for viral replication, from human immunodeficiency virus 1 (HIV-1) was investigated under the influence of copper and mercury ions, Cu^{2+} and Hg^{2+}.[16] This study demonstrated that oxygen was not required for the inactivation of the protease and that approximately stoichiometric concentrations of copper and mercury ions caused rapid and irreversible inactivation. While this research notes that a clear cation binding site exists on aspartic proteases, tests have also shown that copper does not directly inactivate these proteases. Instead, it is postulated that copper acts on the substrates for proteases, though this has not been clearly demonstrated.[16]

Copper ions and particles have also been used in antimicrobial and antiviral textiles, filters, and polymeric materials such as latex.[26–29] Early examples of this include the work by Borkow and Gabbay, which created latex gloves impregnated with copper for testing against HIV-1 and copper filters tested with both HIV-1 and West-Nile virus (WNV).[26] Antiviral effectiveness of latex samples in this study was based on the amount of copper incorporated in a dose-dependent manner, while the filters demonstrated a roughly 5-log reduction for both HIV-1 and WNV. Filters constructed from a layer of nonwoven polypropylene fibers on top of nonwoven carbon fibers were doped with copper-oxide and investigated in a study by Borkow *et al.* that demonstrated reduction in various viruses, starting at a maximum of 2-log reduction of rhinovirus-2, and decreasing reductions were seen with yellow fever, influenza A, measles, respiratory syncytial, parainfluenza

3, Punta Toro, Pichinde, HIV-1, adenovirus type 1, and cytomegalovirus, with vaccinia virus demonstrating the lowest reduction of just 0.47 log (see Table 2.1).[27] Interestingly, copper oxide was incorporated into face masks, which resulted in the elimination of the human influenza A virus within 30 minutes, compared to 4.67 ± 1.35 $\log_{10}$ $TCID_{50}$ (Median Tissue Culture Infectious Dose) recovered from control masks (**Figure 2.3a**) by aerosolized challenge with 5.66 ± 0.51 $\log_{10}$ $TCID_{50}$ of the virus.[28] It has also been demonstrated that by using a cotton textile on which zeolite A was chemically synthesized, the structural component Na^+ can be replaced with Cu^{2+} ions to then allow the textile to inactivate both highly pathogenic H5N1 and less pathogenic H5N3 influenza viruses.[29]

Copper nanoparticles (CuNPs) present great promise for use in antimicrobial and antiviral surfaces due to their smaller size and high surface to volume ratio. This facilitates interaction with microbes and allows broad-spectrum antimicrobial and antiviral activity.[30] Li *et al.* used CuNPs as part of a layered system, by combining the antimicrobial and antiviral properties of copper and chlorine dioxide (ClO_2).[31] This work investigated the use of a polymeric micelle preparation, coated on glass, for the slow release of ClO_2 over a 15-day span. In order to increase the contact killing efficiency of this material, CuNP were covalently clustered on the micelle surface.[31] Testing of this coating demonstrated a broad spectrum of activity that killed a range of microbes including viruses (H1N1), bacteria, and spores. Transmission electron microscope (TEM) images demonstrated significant degradation in virus structure upon contact with this coating (**Figure 2.3b**). The complete inactivation of the influenza virus was demonstrated *via* plaque assay with this coating within one minute.[31]

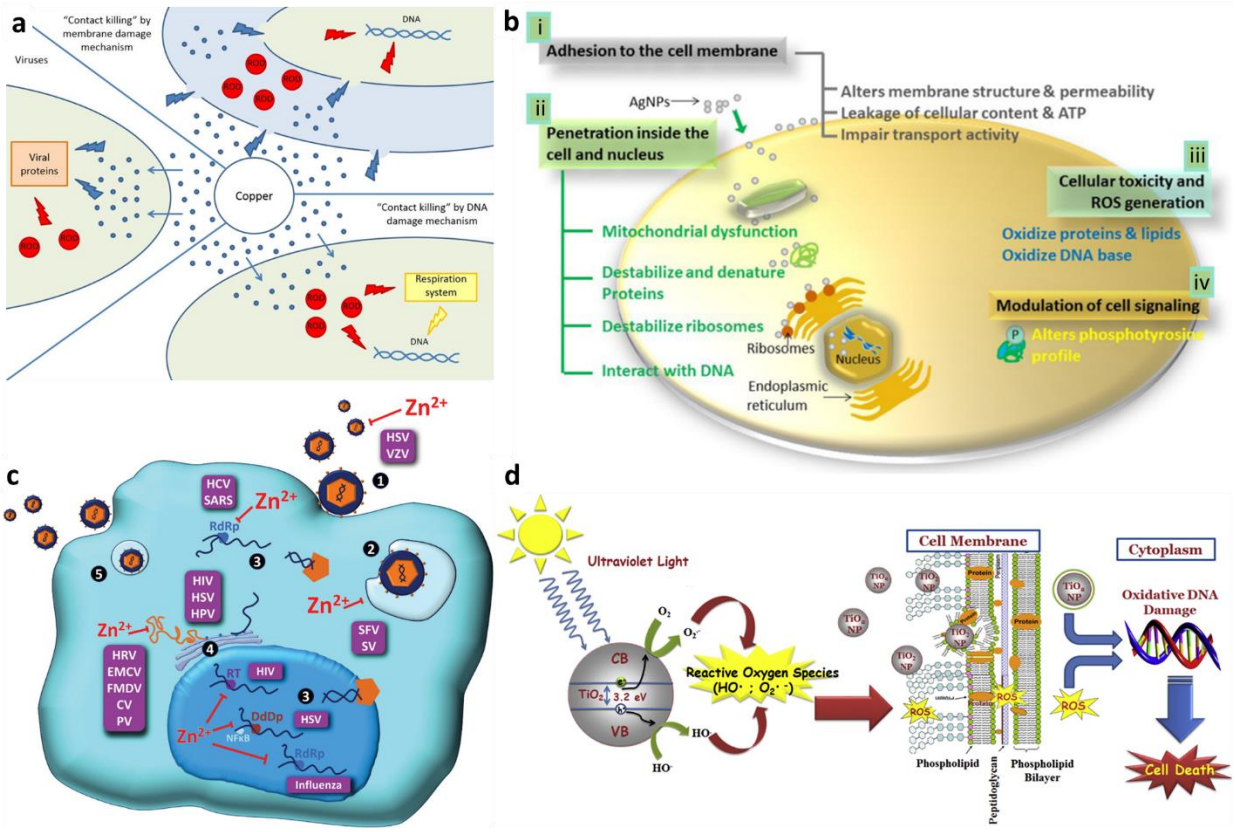

Figure 2.2 – Antiviral mechanisms of inorganic materials **(a)** Antimicrobial contact killing mechanisms for copper, include membrane degradation, genotoxicity and potentially ROS. Reprinted with permission from ref [12]. Copyright 2018 John Wiley and Sons. **(b)** Four prominent routes of antimicrobial action for silver include adhesions to cell membrane (i), penetration into cell and nucleus (ii), cellular toxicity and ROS generation (iii) and modulation of cell signaling (iv). Reprinted from ref [32]. Copyright 2016 Dakal, Kumar, Majumdar and Yadav. **(c)** The actions of zinc throughout the cell and proposed mechanisms for antiviral properties include free virus inactivation (1), inhibition of viral uncoating (2), viral genome transcription (3), and viral protein translation and polyprotein processing (4) Reprinted with permission from ref [33]. Copyright 2019 Oxford University Press. **(d)** The photocatalytic process by which TiO_2 nanoparticles and TiO_2 compounds produce reactive oxygen species (ROS) to cause disturbance of lipid membranes and damage to genetic information, ultimately resulting in bacterial cell death or viral inactivation. Reprinted with permission from ref [34]. Copyright 2017 Elsevier.

Finally, work published by Champagne *et al.* has demonstrated different methods of applying copper powder on surfaces.[35] Specifically, they tested spray coating methods with copper powder to convey antimicrobial and antiviral effects. They also discovered that using a cold-

coating approach, coating at a velocity of 500-1000 m/s and a temperature of 150-400°C, similar to many commercial approaches that exist to apply metal coatings, was most effective against influenza A, with 100% inhibition after just 10 minutes of exposure to a 100 µL aliquot of virus.[35]

2.3.2 Silver

Silver is another antiviral material that deactivates viruses by interaction with the viral envelope and viral surface proteins, blocking of viral penetration into cells, blocking cellular pathways, interaction with the viral genome, and interaction with viral replication factors (**Figure 2.2b**).[36] A significant portion of antiviral research for silver remains in solution.[32] Nevertheless, previous studies have specifically investigated the use of silver in the form of ions, nanoparticles, and hybrid coatings to develop antiviral surfaces (Table 2.1). Work by Lara *et al.* aimed at elucidating the mechanism of viral deactivation for silver using HIV-1, suggesting that silver nanoparticles (AgNPs) function as early-stage antivirals that disrupt viral replication.[37] They hypothesized these to inhibit viral entry by binding or fusion to cells, though AgNPs also demonstrated inhibition at later stages in viral replication for which the mechanism was not confirmed.[37] It is also evident that silver interacts differently with different families of viruses.[38] Unlike copper, solid-state silver compounds do not appear to have strong antiviral capabilities. In a comparative study conducted by Minoshima *et al.*, it was found that while solid-state cuprous oxide effectively inactivated influenza A virus and bacteriophage Qβ, solid-state silver sulfide showed little antiviral activity.[23] Silver as an antimicrobial and antiviral has an affinity toward sulfur and phosphate groups,[39] which can disrupt the cell membrane due to the interaction with phospholipid tails and proteins containing cysteine or methionine. Additionally, Ag^+ produces reactive oxygen species (ROS) within cells, leading to an antimicrobial and antiviral ability.[40] In bacterial studies, AgNPs are thought to disrupt the mitochondrial respiratory chain leading to the

production of ROS.[41] More specific to antiviral activities, AgNPs are thought to inhibit the entry of the virus to cells due to binding of envelope proteins, such as glycoprotein gp120, which prevent CD4-dependent virion binding, fusion and infectivity.[37]

The use of metal ions within coatings is a common approach found in literature. A study conducted by Hodek *et al.* investigated the use of silver, as well as copper and zinc, as part of a sol-gel, hybrid coating.[42] Antiviral tests used HIV-1, dengue virus, herpes simplex virus (HSV), influenza virus, and coxsackievirus to provide comprehensive analysis on enveloped and non-enveloped, as well as DNA- and RNA-based viruses. Results were most favourable with HIV-1, with one method of coating showing a 99.8% reduction in virus titer.[42] Log-scale reductions were significant for all types of viruses (Table 2.1), though this coating was less effective against influenza and coxsackievirus, which is thought to be due to the nature of each virus as negative-sense RNA based or non-enveloped, respectively.[42] Castro-Mayorga *et al.* demonstrated the effectiveness of both silver nitrate and AgNPs in reducing recovered titer levels of norovirus surrogates for up to 150 days.[38] Using feline calicivirus (FCV) and murine norovirus (MNV), statistically significant reductions in surface recovery of both viruses were seen in the presence of the ions and AgNPs (see Table 2.1). Notably, AgNP activity as an antiviral increased or remained constant up to 150 days if the concentration was higher than 2.1 mg/L, however, silver nitrate was most effective over only the first 75 days, likely due to the reduction and aggregation of ions.[38] Here, silver nitrate was more effective against FCV, while AgNPs maintained higher and more prolonged effectiveness against MNV. This study further tested a AgNP film, produced by electrospinning a coating of poly(3-hydroxybutyrate-co-3-hydroxyvalerate) (PHBV)/AgNP fiber mats, which were tested at both 25°C and 37°C.[38] Reductions of 1.42- and 0.14-log were demonstrated for FCV and MNV, respectively at 25°C, which were not shown to be statistically

significant compared to control PHBV films exposed to the virus.[38] At 37°C, the reduction of FCV was greater than 2.26-log, while the reduction in MNV was less successful, at only 0.86-log. It is here hypothesized that the release of silver ions from the immobilized AgNPs are responsible for the viral inactivation observed here; however, further testing and research is required to confirm this mechanism.[38]

Similar to the work of Castro-Mayorga *et al.*, AgNPs are combined with many different materials to lend antiviral capabilities. For example, chitin-nanofiber sheets (CNFS) have been combined with AgNPs to form antimicrobial and antiviral biomaterials including a 2-log decrease in influenza A.[43] Integration of AgNPs into sheets was also the approach taken by Chen *et al.*, with their research on the antiviral activity of graphene-oxide sheets with silver particles (GO-Ag).[44] Using both an enveloped and non-enveloped virus, researchers found that inhibition of viruses depended on the concentration of GO-Ag.[44] The minimum concentration of GO-Ag required to inhibit infectious bursa virus (IBDV) inoculated at 9×10^2 $TCID_{50}$/mL was 0.125 mg/mL, while a higher inoculation of the virus, 9×10^3 $TCID_{50}$/mL IBDV, required 1 mg/mL of GO-Ag for inhibition. For inoculation of 4.7×10^4 $TCID_{50}$/mL of feline coronavirus (FCoV), 0.1 mg/mL concentration of GO-Ag caused 24.8% inhibition.[44] For this study, silver doubled the capability of graphene oxide sheets against enveloped viruses, while it was the sole source of inhibition against the non-enveloped virus.

Integration of nanoparticles into membranes and filters is another common theme throughout the literature. Similar to copper, AgNPs can be incorporated into textiles and membranes in order to confer antiviral capabilities. Zodrow *et al*. investigated the use of AgNPs with polysulfone membranes, which exhibit promising antiviral properties, although a significant loss of silver from the membrane resulted in short-lived antibacterial and antiviral activity.[45] While

the exact mechanism for antiviral capabilities was not confirmed, the possibility of change in membrane permeability, depth of filtration, electrostatic adsorption or inactivation by Ag^+ ions allowed for influent concentrations of up to $5\pm0.2 \times 10^5$ PFU/mL to be completely removed, while membranes without silver retained 10^2 PFU/mL.[45] Similarly, work by De Gusseme *et al.* produced biogenic silver, which is associated with the bacterial cell surface of *Lactobacillus fermentum*, immobilized onto polyvinylidene fluoride (PVDF) membranes.[46] This work tested antiviral properties using bacteriophage UZ1 and based on the slow release of Ag^+, at least a 3.4-log decrease in virus load was achieved. Integration of silver into polylactide (PLA) films functions in the same manner as biogenic silver on PVDF, with the slow migration of silver from the film as demonstrated by Martinez-Abad *et al.* when tested against FCV.[47] Similar to this approach with membranes, silver can be integrated into filters in order to trap airborne virus particles. In research conducted by Joe *et al.*, AgNPs were coated onto a medium air filter, which showed increased filter efficacy over 15 minutes of testing, with a density of 1.5×10^9 particles/cm^2 demonstrating roughly 70% antiviral efficiency without the presence of dust.[48] Importantly, efficiency increased with silver density but decreased as dust buildup accumulated.

Research to date has demonstrated that the size of AgNPs influences their effectiveness as antiviral agents, with 25 nm as their upper size limit.[49] Interestingly, Rogers *et al.* discovered that larger AgNPs – at diameters of 25 nm, 55 nm, and 80 nm – increase the number of plaque-forming units compared to controls, promoting virus survival.[50] A proposed explanation for this is that when the AgNPs are too large to establish a strong physical interaction with the glycoprotein present on viruses, they are unable to inhibit viral binding to cell surfaces and instead, these nanoparticles may agglomerate facilitating interaction of the virus with the host cells.[50]

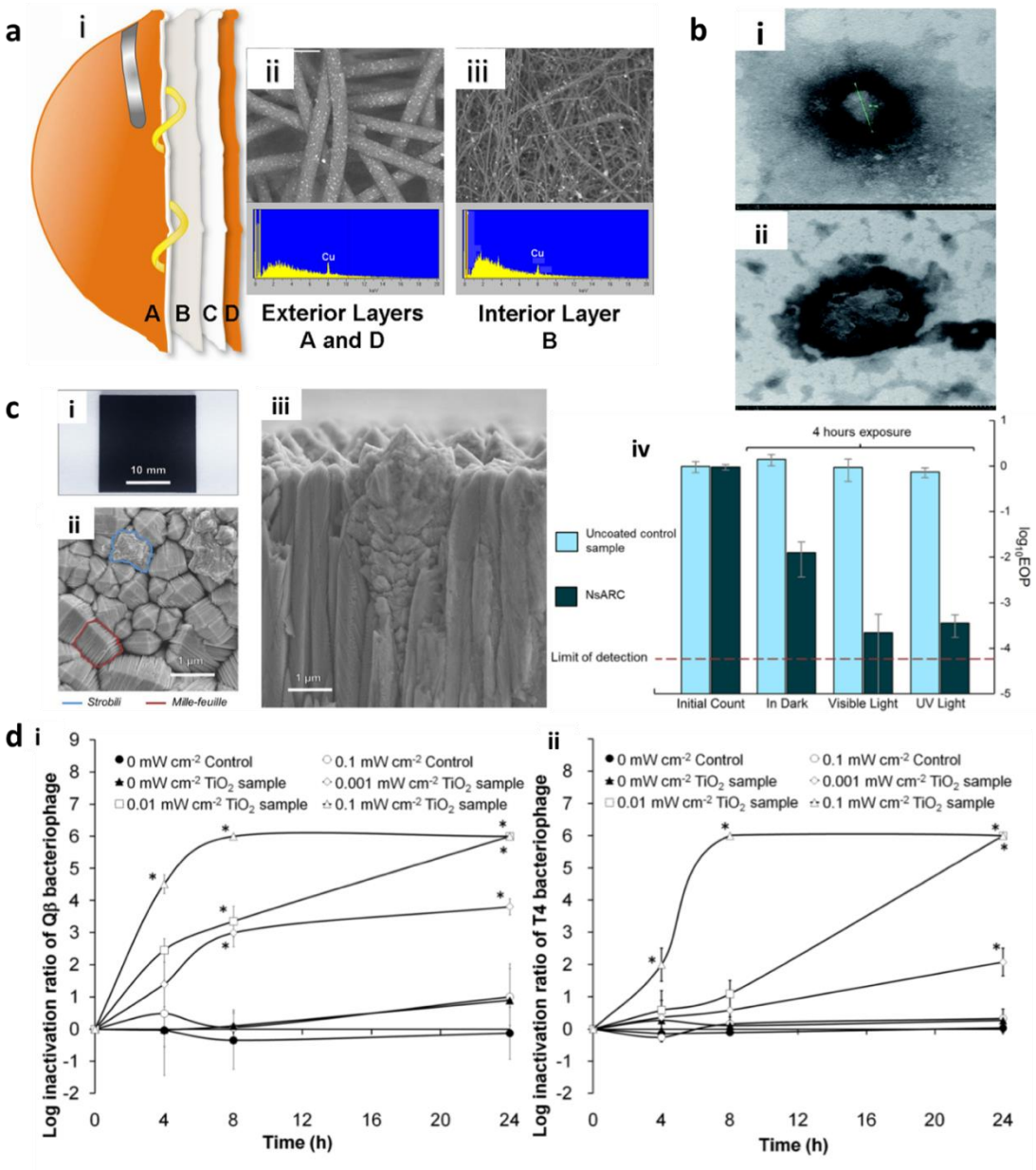

Figure 2.3 – Examples of inorganic antiviral coatings **(a)** Copper impregnation on face mask. Reprinted from ref [28]. Copyright 2010 Borkow *et al*. **(b)** Demonstration of virucidal capabilities conferred through a multi-functional antimicrobial and antiviral coating consisting micelles containing copper nanoparticles. (i) TEM image of influenza H1N1; (ii) TEM image of H1N1 virus after contact with coating. Reprinted from ref [31]. Copyright 2018 Royal Society of Chemistry. **(c)** i. Surface of composite nanostructured anatase-rutile-carbon (NsARC) coating on stainless steel. ii. SEM of NsARC coating surface morphology. iii. SEM of NsARC coating cross section. The nanoscale features resembling anatase sheets (*mille-feuille*) and rutile cones (*strobili*) increase the coating's surface area, promoting efficient charge separation to elicit the photocatalytic effect. iv. Reduction in the number of *E. coli* live cells after 4 h exposure to UV light, visible light, and

dark conditions on uncoated stainless steel and NsARC-coated stainless steel. Reprinted from ref [51]. Licensed under Creative Commons 2019. **(d)** Antiviral performance of a TiO_2 solid coating on glass with UVA irradiation intensities of 0, 0.001, 0.01, and 0.1 mW/cm^2 against (i) Bacteriophage Qβ and (ii) Bacteriophage T4. Reprinted with permission from ref [52]. Copyright 2011 Royal Society of Chemistry.

2.3.3 Zinc

Zinc has also been demonstrated as an antiviral agent since the publication of a study in 1974 by Korant *et al.* demonstrating its effectiveness against the human rhinovirus (HRV).[53] Their use of 0.1 mM zinc chloride provided a 99.99% reduction in the number of plaques formed for HRV. It was also demonstrated in this work that the most dramatic effect of zinc as an antiviral was in inhibiting proteolytic cleavage, thereby halting the synthesis of viral polypeptides.[53] As with most metals, the mechanism for antiviral applications varies between viruses. Studies have shown mechanisms that interfere with viral replication, including free virus inactivation and inhibition of viral uncoating, viral genome transcription, and viral protein translation and polyprotein processing (**Figure 2.2c**).[33] For example, the effects of zinc on HSV-1 and -2 have been studied for over 40 years and research has suggested antiviral functionality in all aspects of the virus life cycle including polymerase function, protein production and processing, and free virus inactivation.[54–56] It is worth noting that many viruses rely on a zinc-finger architecture for their replication by host cells, demonstrating the relevance of zinc as an antiviral agent. Zinc-fingers are protein motifs that contain one or more amino acid sequence that allows the coordination of one of more zinc ions.[57] Williams *et al.* illustrated that subtle changes in the zinc-finger structure of the nucleocapsid protein in HIV-1 reduced the effectiveness of chaperone activity that destabilizes nucleic acids during the reverse transcription process of viral replication.[57]

For antiviral surface applications, zinc is typically combined with other metals, whether as part of an alloy [19] or as an ion within a coating.[42] Researchers have investigated the use of solid surfaces containing zinc combined with copper to create an antiviral alloy. Surfaces showed synergistic capabilities between zinc and copper with up to 40% zinc showing some efficacy to inactivate murine norovirus (MNV) and alloys containing up to 30% zinc completely inactivating 5×10^5 PFU/cm^2 within 2 hours.[19] Notably, this study found a 1-log reduction in the infectivity of MNV using pure zinc, which conveys its capability as an antiviral on its own.

Zinc oxide (ZnO) has also been used to create structures that act as viricidal agents. Mishra *et al.* generated zinc oxide micro-nano structures (ZnO-MNSs), which mimicked the naturally-occurring filopodia-like structures observed on the surface of HSV-1. These structures are thought to compete with the virus to bind heparan sulfate on the cell surface and also efficiently trap virions outside cells due to partial negatively charged oxygen vacancies.[58] Pre-incubation of ZnO-MNSs with HSV-1 for 90 minutes significantly blocked viral entry. Monitoring the enzymatic activity of infected cells measured using optical density showed that at a ZnO-MNSs concentration of 100 µg/mL, below 20% of HSV-1 entered the cell, which increased to just below 30% entry when the ZnO-MNSs concentration is at 0.1 µg/mL, while the PBS control showed roughly 70% HSV-1 entry into cells.[58] This reduction of virus cell entry was increased by the use of ultraviolet (UV) light to create oxygen vacancies in the structure of ZnO-MNSs.

Zinc ionophores, substances responsible for transporting zinc ions across lipid membranes, are another intriguing use of the metal for antiviral capabilities. In research conducted by Qiu *et al.*, the use of pyrithione (PT), which is a zinc ionophore, proved effective in inhibiting HSV-1 and HSV-2 replication.[59] Here, PT facilitated the inhibition of HSV late gene expression and the

production of viral progeny, which is presumed to be due to its role in the transport of Zn^{2+}, as inactivation was dependent on ion presence.

2.3.4 Titanium Dioxide (TiO_2)

TiO_2 has attracted much attention for its photocatalytic properties and its resultant applications to the inactivation of bacteria and viruses. The mechanism of pathogenic inactivation in TiO_2 is related to light absorption, electron/hole generation, and the oxidation of organic material by ROS, such as superoxide anions and hydroxyl radicals, generated *via* valence band holes and conduction band electrons (**Figure 2.2d**).[34,60–63] As with other compounds, research into the antimicrobial properties of TiO_2 has largely focused on antibacterial applications, leaving studies into its virucidal activity relatively scarce.

Early studies investigated the mechanisms of TiO_2 photoinactivation of microbes in solution. Akhtar *et al.* developed TiO_2 colloidal nanoparticles by a sonochemical method and demonstrated antibacterial and antiviral activity.[64] The authors note that gram-negative bacteria were more resistant to TiO_2, citing enzymatic and DNA damage as probable mechanisms alongside membrane disruption. They qualitatively demonstrated antiviral activity by inoculating chick allantoises with Newcastle disease virus (NDV) and a sample of nano-colloids (see Table 2.1). The presence of active virus was characterized by hemagglutination of the allantois; virucidal behaviour was demonstrated at concentrations above 6.25 μg/mL.[64]

Planar surface coatings of TiO_2 have been effective antibacterial agents. Nakano *et al.* tested the antibacterial activity of TiO_2-coated glass slides on a range of bacteria, finding that all tested strains were photocatalytically inactivated on TiO_2-coated glass under UVA exposure. They also demonstrated that gram-negative bacteria were significantly more resistant to TiO_2 catalysis, further implicating the lipid membrane as a locus of ROS activity.[65] Krumdieck *et al.* report

growing a nanostructured, solid, composite surface coating of anatase and rutile formations of TiO_2 with carbon on stainless steel by a scalable vapour deposition method.[51] The co-deposition of amorphous carbon enhances the photocatalytic activity of the coating by broadening the range of excitation wavelengths. They reported sizeable reductions of bacterial activity under UV and visible light irradiation and under totally dark conditions (**Figure 2.3c**).[51] Several studies have identified alterations to cell membrane potential, increasing permeability to damaging agents, as a possible "dark" mechanism of TiO_2 antimicrobial action.[51,66,61] These techniques are likely to be effective in antiviral applications, particularly against enveloped viruses in which the outer lipid membrane is susceptible to the same disruption mechanisms as the bacterial plasma membrane.

With the antibacterial nature of TiO_2 nanoparticles and coatings well-established, some recent studies have focused on the direct application of TiO_2 compounds to the development of antimicrobial – and, in growing numbers, antiviral – surfaces for use in areas with high rates of infection, such as hospitals (Table 2.1). Nakano *et al.* demonstrated virucidal photocatalytic activity in TiO_2 coatings using the enveloped influenza virus and non-enveloped FCV.[65] They report a 3.6-log reduction in influenza virus activation after 4 h of UVA exposure on the TiO_2-coated glass and 1.7-log inactivation of FCV after 8 h. Inactivation of the viruses past the lower detection limit of their experiment occurred at 8 h and 16 h for influenza virus and FCV, respectively.[65] Similarly to the bacterial case, they ascribe this stark difference to the absence of a phospholipid bilayer in non-enveloped viruses like FCV.[65] Ishiguro *et al.* demonstrated antiviral activity of TiO_2 spin-coated on glass plates against bacteriophages Qβ and T4 upon exposure to 0.1, 0.01, and 0.001 mW/cm^2 intensity UVA light (351 nm) (**Figure 2.3d**).[52] The lowest intensities they tested are representative of the typical UVA irradiation encountered indoors. At the lowest intensity, they showed 5-log and 2-log reductions in viral activity after 24 h of irradiation for

bacteriophages Qβ and T4, respectively.[52] More rapid inactivation was observed at 0.1 and 0.01 mW/cm^2 for both viral species. They also hypothesized that the probable target of ROS released by photocatalysis is the protein capsid of the bacteriophage after performing tests with bovine serum albumin in solution as a competitor,[52] which resulted in lower bacteriophage activation. The results of Nakano *et al.* discussed above indicate that this surface coating may perform better against enveloped viruses, in which the outer lipid envelope would be more effectively targeted than a protein capsid.[65]

The effect of modifications to TiO_2 surface coatings with fluorine compounds to increase the efficiency of ROS production is also an active area of research. Park *et al.* investigated the virucidal activity of fluorinated TiO_2 surface coatings on bacteriophage MS2, FCV, and MNV.[60] Their goal was to adapt the high-energy photon requirements of normal TiO_2 photocatalytic activity through fluorination, which would allow the phenomenon to occur with only the intensity of UVA irradiation encountered in a typical office with fluorescent lighting (3.5 μW/cm^2 of UVA at a wavelength of ~365 nm).[60] They suspended TiO_2 nanoparticles in a PEG solution before spreading, drying, and calcifying the mixture onto glass slides, followed by immersion in a NaF solution to achieve fluorination.[60] They obtained 90% inactivation of bacteriophage MS2 under 3.5 μW/cm^2 of UVA (~365 nm) intensity after 42 mins on glass with an F-TiO_2 surface coating. In a realistic office setting, residual UVA exposure from fluorescent lighting is typically around 2.4 μW/cm^2. Infectivity of MS2 on their coating fell below detection levels after 12 h under these conditions, validating the potential for F-TiO_2 coatings to prevent viral transmission in indoor environments.[60]

In addition, creating coatings that combine TiO_2 with other metals demonstrates higher viral inactivation (*e.g.* bacteriophage MS2) compared to coatings that contain only TiO_2. As

demonstrated by Rao *et al.*, loading TiO_2 nanowire membranes with silver and copper increased the disinfection of drinking water in comparison to TiO_2 alone, or in combination with just one metal.[67] Testing with bacteriophage MS2 demonstrated a 4.02-log reduction for Cu-Ag-TiO_2 in the UV light irradiation condition compared to less than 3-log reduction for TiO_2 alone, a difference that was attributed directly to the co-loading of Ag and Cu.[67] Furthermore, Moongraksathum *et al.* demonstrated the antiviral capability of a silver-doped TiO_2 coating prepared using a sol-gel method and deposited on a glass substrate.[62] They achieved photocatalytic activity under both UVA and visible light irradiation, demonstrated by the degradation of a methylene blue solution, and observed that a 1 wt% concentration of Ag in the TiO_2 sol-gel produced the most photoactive coatings.[62] They tested the antiviral capability of their coating against influenza A and enterovirus and achieved a >99.99% (>4.17-log) reduction in viral activity after irradiation with a 15 W UVA lamp for 20 mins. They also confirmed that the Ag-TiO_2 composite outperformed a simple TiO_2 coating in terms of percent antibacterial effectiveness by more than six times.[62]

2.3.5 Other inorganic antiviral materials

Although copper, silver, zinc, and TiO_2 are the most widely studied inorganic materials, other inorganic materials and nanoparticles (*e.g.* gold, magnesium, transition metals, silica, and perovskites) have also been investigated in the antiviral research literature (Table 2.1).

Gold nanoparticles (AuNPs) have historically been used for drug delivery alone or in combinations with other, more viricidal, metals such as copper.[68] Different surface modifications, such as increased porosity or sulfate-ended ligands, as well as combination with other bioactive metals, such as copper or iron, have been used to achieve antiviral and, more often, antibacterial functionality.[68–70] Broglie *et al.* investigated a gold/copper sulfide core/shell nanoparticle which

was able to rapidly inactivate norovirus GI.1 (Norwalk) virus-like particles, that replicate the activity of human norovirus in solution.[68] This work provided evidence that capsid protein degradation and capsid damage appeared to be the mechanism associated with viral inactivation, showing a direct reliance on nanoparticle concentration as well as treatment time. Reports as far back as 2010 from Di Gianvincenzo *et al.* hold promise for the use of capped gold nanoparticles as functional units that could be applied to surfaces to convey antiviral capabilities.[70] These AuNPs were coated with multiple copies of an amphiphilic sulfate-ended ligand that is able to bind to HIV and inhibit the infection *in vitro*. More recent work by Cagno *et al.* seems to suggest a similar possibility for surface coating, this time implementing gold nanoparticles as well as iron oxide.[71] Using long and flexible linkers that mimic heparan sulfate proteoglycans (HSPG), tests with HSV-2, vesicular stomatitis virus pseudo-typed lentivirus (LS-VSV-G), human papillomavirus (HPV) and respiratory syncytial virus (RSV) illustrated the effectiveness as an antiviral agent.[71]

Use of transition metals, including iron, magnesium, and manganese, has also proven effective in combination with TiO_2 due to their higher sensitivity to visible light for the creation of radicals. Choi and Cho created a visible-light-induced photocatalyst coating using a sol-gel method, which eradicated more than 99% of influenza virus H1N1 within 30 minutes.[72] Here, the proposed mechanism of action is through the hydroxyl radicals that are generated in photocatalytic reactions, similar to the mechanisms discussed for TiO_2 itself.[72]

A silica nanoparticle-based antimicrobial and antiviral coating was developed by Botequim *et al.* by incorporating quaternary ammonium cationic surfactant, didodecyldimethylammonium bromide (DDAB) on the surface of nanoparticles.[73] They showed complete inactivation of influenza A/PR/8/34 (H1N1) virus on glass coated with DDAB treated nanoparticles with 0% virus survival. Notably, the antiviral mechanism does not require leaching of DDAB from the particle's

surface and is predicted to be similar to polycations with quaternary ammonium monomeric unity where they attract the viruses through favorable surface charges.[73]

Use of perovskites for antimicrobial capability is another growing area of research. Perovskites, referring to all compounds with the same crystal structure as calcium titanate, have been the subject of recent energy research, with perovskite-based solar cells reported in 2009.[74] The application of these materials for antimicrobial and antiviral use has gained traction due to their superb oxidative ability, as reported by Weng *et al.*.[75] Using nonstoichiometric perovskite-type La_xMnO_3, research has demonstrated the oxidation of amino acid residues within the viral envelope which neutralized the infectivity of influenza A virus. The best disinfection was achieved using $La_{0.9}MnO_3$ drop-coated onto glass coverslips, which neutralized 76% of influenza A within 15 minutes.[75] Additional research has remained focused on antibacterial capabilities of materials such as perovskite lanthanum aluminate (PLA) and $La_{0.8}Ag_{0.15}MnO_3$ (LAMO) magnetic nanoparticles (MNPs), which are thought to function through the interaction of positively charged NPs with the negatively charged cell wall of bacteria such as *S. aureus*, *Bacillus subtilis*, *E. coli*, and *Pseudomonas aeruginosa*.[76,77]

Table 2.1 Metal and inorganic antiviral materials

Material Form	Virus			Virucidal Activity	Deactivation time	Proposed applications	Ref.
	Name	Envelope	Genetic Material				
Copper							
Solid state	Influenza A	Enveloped	Negative sense ssRNA	2 x 10^6 reduced to 500 infectious virus particles	6 hours	Replacement of steel fittings; Copper surfaces in schools and healthcare facilities	22
Solid (coupons)	Bacteriophage Φ6	Enveloped	dsRNA	2-log decline	1 hour	Noted copper usage in sanitary and medical contexts	24
Solid state (coupons)	Monkeypox	Enveloped	dsDNA	Complete viral inactivation uponcontact	3 minutes	Positioned as useful in hospital trials	21
	Vaccinia virus	Enveloped	dsDNA	Complete viral inactivation upon of contact	3 minutes		
Copper alloys	Murine norovirus	Non-enveloped	Positive sense ssRNA	**Dependent on alloy composition** *Dry touch*: Complete inactivation *Wet fomite:* Range from complete inactivation to a 2-4 log reduction	*Dry touch*: 5 to 120 minutes *Wet fomite:* Within 2 hours	Suggest use of copper alloys as dry surfaces in health care and community environments to prevent spread of pathogens, in combination with regular and efficient cleaning and decontamination regimes	20
Copper/Zinc alloy	Human coronavirus 229E	Enveloped	Positive sense ssRNA	Inactivation for dry fingertip method 10^3 PFU in wet-droplet contamination (20 µl per cm^2) inactivated	*Dry fingertip*: 5 mintues *Wet Droplet*: <60 minutes	Incorporation of copper alloy surfaces along with effective cleaning regimens and good clinical practice.	25
Solid state oxide (Cuprous oxide)	Influenza A	Enveloped	Negative sense RNA	3.7-log reduction after exposure to 2.1 µmol on glass slide	30 minutes	Tackle novel forms of the virus and potential resistance to drugs to reduce transmission. Treatment of both public and living spaces to help limit or prevent future pandemics	23
Solid state oxide (Cuprous oxide)	Bacteriophage Qβ	Non-enveloped	Positive sense ssRNA	6-log reduction	30 minutes	Demonstrated potential for public and private living environments to reduce the risk of infections from pathogens	18

Material Form	Virus			Virucidal Activity	Deactivation time	Proposed applications	Ref.
	Name	Envelope	Genetic Material				
Copper-oxide within filters	Rhinovirus-2	Non-enveloped	Positive sense, ssRNA	2 ± 1.7 log reduction	2 minutes	Represent an inexpensive way to quickly deactivate viruses in contaminated liquids.	27
	Yellow fever virus	Enveloped	Positive sense ssRNA	1.1 ± 0.5 log reduction	2 minutes		
	Influenza A	Enveloped	Negative sense RNA	1.77 ± 0.87 log reduction	2 minutes		
	Measles virus	Enveloped	Negative sense ssRNA	≥3.67 log reduction	2 minutes		
	Respiratory syncytial	Enveloped	Negative sense ssRNA	1.5 ± 0.5 log reduction	2 minutes		
	Parainfluenza virus 3	Enveloped	Negative sense ssRNA	1.11 ± 0.5 log reduction	2 minutes		
	Punta Toro virus	Enveloped	Negative sense ssRNA	1.73 ± 1.55 log reduction	2 minutes		
	Pichinde virus	Enveloped	Negative sense ssRNA	1.7 ± 1.47 log reduction	2 minutes		
	HIV-1	Enveloped	Positive sense ssRNA	4.6 ± 0.6 log reduction	2 minutes		
	Adenovirus	Non-Enveloped	dsDNA	2.2 ± 0.36 log reduction	2 minutes		
	Cytomegalovirus	Enveloped	dsDNA	4.3 ± 0.26 log reduction	2 minutes		
	Vaccinia virus	Enveloped	dsDNA	0.47 ± 0.45 log reduction	2 minutes		
Copper oxide impregnated face masks	Influenza A	Enveloped	Negative sense RNA	No infectious titers recovered from surface	30 minutes	Reduction of contamination risk during use or removal of masks	28
Ionic impregnation of latex and filters	HIV-1	Enveloped	Positive sense ssRNA	*Latex:* Dose dependent withincubation on glove surface *Filter:* 5-log reduction	*Latex:* 20 minutes *Filter:* 5 mL/min	Example of reduction of nosocomial infections in hospitals using copper in fabrics, paper, latex, *etc.*	26
	West Nile Virus	Enveloped	Positive sense ssRNA	5-log reduction	5 mL/min		

Material Form	Virus			Virucidal Activity	Deactivation time	Proposed applications	Ref.
	Name	Envelope	Genetic Material				
Zeolite textiles, Cu^{2+}	H5N1 avian influenza	Enveloped	Negative sense ssRNA	*Ck/Yamaguchi/7/04:* > 5.0 log reduction *Who.s/Hokkaido/1/08:* 2.3-log reduction	*Ck/Yamaguchi/7/04:* 30 seconds *Who.s/Hokkaido/1/08:* 1 minute	CuZeo-textile has wide applications as a microbicidal agent or in environmental healthcare goods. Can be applied as a comprehensive healthcare item such as in protective wear (clothes, masks and gloves), sheets covering beds or pillows in hospitals, and air or water purifiers in facilities such as hospitals or farms, *etc.*	29
	H5N3 avian influenza	Enveloped	Negative sense ssRNA	> 5.0 log reductionfor Whi.s/Shimane/499/83	10 minutes		
Nanoparticles within coating	Influenza H1N1	Enveloped	Negative sense ssRNA	Complete inactivation	1 minute	Authors propose that this anti-pathogen coating can provide an additional measure of protection against the spread of diseases in natural and manmade disasters, and during outbreaks of disease in either human or animal populations.	31
Copper powder within spray	Influenza A	Enveloped	Negative sense RNA	100% inhibition	10 minutes	Demonstration of spray coating that is effective as an antimicrobial, which can be used on surfaces within healthcare facilities.	35
Silver							
Hybrid coating (ionic)	HIV-1	Enveloped	Positive sense ssRNA	99.8% reduction	20 minutes	A broad-spectrum antimicrobial surface coating would have great impact on the battle against hospital-acquired infections. Potential to provide antimicrobial protection on surfaces and materials in hospital settings.	42
	Dengue virus	Enveloped	Positive sense ssRNA	1.1log $TCID_{50}$ reduction	4 hours		
	HSV	Enveloped	dsDNA	Complete inactivation	4 hours		
	Influenza	Enveloped	Negative sense ssRNA	0.7-log $TCID_{50}$ reduction	4 hours		
	Coxsackie	Non-enveloped	Positive sense ssRNA	0.2-log $TCID_{50}$ reduction	4 hours		

Material Form	Virus			Virucidal Activity	Deactivation time	Proposed applications	Ref.
	Name	Envelope	Genetic Material				
Silver Nitrate in solution	Feline calicivirus	Non-enveloped	Positive sense ssRNA	3-log reduction in recovery in 2.1mg/L concentration	75 days	Technology proposed here would allow for custom design of active, adaptive packaging and contact surfaces.	38
	Murine norovirus	Non-enveloped	Positive sense ssRNA	1 log reduction after 75 days with 2.1mg/L concentration	75 days		
Nanoparticle in solution or film	Feline calicivirus	Non-enveloped	Positive sense ssRNA	*In solution*: 4-log reduction in recovery of virus if concentration was higher than 10.5mg/L *As film:* 1.42 log reduction of FCV at 25°C Complete inactivation of FCV at 37°C	*In solution:* Maintained over 150 days *As film:* Overnight incubation		
	Murine norovirus	Non-enveloped	Positive sense ssRNA	*In solution*: Initial 3-log reduction in recovery of virus, increased to complete inactivation over 150 days if concentration was higher than 10.5mg/L *As film:* 0.14 log reduction of MNV at 25°C 0.86 log reduction of MNV at 37°C	*In solution:* 1 day, increased over 150 days *As film:* Overnight incubation		
Nanoparticle impregnation of nanofiber sheets	Influenza A (A/PR/8/34 (H1N1))	Enveloped	Negative-sense RNA	2-log decrease at concentration of AgNPs at 8.5 µl/cm^2	1 hour	Chitin-nanofiber sheets with potential to act as wound dressings	43
Nanoparticle within Graphene Oxide	Infectious bursa virus	Non-enveloped	dsRNA	0.125mg/mL led to complete inhibition of 9 x 10^2 $TCID_{50}$/mL; 1 mg/mL against the infection of 9 x 10^3 $TCID_{50}$/mL	1 hour	Further application of GO and GO-Ag can be considered for personal protection equipment to decrease the transmission of viruses	44
	Feline coronavirus (FCoV)	Enveloped	Positive sense, ssRNA	0.1mg/mL caused 24.8% inhibition for 4.7 x 10^4 $TCID_{50}$/mL	1 hour		
Nanoparticle within membrane	Bacteriophage MS2	Non-enveloped	Positive sense ssRNA	5 ± 0.2 x 10^5 PFU/mL completely removed	Flow rate not reported	Membranes used for water treatment	45
Nanoparticle within membrane	Bacteriophage UZ1	-	-	3.4-log decrease in virus load	Flux of 3.1 L m^{-2} h^{-1}	Development of an innovative strategy for preventing outbreaks of waterborne diseases	46

Material Form	Virus			Virucidal Activity	Deactivation time	Proposed applications	Ref.
	Name	Envelope	Genetic Material				
Nanoparticle within film	Feline Calicivirus (FCV)	Non-enveloped	Positive sense ssRNA	> 4.4 log $TCID_{50}$/mL reduction after contact with films	24 hours	Excellent potential for PLA-silver films for food contact applications as well as in active packaging technologies for food safety and quality.	47
Nanoparticle within filter	Bacteriophage MS2 virus	Non-enveloped	Positive sense ssRNA	Density of 1.5 x 10^9 particles/cm^2 demonstrates roughly 70% antiviral efficiency without the presence of dust	15 minutes	Use as air filters within all types of public facilities.	48
Zinc							
Solid state	Murine norovirus	Non-enveloped	ssRNA	1-log reduction for pure zinc	2 hours	Suggests the incorporation of copper alloy surfaces to help prevent infection spread, such as within hospitals	19
Zinc Oxide filopodia-like structures	Herpes simplex virus type 1	Enveloped	dsDNA	Dose dependent reduction of viral entry; incubation with 100ug/mL ZnO-MNSs led to below 20% entry	90 minutes	Suggests development of these micro-nanostructures as a topical agent for prevention of HSV-1 infection.	58
Ionic solution	Human rhinovirus	Non-enveloped	Positive sense, ssRNA	99% reduction in number plaques using zinc chloride after virus exposure	1 hour	Investigation focused on the mechanism of action.	53
TiO_2							
Colloidal nanoparticles	Newcastle disease virus	Enveloped	Negative sense ssRNA	Qualitative; chick allantoises did not hemagglutinate after incubation with nano-colloids	96 hours	Starting point for the development of antiviral drugs	64
Solid state coating	Influenza virus	Enveloped	Negative sense ssRNA	3.6-log reduction (UVA intensity 0.1 mW/cm^2)	4 hours	Integration into surfaces in high-risk environments to reduce the spread of infection, such as at hospitals and daycare centers	65
	Feline calicivirus	Non-enveloped	Positive sense ssRNA	1.7-log reduction (UVA intensity 0.1 mW/cm^2)	8 hours		
Solid-state anatase coating	Bacteriophage Qβ	Non-enveloped	Positive sense ssRNA	4.5-log reduction (UVA intensity 0.1 mW/cm^2)	4 hours	Prevention of viral transmission in indoor and outdoor living spaces	52
	Bacteriophage T4	Non-enveloped	dsDNA	2-log reduction (UVA intensity 0.1 mW/cm^2)	4 hours		

Material Form	Virus			Virucidal Activity	Deactivation time	Proposed applications	Ref.
	Name	Envelope	Genetic Material				
Fluorinated nanoparticles	Bacteriophage MS2	Non-enveloped	Positive sense ssRNA	2.6-log reduction (UVA intensity 0.01 mW/cm^2)	60 minutes	Prevention of viral transmission in indoor commercial spaces with fluorescent lighting	60
	Feline calicivirus	Non-enveloped	Positive sense ssRNA	2.0-log reduction (UVA intensity 0.01 mW/cm^2)	60 minutes		
	Murine norovirus	Non-enveloped	Positive sense ssRNA	2.6-log reduction (UVA intensity 0.01 mW/cm^2)	6 minutes		
Ag- and Cu-doped nanowire membranes	Bacteriophage MS2	Non-enveloped	Positive sense ssRNA	4.02-log reduction after filtration	30 minutes	Filtration and disinfection of drinking water	67
Ag-doped solid-state coating	Influenza A	Enveloped	Negative sense ssRNA	≥4.17-log reduction 15 W UVA light from 35 cm)	20 minutes	Disinfection of publicly-used surfaces and breakdown of organic pollutants	62
	Enterovirus	Non-enveloped	Positive sense ssRNA	≥4.17-log reduction (15 W UVA light from 35 cm)	20 minutes		
Other inorganic antiviral materials							
Modified Gold Nanoparticle in solution	Virus-like particles (VLPs), replicating human norovirus, GI.1 VLPs	Replicates Non-enveloped	Replicates RNA	Complete inactivation of VLPs at a concentration of 0.37 µg/mL using 0.083 µM Au/CuS NPs	1 hour	Proposed as an antiviral	68
Multivalent gold nanoparticles with sulfate ligands	HIV	Enveloped	Positive sense ssRNA	<20% infection rate of T-cells after incubation with sulfonated gold nanoparticles	30 minutes	Development of a multifunctional therapeutic anti-HIV system	70

Material Form	Virus			Virucidal Activity	Deactivation time	Proposed applications	Ref.
	Name	Envelope	Genetic Material				
Gold nanoparticles with undecanesulfonic acid(MUS)-containing ligands	HSV-1	Enveloped	dsDNA	Irreversible loss of infectivity (0 PFU) after pre-incubation of virus with gold NPs	1 hour	Production of virucidal drugs to fight viral infections	[71]
	HSV-2	Enveloped	dsDNA	Irreversible loss of infectivity (0 PFU) after pre-incubation of virus with gold NPs	1 hour		
	Human papillomavirus type 16 (HPV-16)	Non-Enveloped	dsDNA	Irreversible loss of infectivity (0 FFU) after pre-incubation of virus with gold NPs	1 hour		
	RSV	Enveloped	Negative sense ssRNA	Irreversible loss of infectivity (0 PFU) after pre-incubation of virus with gold NPs	1 hour		
	Vesicular stomatitis virus pseudo-typed lentivirus (LV-VSV-G)	Enveloped	Negative sense ssRNA	Irreversible loss of infectivity (0 transduction units) after pre-incubation of virus with gold NPs	1 hour		
	Adenovirus-5(AD5)	Non-Enveloped	dsDNA	No inhibition (virus is not HSPG-dependent)	1 hour		
Ion doping of coating with Transition Metals (*i.e.* iron, magnesium, manganese)	Influenza H1N1	Enveloped	Negative-sense RNA	99% eradication with a fluorescent lamp	30 minutes	Suggest use for inactivation of virus inside buildings with fluorescent light.	[72]
Silica Nanoparticle in coating	Influenza A/PR/8/34 (H1N1)	Enveloped	Negative-sense RNA	Complete inactivation after incubation of virus suspension on surface	30 minutes	Use as a microbicidal coating	[73]
Nonstoichiometric perovskite-type LaxMnO3	Influenza A	Enveloped	Negative-sense RNA	Neutralized 76% of influenza A	15 minutes	Proposed as a sterilizing method to minimize transmission of virus *via* multiple routes, including aerosol and contaminated fluids	[75]

2.4 Polymeric and Organic Antiviral Coatings

2.4.1 Polyelectrolyte-coated Surfaces

It has been shown that the positive charge of polycations in polymers such as polyethylenimine attracts viruses having an inherent negative charge, interferes with their genomic content or structural units, and causes complete viral disintegration (**Figure 2.4a**).[78,79] It has been claimed that this class of coating, typically applied through "painting", can permanently convey antiviral and antibacterial properties even after being subjected to multiple washes.[80] Herein, the literature involving polycations, mainly polyethylenimines, is discussed and is summarized in Table 2.2.

Immobilizing polycations on various surfaces has been shown to convey antiviral properties for both enveloped and non-enveloped viruses.[81,82] Immobilized hydrophobic polyethylenimine-based and dendrimer-based polycations have reduced the titer of viruses. A study on bacteriophage PRD1 interaction with polyethylenimine coated glass slides demonstrated that positive charges and hydrophobicity (conferred by 4-bromobutyrylated polyethylenimine treated glass with N,Ndimethylhexadecylamine) result in a significant decrease in the virus titer compared to uncoated glass.[82] Overall, having only polycations (minimal hydrophobicity) also showed a reduction in the virus titer, however, the combination of hydrophobicity with acetylated surfaces and positive charges of polyethylenimine was more effective.[82] The antiviral activity was also proportional to the surface area of the treated glass. This was also confirmed by exposing treated glass powders to the virus solution, demonstrating higher titer reduction compared to treated surfaces.[82] Moreover, N-alkylated polyethylenimines, namely linear N,N-dodecyl,methyl polyethylenimines, have also demonstrated antiviral properties for non-enveloped viruses when "painted" on polyethylene.[81] Using this method, Larson *et al.* showed slightly elevated antiviral

activity as incubation time was increased and nearly 100% virucidal activity after 15 minutes of incubation.[81] Furthermore, they tested another N-alkylated polyethylenimine, branched N,N-hexyl,methyl *via* covalent attachment to glass slides, and similarly demonstrated complete elimination of the rotavirus after 30 minutes of incubation.[81] Their studies showed effective antiviral behaviour of the polycation coating not only on enveloped viruses such as influenza but also on non-enveloped viruses such as poliovirus and rotavirus.[81] To elucidate the role of the polyethylenimines, Haldar *et al.* demonstrated that their molecular weight is important for the virucidal characteristics, as they must be large enough to penetrate the viruses.[83] They tested 750 kDa, 25 kDa, and 2 kDa sizes of polyethylenimines, with only the 750 kDa polyethylenimine showing complete inactivation of the influenza virus. Moreover, the polycation (polyethylenimines) was compared to a polyanion and a neutral coating.[83] It was shown that the polyanion has partial virucidal activity, while the neutral coating was not virucidal. The fact that both polycations and polyanions showed antiviral characteristics was hypothesized to be due to availability of both positively and negatively charged domains on the virus (*i.e.* influenza virus), with the negatively charged domains being dominant, which explains the superiority of polycations in antiviral activity (polycation and polyanion having 100% and 66% viricidal activity respectively).[83] Similarly, a study by Dang *et al.* showed positively- and negatively-charged polyelectrolyte multilayers (PEMs) deposited on a quartz crystal microbalance (QCM).[84] They claimed that with various designs for the PEMs it is possible to manipulate the adhesive properties of the surfaces towards viruses. Negatively charged surfaces (*e.g.* poly(styrene-4-sulfonate) terminated) showed relatively lower amounts of bacteriophage MS2 due to the unfavorable electrostatic interaction between the bacteriophage and the anionic surface.[84] On the other hand, positively charged PEMs showed higher amounts of MS2 deposition, which is in line with the

findings by Haldar *et al.* From the molecular perspective, polycations with both branched and linear polyethylenimines (*e.g.* N,N-dodecyl,methyl-polyethylenimine) were lethal towards influenza virus A,[85–87] even to strains which were resistant towards commercial drugs.[87] PEMs can be easily applied to surfaces using methods such as spray coating, dip coating, and painting, for the development of scalable antiviral coatings.

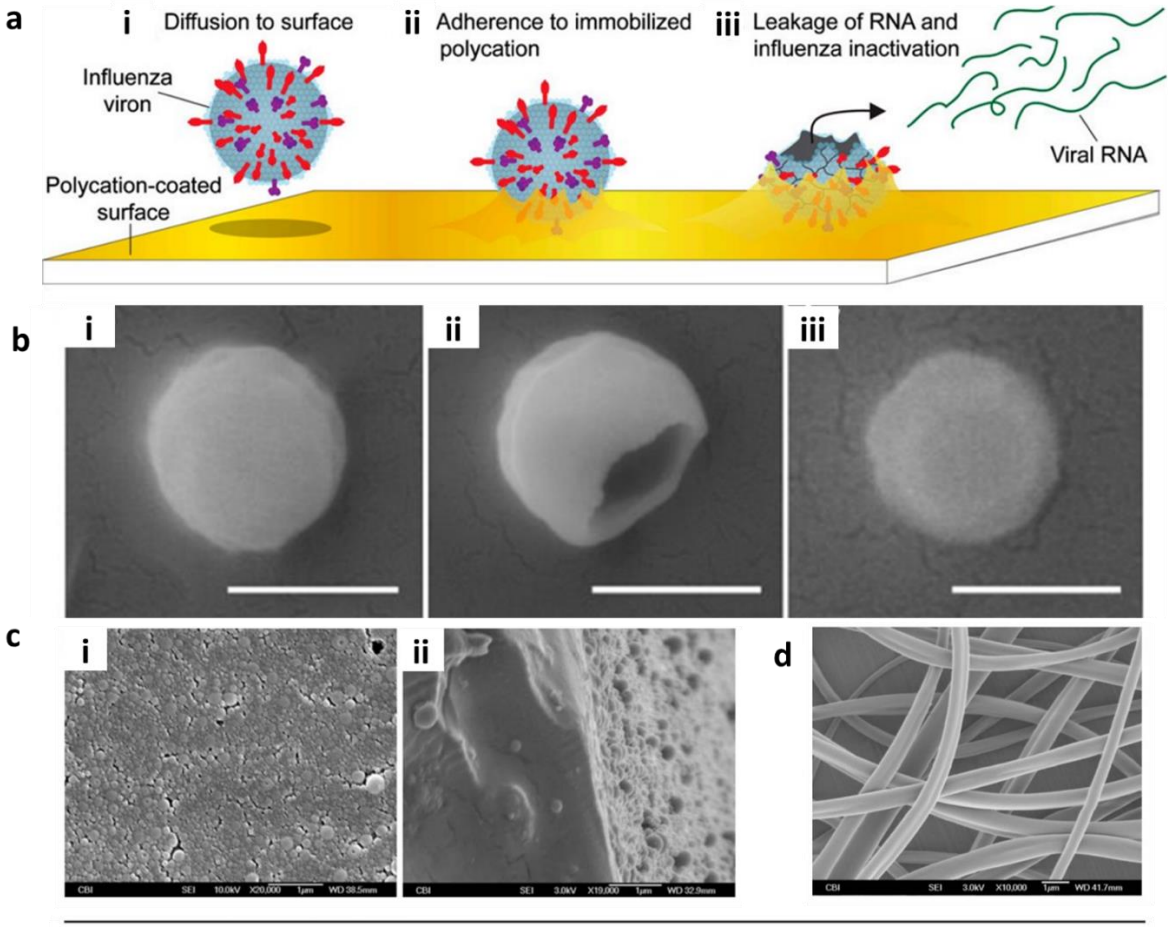

e

Virus	No slide	Uncoated slide	Slide coated with a solution	Slide coated with a nanosuspension
Influenza (pfu/ml)	$(5.9\pm1.7)\times10^4$	$(2.2\pm0.3)\times10^4$	0	0
Poliovirus (pfu/ml)	$(3.8\pm1.0)\times10^5$	$(1.7\pm0.4)\times10^5$	$(1.6\pm0.4)\times10^5$	$(1.4\pm0.5)\times10^5$

Figure 2.4 - Polycation coatings. **(a)** Mechanism of enveloped virus inactivation by polycation coating. (i) diffusion of the virus particle to the surface from solution (ii) adhesion on polycation surface (iii) the genomic material leaks out and the virus gets inactivated. Reprinted from ref [79].

Copyright 2011 National Academy of Sciences. **(b)** SEM images of influenza virus after exposure to uncoated (i) and N;N-dodecyl,methyl-PEI-coated (ii and iii) silicon wafers. Reprinted from ref [79]. Copyright 2011 National Academy of Sciences. **(c)** SEM images of a polyethylene surface coated with Quat-12-PU nanoparticles. (i) Top view (ii) cross-section. Reprinted with permission from [88]. Copyright 2013 Springer Nature. **(d)** The SEM of Quat-12-PU electrospun nanofibers. Reprinted with permission from ref [88]. Copyright 2013 Springer Nature. **(e)** Antiviral activities of uncoated and Quat-12-PU coated polyethylene slides solution-based or nanosuspension deposition. Reprinted with permission from ref [88]. Copyright 2013 Springer Nature.

Further studies by Hsu *et al.* investigated the role of the underlying substrate on the antiviral properties.[79] Polyethylene and polypropylene were used as alternatives to glass. It was discovered that all three types of substrates used for coating demonstrated complete disinfection of the virus, proving that the polycation painting is the key to the antiviral activity of the materials.[79] In order to better understand the mechanism and fate of viruses when coming in contact with the polycation coating, the viral nucleoprotein was assayed using colorimetric ELISA as a marker indicating viral rupture.[79] The assay demonstrated the disappearance of the viral particles from the solution exposed to the polycation, indicating that the viruses attach to the hydrophobic polycationic coatings (**Figure 2.4a**). Furthermore, real-time reverse-transcriptase PCR (qRT–PCR) was used to evaluate the detectable viral RNA in solution where its presence would indicate loss of infectivity of the virus due to the viral genomic material being exposed.[79] It was shown that a significant amount of viral RNA was detectable, therefore the polycation layer is not only attracting the virus but also inactivating the virus.[79] This was also validated with scanning electron microscopy (SEM) (**Figure 2.4b**) of the influenza virus, showing that the integrity of the influenza virus was compromised for 54% of the 132 surveyed viruses.[79] The monomer of the polycation N;N-dodecyl,methyl-polyethylenimine, dodecyltrimethylammonium bromide (DTAB), was also capable of inactivating the influenza virus in test solutions. This hinted towards the antiviral

activity being related to the hydrophobic quaternary ammonium salt moiety, that is maintained within the polymeric and surface-immobilized form of the polycation.

In another approach for coating the polycations, a study by Liu *et al.* demonstrated use of N,N-hexyl,methyl-polyethylenimine with an aerosol-assisted plasma deposition technique on glass surfaces.[89] This allows for the covalent immobilization of N,N-hexyl,methyl-polyethylenimine through a one-step method and has been shown to be thermally stable (up to 150 ºC) and durable upon exposure to vigorous washes and exposure to detergents. This study demonstrated a greater than 4-log reduction in the influenza H1N1 virus for N,N-hexyl,methyl-polyethylenimine treated surfaces.[89]

Another class of polyelectrolytes used as antiviral coatings is polyurethane-based materials, such as N,N-dodecyl,methyl-polyurethane (Quat-12-PU), which are versatile, abrasion-resistant, and robust for long periods of time.[88] Quat-12-PU can be coated onto surfaces through three different methods: (1) spray coating on polyethylene or glass slides, (2) synthesizing Quat-12-PU nanoparticles by dissolving Quat-12-PU in Tetrahydrofuran (THF) and subsequently spraying the nanoparticle solution on glass slides (SEM image shown in **Figure 2.4 c(i),(ii)**) or, (3) by electrospinning Quat-12-PU nanofibers onto glass slides (scanning electron microscopy image shown in **Figure 2.4d**).[88] The study by Park *et al.* demonstrated antiviral properties with complete inactivation of influenza virus (enveloped, with 0 PFU/ml of virus detected) but not poliovirus (non-enveloped) by subjecting the solution-treated or nanoparticle-treated surfaces to the respective virus solutions and comparing each to uncoated substrates (**Figure 2.4e**).[88] The antiviral properties were attributed to the Quat-12-PU interfering with the lipid envelope of the virus protecting its RNA. Comparing the Quat-12-PU to the N,N-dodecyl,methyl-polyethylenimine coated surfaces, it was previously shown that the latter disinfects poliovirus.[81]

Park *et al* showed that the polioviruses adhere to N,N-dodecyl,methyl-polyethylenimine surfaces but not to Quat-12-PU coated ones by subjecting N,N-dodecyl,methyl-polyethylenimine surfaces to detergent washes and assessing the extent of the recovered viruses. This can be attributed to the different chemistries on these surfaces.[88]

A polyelectrolyte-based method was used to develop filtration membranes for reducing the amount of virus in drinking water.[78] Through a covalent layer-by-layer deposition method, multiple layers of polyethyleneimine were created with use of terephthalaldehyde as the cross-linking agent. It was found that there was a 4-log reduction in the virus titer from the solution.[78] Furthermore, silver and copper nanoparticles were incorporated within the polyethyleneimine layer and tested for antiviral properties, indicating 4.5- to 5-log reduction in PFU.[78] They also ran qRT-PCR on the permeates of the membrane, which confirmed the hypothesis that the polycationic coating actually inactivates the virus and exposes the genomic content.[78] Their overall findings suggested that this polyelectrolyte coating can be integrated on a planar surface (*e.g.* glass), as well as on irregular surfaces (*e.g.* porous membranes).[78]

In another study, quaternary ammonium compounds (QACs) were coated onto glass and plastic surfaces in order to add antiviral properties. The QAC polymer was dissolved in acetone and a thin layer was added to either glass or well plates and subsequently dried, making a positively charged layer.[90] Enveloped influenza A (H1N1) virus and non-enveloped poliovirus Sabin 1 were tested for virucidal activity on the surfaces. Influenza A showed reduction in the virus infectivity after 2 minutes; on the other hand, poliovirus did not show reduction even after longer incubation times.[90]

2.4.2 Photosensitizer materials

A number of recent studies have integrated photosensitive compounds other than TiO_2, such as rose bengal and C_{60}, onto surfaces to exploit the ROS-dependent antimicrobial and antiviral pathways.[91] Photosensitizers, light-activated molecules, are also used for antimicrobial photodynamic therapy as an alternative for antibiotic chemotherapies.[92] Antimicrobial photodynamic inactivation operates on the principle that a photosensitizer gets excited *via* visible light absorption and subsequently reacts with oxygen.[92] There are two pathways (type I and type II), shown in **Figure 2.5a**, through which active products are generated that induce damage to viruses, bacteria, or other organic species. In the type I pathway, the photosensitizer reacts with bio-organic molecules and produces ROS (*e.g.* superoxide, hydroxyl radicals, and hydrogen peroxide). The type II pathway occurs as the excited photosensitizer transfers energy to molecular oxygen and generates singlet oxygen ($^1O_2$), which induces oxidative damages to biological species.[92,93] More specifically, saturated lipids are the target for free radicals and singlet oxygen attacks. This leads to lipid peroxidation and the alteration of surrounding proteins, nucleic acids (mainly guanine) and other molecules. Therefore, it is hypothesized that the generation of ROS damages the viral envelope and causes viral inactivation.[93] This makes enveloped viruses more susceptible to photodynamic inactivation than non-enveloped ones. However, non-enveloped viruses have also shown photodynamic inactivation of their viral proteins.[93] The advantages of such antimicrobial pathways over antiviral and antimicrobial drugs include non-specific damage leading to an inability to develop resistance, $^1O_2$ being environmentally benign, and the non-toxicity of photosensitizers.[92,93]

Si *et al*. reported on developing a fine membrane of electrospun poly(vinyl alcohol-co-ethylene) nanofibers functionalized with benzophenone tetracarboxylic dianhydride and

chlorogenic acid.[94] They recognized the limitations of UV-dependent photoactivity exhibited by most photoactive materials and sought to develop an antibacterial and antiviral surface excitable in daylight conditions by ambient visible and UVA light. They achieved a 5-log reduction in viral activity of bacteriophage T7 in daylight conditions, with similar results for antibacterial action against *E. coli* and *L. innocua*.[94] As mentioned previously, non-enveloped bacteriophages such as T7 generally show increased resistance to most ROS- or contact-killing-based antiviral mechanisms, and the authors predicted that enveloped viruses would be targeted even more effectively due to the presence of a lipid membrane.[94] The nanofiber membrane is also notable for its filtration capabilities, which effectively impedes the penetration of small particles and microorganisms. It also possesses the ability to "store" photoactivity by achieving a metastable electronic structure in the event that hydrogen abstraction is not completely reversed by ROS production.[94] This allows it to maintain its antimicrobial characteristics in the dark. Si *et al.* tested their nanofiber membrane on personal protective equipment such as lab coats and N100 masks and demonstrated that it provided a nearly 6-log reduction in T7 phage plaque-forming units compared to the unmodified materials.[94]

Cellulose has been researched with the aim to reduce nosocomial infections in hospital textiles.[95] In order to introduce antimicrobial and antiviral characteristics to cellulose, Alvarado *et al.* developed photosensitizer-linked nanofibrillated cellulose (PS-NFC) through utilizing triazine linking and covalently bonding a porphyrin-based photosensitizer to nanofibrillated cellulose (NFC).[95] The antiviral behaviour of this technology relies on the production of reactive singlet oxygen ($^1O_2$) and other ROS upon illumination of the photosensitizer and the extremely high surface area of NFC is a contributing factor. Free-base, [5-(4-aminophenyl)-10,15,20-tris-(4-N-methylpyridinium)porphyrin (A^3B^{3+})], and metallated, [5-(4-aminophenyl)-10,15,20-tris-(4-N-

methylpyridinium)porphyrinato]zinc(II) (Zn-A_3B^{3+}), photosensitizers were applied to NFC (A^3B^{3+}-NFC and Zn-A_3B^{3+}-NFC) (**Figure 2.5b,c**) in order to integrate photoactive behaviour to NFC.[95] Vesicular stomatitis virus (VSV) and dengue-1, both enveloped viruses, were used to assess the antiviral behaviour of the modified NFC. After illumination, both treated NFC materials showed complete inactivation of the viruses (**Figure 2.5d,e**).[95] A study by Carpenter *et al.* conjugated cationic, anionic, and neutral porphyrins to cellulose fibers to add antimicrobial properties to the surface against enveloped (dengue-1 and influenza A) and non-enveloped viruses (human adenovirus-5 (Had-5)).[96] The anionic and neutral porphyrins did not show promising results in a reduction in CFU/mL in their bacteria studies, which they attributed to electrostatic repulsion and/or hydrophobicity of those surfaces not allowing interaction of the porphyrins with the bacteria.[96] For the virus studies, they implemented porphyrin-positive treated cellulose, due to its better performance with bacteria. Dengue-1 and influenza A showed >99.995% and ~99.5% reduction in FFU/mL, however, the non-enveloped viruses (HAd-5) were harder to inactivate and showed ~99% reduction in FFU/mL using immunofoci staining. The reductions in FFU were attributed to the protein-based capsid and the lipid-bilayers, which in the case of enveloped viruses, were found less resistant towards photosensitization.[96] In another study, wipes with polypropylene fibers were coated with the photosensitizer rose bengal, which is immobilized on the fibers through multiple amide bonds and produces singlet oxygen during exposure to visible light.[97] Wipes were spiked with various viruses including the human norovirus GI.4 and GII.4, murine norovirus 1 (MNV-1), human adenovirus type 5 (hAdV-5), and influenza virus H1N1. The non-enveloped viruses did not exhibit prompt inactivation, with the time needed for the first 1-log reduction being more than 7 hours, while enveloped viruses showed immediate and complete inactivation (more than 4-log).[97] Furthermore, the transfer and persistence of viruses from a steel surface were tested

after being wiped with the treated and untreated wipes, and the proportion of viruses recovered from the wiped surface to the unwiped one through viral genome quantification was reported. For MNV-1 and influenza virus, no viruses were discovered after wiping the contaminated steel surfaces. However, residual amounts (0.2%-0.6% residual virus proportions) of norovirus were found on the steel surfaces.[97] Notably, in this case, no difference was found between the treated and untreated wipes. They further tested the already used wipes (used on steel surfaces) on a secondary steel surface to investigate cross contamination and revealed that non-enveloped viruses demonstrated cross-contamination.[97] The development of wipes that remain clean is an avenue for reducing cross-contamination and halting the spread of infection *via* surfaces.

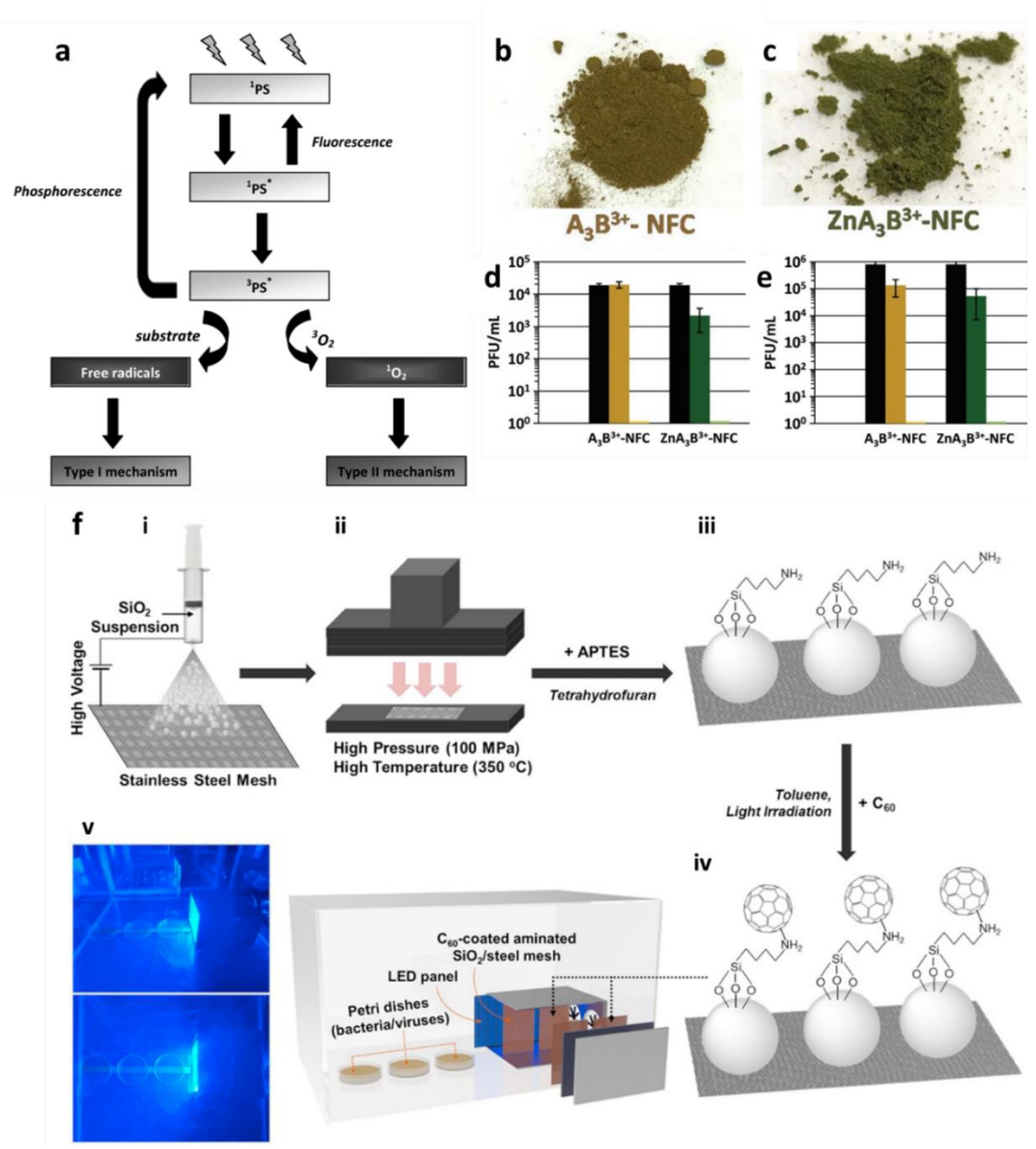

Figure 2.5 - Photosensitizer–cellulose conjugate materials. **(a)** Schematic representation of the photosensitization process. Reprinted from ref [93]. Copyright 2012 Costa *et al*. **(b)** A3B3+-NFC and **(c)** Zn-A3B3+-NFC. Photodynamic inactivation studies of the **(d)** dengue-1 and **(e)** vesicular stomatitis virus (VSV). Dark yellow and dark green bars are dark controls. Light yellow and light green bars are illuminated. Black bar is the initial virus concentration. Slight decrease in the virus infectivity was observed in dark environments, which, due to observed strong virucidal behaviour in illumination conditions, was attributed to the accidental light exposure while running the assays. Reprinted with permission from ref [95]. Copyright 2019 Royal Society of Chemistry. **(f)** Fabrication process of C_{60} coated stainless-steel mesh and virus assay setup. (i) Electrospraying silica particles on stainless-steel mesh; (ii) hot pressing (iii) APTES treating silica (iv) covalent C_{60} attachment (v) visible-light-sensitized remote singlet oxygenation and virus inactivation setup. Reprinted with permission from ref [98]. Copyright 2020 Elsevier.

A C_{60}-based sensitizer was developed to evaluate virus inactivation in air due to its high yield of singlet oxygen production. Briefly, SiO_2 was electrosprayed on a stainless-steel mesh to serve as a support for a layer of (3-aminopropyl)triethoxysilane (APTES).[98] This allowed for the SiO_2 to attach to the double bonds of C_{60}. To assess antiviral activity in air, inactivation rates of bacteriophage MS2 were evaluated at various distances from the singlet oxygen source (C_{60} coated mesh).[98] The schematic of the production process and virus assay setup are shown in **Figure 2.5f**. It was found that bacteriophage MS2 was deactivated ((N0-N)/N0, the quantity of the residual bacteriophage MS2 remaining relative to the initial quantity in PFU/mL) by 55.8%, 37.7%, and 24.3% respectively when the C_{60} coated mesh was used at 5, 15, 30 cm distances after 3 hours.[98]

Within the field of photosensitized material and their virucidal activity, there are some studies that produce polycaprolactone, polyurethane, and polyacrylonitrile nanofibers, and dope them with photosensitizers such as 5,10,5,20-tetraphenylporphyrin, polyacrylonitrile, and porphyrin positive mixtures while electrospinning the fibers.[99,100] These have been shown to inactivate non-enveloped viruses such as polyomaviruses (30 minutes, quantification was not elaborated) and adenovirus 5 (30 minutes, ~99.8% reduction in PFU/mL), as well as enveloped viruses such as baculoviruses and VSV.[99,100]

2.4.3 Other coatings

To introduce antiviral properties to textiles, Iyigundogdu *et al.* immersed cotton fabrics into a solution containing sodium pentaborate pentahydrate and triclosan.[101] They tested adenovirus type 5 and poliovirus type 1, demonstrating that the amount of decline for the virus titer is 3-log on the sodium pentaborate pentahydrate and triclosan solution-treated textiles, whereas the non-treated textiles do not show any decrease.[101] This was confirmed by observing the cell deaths as a result of contact with the virus solution passed through the fabrics.

Table 2.2 Polymeric and organic antiviral coatings

Material			Virus			Virucidal Activity	Deactivation time	Proposed applications	Ref.
Coating	Method	Backbone Material	Name	Envelope	Genetic Material				
Polycations									
4-bromobutyrylated N,Ndimethylhexadecylamine	Covalent bonding	Glass, glass powder	Bacteriophages PRD1	Non-enveloped	dsDNA	77± 3% titer reduction	24 hours	Removing viruses from water by adsorption	[82]
N,N-hexyl,methyl polyethylenimines (750 kDa)	Covalent bonding	Glass	poliovirus	Non-enveloped	Positive sense ssRNA	100% virucidal activity (PFU/mL)	30 minutes	disinfect aqueous solutions	[81]
N,N-dodecyl,methyl-polyethylenimines (217 kDa)	Physical absorption (painting)	Polyethylene	poliovirus	Non-enveloped	Positive sense ssRNA	~100% virucidal activity (PFU/mL)	30 minutes	disinfect aqueous solutions	[81]
	Physical absorption (painting)	Polyethylene	rotavirus	Non-enveloped	dsRNA	100% virucidal activity (PFU/mL)	15 and 30 minutes	disinfect aqueous solutions	[81]
	Physical absorption (painting)	Glass, Polypropylene, Polyethylene	WSN influenza strain WSN/33 (H1N1), PR/8/34 (H1N1), turkey/MN/833/80 (H4N2	Non-enveloped	Negative sense dsRNA	Final viral titer (PFU/ml) = 0 100% virucidal activity (PFU/mL) viral nucleoprotein by ELISA =< 0.1 (pfu/ml) qRT–PCR RNA leakage detection <50% viral RNA in solution Scanning electron microscopy survey for damaged viruses, 54% showed structural damage	5 minuutes	Not specified Antimicrobial surfaces	[79]
N,N-hexyl,methyl-polyethylenimine	Covalent aerosol-assisted	Glass	Influenza A/PR/8/34 (H1N1)	Non-enveloped	Negative sense dsRNA	>4 log reduction in viral titer	10 minutes	Not specified Antimicrobial surfaces	[89]

Material			Virus			Virucidal Activity	Deactivation time	Proposed applications	Ref.
Coating	Method	Backbone Material	Name	Envelope	Genetic Material				
(Mw non specified)	plasma deposition								
N,N-dodecyl,methyl-polyethylenimines (750 kDa)	Physical absorption (painting)	Glass	influenza virus A/WSN/33 (H1N1)	enveloped	Negative sense ssRNA	100% virucidal activity (PFU/mL)	30 minutes	Preventing the spread of infection	83
	Physical absorption (painting)		influenza A Wuhan (H3N2), avian influenza A turkey (H4N2) virus, drug-resistant strains of a human influenza A Wuhan (H3N2) and an avian influenza A turkey (H4N2)	enveloped	Negative sense ssRNA	Final viral titer (PFU/ml) = 0	30 minutes	preventing the spread of influenza	87
N,N-dodecyl,methyl-polyurethane (Quat-12-PU)	solution treated or nanoparticle treated by spray coating (physical absorption)	Glass	Influenza virus	enveloped	Negative sense ssRNA	Final viral titer (PFU/ml) = 0	15 minutes	Not specified Antimicrobial surfaces	88
Polyethyleneimine (25 kDa)	chemical-crosslinking (covalent)	Glass, micro-filtration membranes	Bacteriophage MS2	Non-enveloped	Positive sense ssRNA	4-log of reduction in the virus titer 3–3.5-log of reduction in the virus titer qRT- PCR for quantification of genome copies ~2-log reduction	30 minutes	filtration membranes for drinking water	78

Material			Virus			Virucidal Activity	Deactivation time	Proposed applications	Ref.
Coating	Method	Backbone Material	Name	Envelope	Genetic Material				
Polyethyleneimine (25 kDa)+ AgNP and/or CuNP	chemical-crosslinking (covalent)	Glass, micro-filtration membranes	Bacteriophage MS2	Non-enveloped	Positive sense ssRNA	4.5- to 5-log reduction in the virus titer qRT- PCR for quantification of genome copies >2-log reduction	30 minutes	filtration membranes for drinking water	78
Quaternary ammonium compounds (QACs)	Physical absorption by thin layer deposition	Glass, Plastic	influenza A (H1N1)	enveloped	Negative sense ssRNA	Complete inactivation,	1 hour	Not specified Antimicrobial surfaces	90
			poliovirus Sabin 1	non-enveloped	Positive sense ssRNA	No inactivation observed	1 hour		
Photosensitizer materials									
poly(vinyl alcohol-co-ethylene) nanofibers functionalized with benzophenone tetracarboxylic dianhydride and chloro- genic acid	Electrospinning followed by grafting	N/A (standalone membrane)	Bacteriophage T7	Non-enveloped	dsDNA	5-log PFU/mL reduction	5 mins daylight exposure	Protection of high-risk surfaces and personal protective equipment (*e.g.* protective suit)	94
free-base 5-(4-aminophenyl)-10,15,20-tris-(4-N-methylpyridinium)porphyrin (A^3B^{3+})	Covalent bonding	nanofibrillated cellulose	Vesicular stomatitis virus (VSV)	enveloped	Negative sense ssRNA	Final viral titer (PFU/ml) = 0	30-minute illumination	Integration in textiles for the prevention of nosocomial infections	95
			Dengue-1	enveloped	Positive sense ssRNA	Final viral titer (PFU/ml) = 0	30-minute illumination		

Material			Virus			Virucidal Activity	Deactivation time	Proposed applications	Ref.
Coating	Method	Backbone Material	Name	Envelope	Genetic Material				
metallated [5-(4-aminophenyl)-10,15,20-tris-(4-N-methylpyridinium)porphyrinato]zinc(II) (Zn-A^3B^{3+})	Covalent bonding	nanofibrillated cellulose	Vesicular stomatitis virus (VSV)	enveloped	Negative sense ssRNA	Final viral titer (PFU/ml) = 0	30-minute illumination	Integration in textiles for the prevention of nosocomial infections	95
			Dengue-1	enveloped	Positive sense ssRNA	Final viral titer (PFU/ml) = 0	30-minute illumination		
cationic porphyrin	Covalent bonding	cellulose fiber (paper)	dengue-1	Enveloped	Positive sense ssRNA	>99.995% reduction in FFU/mL	30-minute illumination	autonomously sterilize materials for hospitals and healthcare-related industries, preventing the spread of infection	96
			Influenza A	Enveloped	Negative sense ssRNA	~99.5% reduction in FFU/mL	30-minute illumination		
			human adenovirus-5 (HAd-5)	non-enveloped	dsDNA	~99% reduction in FFU/mL	30-minute illumination		
rose bengal	Covalent bonding	wipes with polypropylene fibers	murine norovirus 1 (MNV-1),	non-enveloped	Positive sense ssRNA	8.7 hours first 1-log reduction	8.7 hours	one-step procedure for cleaning and disinfecting influenza virus-contaminated surfaces	97
			human adenovirus type 5 (hAdV-5),	non-enveloped	dsDNA	7 hours first 1-log reduction	7 hours		
			influenza virus H1N1	enveloped	Negative sense ssRNA	Immediate and complete inactivation (more than 4-log)	0 minutes		

Material			Virus			Virucidal Activity	Deactivation time	Proposed applications	Ref.
Coating	Method	Backbone Material	Name	Envelope	Genetic Material				
C_{60}	Covalent bonding	SiO_2 electrosprayed on a stainless-steel mesh	Bacteriophage MS2	Non-enveloped	Positive sense ssRNA	inactivation levels at 5 cm distance = 55.8%	3-hour illumination	remote disinfection	98
Other									
Sodium pentaborate pentahydrate and triclosan	Physical absorption by immersion	Fabric	adenovirus type 5	non-enveloped	dsDNA	3-log decline in virus titer based on microscopic observation of the infected cells	Not Given	antiviral textile finishes for medical applications, daily use, and technical textiles	101
			poliovirus type 1	non-enveloped	Positive sense ssRNA	3-log decline in virus titer based on microscopic observation of the infected cells	Not Given		
			poliovirus Sabin 1	non-enveloped	Positive sense ssRNA	No inactivation observed	Not applicable		

2.5 Toxicity and environmental considerations

The use of metals and inorganic materials can present health and environmental risks. Bowkow and Gabbay conducted animal studies with antimicrobial and antiviral fabrics impregnated with copper to determine the fabric's skin-sensitizing potential in both guinea pigs and rabbits.[26] In studies that looked at exposure to these fabrics, no skin irritation was demonstrated over a 14 day period.[26] Furthermore, Gerhard *et al.* reviewed the effects of TiO_2 on the skin and found that there was little evidence to suggest that the use of TiO_2 nanoparticles in cosmetics pose a risk to human health.[102] However, Scokaj *et al.* reported in a similar review that the evidence for the safety of TiO_2 in humans is still under debate, especially for its nanoparticulate forms.[103] For example, Qiang *et al.* demonstrated that a culture of HFL1 cells treated with a 0.50 mg/mL suspension of TiO_2 nanoparticles and incubated for 48 h experienced a 40% reduction in viability relative to control cultures using an MTT assay (for cell metabolic assessment).[104]

Research conducted by Hodek *et al.* performed cytotoxicity tests of their hybrid coating containing silver, copper, and zinc on Vero and HeLa cells, demonstrating viability values above 90% for both cell lines after 4 hours.[42] Similarly, the graphene-oxide-silver nanocomposite created by Chen *et al.* successfully immobilized AgNPs to prevent toxicological effects and reduce potential downstream environmental impacts caused by free AgNPs.[44] Additionally, some research has suggested that AgNP exposure induces metabolic arrest rather than cell death and that human cells have greater resistance than other organisms, providing some justification for their use for healthcare.[105,106]

Polyethyleneimine compounds have shown minimal cytotoxicity in mammalian cells.[78] A study by Shi *et al.* evaluated the cytotoxicity of polyethyleneimines through an MTT assay on 3T3 mouse fibroblasts, showing no statistically significant difference between the polyethyleneimine

treated surfaces, untreated surfaces, and growth culture medium.[107] Furthermore, photosensitizer materials such as rose bengal, which have been implemented in wipes, have also shown no toxic effect on mammalian cells.[97]

Impact of metal nanoparticles on the environment has been a concern since their popularity increased due to antimicrobial activity without the possibility for resistance.[36] The mechanism of toxicity for nanoparticles is through association with the cell surface, dissolution of material by releasing toxic ions which impair enzyme function or DNA, or generation of ROS leading to oxidative stress.[108] Recent studies have considered the environmental toxicity of the fabrication of these nanoparticles. In the study conducted by Li *et al.*, copper nanoparticles were generated *via* a biosynthesis method, which incorporates L-vitamin C to avoid the toxicity of ROS created when CuNPs are exposed to air.[31,109] Additionally, strategies have been considered which will reduce the environmental impact of nanoparticles, such as negative surfaces on nanomaterials to reduce cell surface interactions,[110] capping of nanoparticles to reduce dissolution *via* toxic ions,[111] and tethering of antioxidant molecules to nanoparticle surfaces to reduce ROS impact.[112]

2.6 Emerging technologies and future perspective

In the previous sections, we introduced antiviral agents and coatings that have shown antiviral effects. Although these technologies have been effective in inactivating viruses on various surfaces, they still suffer from several shortcomings that inhibit their practical application for use in daily life. Most of these methods are not universal and their effectiveness depends on the type of the virus. In addition, they might require long incubation times with the attached viruses that could contribute to the interim transmission of the virus. Challenges with mass production and material cost are other drawbacks to many of these technologies, including polyethyleneimine-based antiviral coatings and nanoparticle-based antiviral solutions. In this section, we introduce

potential emerging technologies that could be used stand-alone or in combination with the currently-available antiviral technologies to provide synergistic effects for creating antiviral surfaces (Table 2.3).

Pathogen-repellent surfaces, rather than surfaces impregnated with microbicides, have shown great promise for preventing bacterial adhesion and biofilm formation;[2] however, there is limited information on the applicability of these surfaces in repelling viruses. These repellent surfaces are mostly inspired by natural systems and involve combining nanostructures, microstructures, and chemical functionality. Bioinspired hierarchical micro and nanostructures have been shown to demonstrate antimicrobial effects, while also preventing the binding and attachment of pathogenic organisms to the surface in the first place.[2] Due to the unique wetting properties/states of hierarchical structures, many biological contaminants have been shown to have poor adhesion to these surfaces.[2] This has been most commonly seen with complex fluids such as blood,[113] as well as with solutions containing bacteria, showing low surface contamination and bacterial growth.[114] Nanostructuring of surfaces is a bioinspired technique that researchers regularly employ to obtain self-cleaning characteristics and varying levels of repellency. Similar to the lotus leaf and pitcher plant providing inspiration for self-cleaning surfaces,[115] insect wings have inspired a nanostructured approach for antimicrobial capability.[116] In addition to this, combining the chemical modifications, micro and/or nanostructures with an infused liquid layer, mimics the effect of the pitcher plant,[117,118] thus creating a class of surfaces called lubricant-infused surfaces. These surfaces have displayed superior performance in suppressing blood contamination and clotting,[119–124] while also preventing the growth and attachment of bacteria and their biofilms.[5,125–127] **Figure 2.6a** shows the growth of planktonic bacteria biofilm after 21 days of incubation on dissolved oxygen-permeable membranes with and without a lubricant-infused

coating. Although lubricant-infused surfaces show superior properties for pathogen repellency compared to other technologies, the stability of the lubricant layer, especially on surfaces open to air, is a current drawback of these coatings that could be addressed by choosing more stable lubricants.

Recently, nanostructured surfaces were tested by Hasan *et al.* for the purpose of antiviral capabilities (**Figure 2.6b**). Studying the impact of wet etching with NaOH on aluminum alloy Al 6063, it was found that rhinovirus-16 (RV-16) was very susceptible to loss of viability over a 24 hour period, showing a 3- to 4-log reduction.[128] The same research revealed a lesser impact on the viability of respiratory syncytial virus 4 (RSV4), with the virus naturally showing reduction after 24 hours on Al 6063 alone, though significant decreases were recorded after just 2 hours when nanostructures were present.[128]

We recently developed a flexible omniphobic wrap featuring hierarchical structures (*i.e.* multiple length-scale structures) with repellent properties towards a multitude of fluids and pathogenic bacteria, including *Staphylococcus aureus and Pseudomonas aeruginosa*, as well as inhibition of biofilm formation on the surface (**Figure 2.6c**).[2] To evaluate the repellency, a pathogen transfer analysis was demonstrated with GFP-expressing *E. coli* contaminating the repellent wrap and a commercial wrap through a simulated touch experiment (**Figure 2.6c**). The repellent wraps showed a significant reduction in the transferred bacteria between surfaces. In another work by Chauhan *et al.*,[129] cotton fabrics were modified with hexadecyltrimethoxysilane (HDTMS) to create a superhydrophobic and durable surface. To investigate antimicrobial effects, these surfaces were incubated with *E. coli* (1×10^5 CFU/mL) at 37 ºC for 24 hours and *E. coli* was unable to bind to the surface resulting in cell death and the formation of an inhibition zone around the treated substrates.[129]

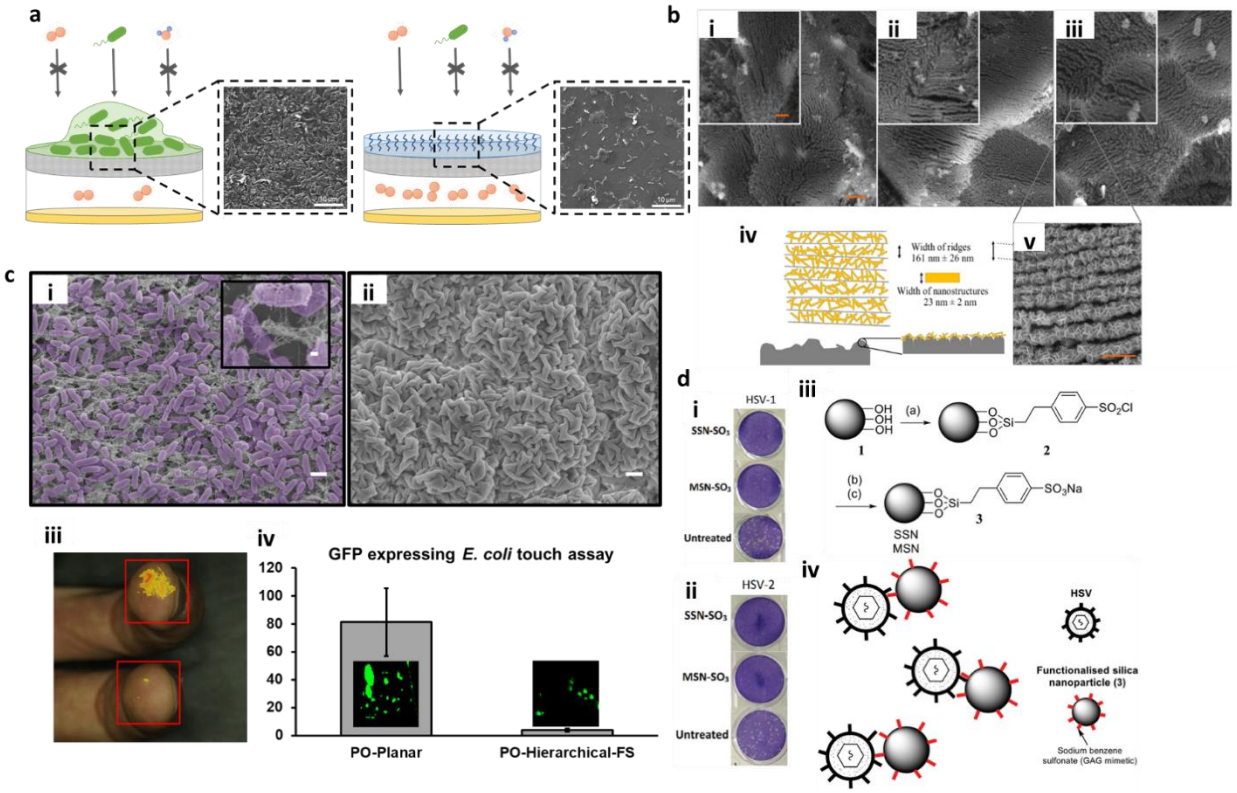

Figure 2.6 – Emerging technologies with potential applications as antiviral coatings. **(a)** Permeable membrane with fluorosilane based lubricant-infused coating (i, ii, iii) schematic of biofouling on membrane with and without the lubricant-infused layer, (iv) SEM of biofouling on untreated membrane and (v) SEM of biofouling on lubricant-infused membrane, after 21 days of incubation. Reprinted from ref [125]. Copyright 2019 American Chemical Society. **(b)** The induced nanostructures on Aluminum 6063 are shown here *via* SEM, created by wet etching for (i) half hour, (ii) one hour and (iii) three hours (Scale bars = 2 µm, inset scale bars = 1 µm). (iv) Schematic representations of the etched samples at higher (top) and lower (bottom) magnification. (v) SEM of the three-hour etched surface at higher magnification revealing the presence of random nanostructures (Scale bar = 500 nm). Reprinted from ref [129]. Copyright 2020 American Chemical Society. **(c)** An omniphobic hierarchical wrinkled structure that prevents the adhesion of bacteria and the growth of their biofilms. SEM of the fixed biofilm of *P. aeruginosa* on (i) planar polystyrene and (ii) hierarchically structured polystyrene surface. The scale bars on larger SEM are 1 µm and the inserted are 100 nm. (iii) analysis of bacterial transfer from an intermediate surface to human hands (iv) bacterial transfer from contaminated surface to planar plastic shrink film and hierarchically structured shrink film. Reprinted from ref [2]. Copyright 2019 American Chemical Society. **(d)** GAG mimetic modified mesoporous silica nanoparticles (i, ii) plaque reduction assay of SSN-SO3 and for HSV1 and HSV2 respectively, (iii) synthesis of GAG mimetic silica nanoparticles, (iv) schematic of proposed mode of antiviral activity. Reprinted from ref [130]. Copyright 2016 Royal Society of Chemistry.

Mannelli *et al.* demonstrated the effect of wetting properties on the stability of influenza A on glass surfaces treated with various hydro and fluoro-carbon chain lengths silanes. Three wetting condition combinations were considered; hydrophilic/oleophilic, hydrophobic/oleophilic, and hydrophobic/oleophobic.[131] They were able to demonstrate the degradation of the viral envelope in the latter two cases, with the hydrophobic/oleophilic surface showing the largest amount of viral inactivity, an 80% reduction in viral activity, while for glass there was little to no reduction in the virus activity.[131] These emerging natural pathogen repellent/inactivating technologies could potentially be used for preventing viral contamination of high-contact surfaces in various settings.

Other emerging materials that utilize micro and nanostructures to create antimicrobial effects are being investigated and developed using safe compounds while still displaying promising antimicrobial properties. For example, solid and mesoporous silica nanoparticles (SSN and MSN, respectively) functionalised with glycosaminoglycan (GAGs) have been implemented to attract viral glycoproteins and eliminate virus entry to host cells in solution.[130] This method could provide a close proximity for virucidal agents to act on the virus, providing a dual functionality (*i.e.* capture and deactivation). The electrostatic and hydrophobic interaction between the GAGs and the virus (*e.g.* HSV-1 and -2), along with the facility of surface functionalization and biocompatibility of silica nanoparticles, make this system a promising method for eliminating infection in solution.[130] This effect can be seen with the plaque reduction assay run on both HSV-1 (**Figure 2.6d(i)**) and HSV-2 (**Figure 2.6d(ii)**) which both displayed significant antiviral activity compared to the control case. Micro-sized SiO_2 particles (SiO_2 MPs) were also used for antiviral studies in solutions where the surface of the SiO_2 MPs were treated with APTES to add C_{60} to their surface as a photosensitizer. Under blue LED light at a wavelength of 470 nm, these particles

showed antiviral behaviour. These treated particles could potentially be coated on to existing surfaces to confer antiviral properties.[98]

Another class of materials based on pyridinium has been used to capture viruses in solution,[132] and air,[133] and could potentially be used as surface coatings. Cross-linked poly(N-benzyl-4-vinylpyridinium bromide) (BVP) and crosslinked poly(N-benzyl-4-vinylpyridinium chloride) have been used for removing pathogenic viruses and have been shown to remove more than 99.5% of viruses such as of enterovirus, HSV, poliovirus, and HIV.[132,133] The affinity of the viruses towards pyridinium was attributed to the combination of the positive charge of the resin and the negative charge on the surface of the viruses, as well as the hydrophobic interactions. This affinity can potentially be exploited to incorporate antiviral agents within the matrix of the resin to attract and inactivate the viruses on site. Xue *et al.* showed more than 90% virucidal effect in solution with only 50 ppm of the synthesised polymers, which consisted of quaternary pyridinium-type polymers (*e.g.* Poly(4VP-co-NVP)), comprising of 4-Vinylpyridine (4VP) and N-vinyl pyrrolidone (NVP), quaternized with benzyl halides,[134] which can potentially be added as a coating to surfaces.

Quantum dots (QDs) are another category of optically active nanomaterials that have potential for use in antimicrobial coatings. More recently, research has been directed at fabricating antimicrobial coatings using QDs as an active agent. Ristic *et al.* evaluated the antibacterial effectiveness of graphene quantum dots (GQDs), which, unlike other types of semiconducting QDs, are biocompatible while retaining the ability to produce ROS.[135] They suspended MRSA and *E. coli* with varied concentrations of GQDs before irradiation with blue light (465-475 nm, 1W). They used propidium iodide (PI) staining to visualize membrane damage and found that approximately 90% of both cell species were not viable after 15 min of irradiation in a 200 µg/mL

GQD suspension.[135] Similarly, Habiba *et al.* demonstrated antibacterial activity in Ag-NPs decorated with GQDs, which were further surface modified with PEG to promote biocompatibility. Minimum inhibitory concentrations of 50 µg/mL and 25 µg/mL were obtained for the nanoparticle suspensions against *P. aeruginosa* and *S. aureus,* respectively.[136] The non-toxicity of GQDs has been well-established. For example, Zhu *et al.* demonstrated that adding 400 µg of GQDs to 150µL of MG-63 cell culture medium resulted in no significant reduction to cell viability in an MTT assay.[137] To the best of our knowledge, research has yet to test the antiviral potential of QDs on surfaces, however, based on the ROS mechanism seen with other antiviral agents this material shows promise for antiviral capabilities.

In an effort to develop technologies with antiviral properties, several companies have utilized antiviral strategies to manufacture products and coatings. EnvisionSQ has developed a product called GermStopSQ,[138] a coating that claims to adhere to any surface and is semi-permanent. The EnvisionSQ website states that their technology is 99.9999% effective in eliminating bacteria, fungi and viruses (both enveloped and non-enveloped). Covalon has recently introduced a product called CovaGuard,[139] which they assert is formulated to inactivate SARS-CoV-2 and other viruses, as well as bacteria, both immediate and sustained. They highlight the use of benzalkonium chloride (BAC) in their formulation, which can be applied (through spraying) on any surface and remains antimicrobial and antiviral for four days. Biogate is another company which has a product called MicroSilver BG™,[140] comprising of microporous silver additive. They have claimed that their product is not cytotoxic and can be incorporated into various materials. Bio-Fence has fabricated chlorine-binding polymer coatings that are antimicrobial and antiviral.[141] Once the surface is depleted, it can be coated again by spraying the Chlorine, according to their website. SurfaceWise^2 is another surface coating approved by United States Environmental

Protection Agency (EPA) to have antiviral activity with a single application.[142] Caliwel™ BNA Coating, based on calcium hydroxide, has also been approved by EPA for its antiviral and antimicrobial behavior.[143,144] BioFriend™ BioMask™ is another company with FDA approval that produces masks that are able to trap pathogens including viruses and inactivate them.[145]

In the future, a combination of pathogen-repellent coatings with antiviral materials could create synergistic effects, through which the surface repels the majority of the viruses while the coated antiviral agents inactivate any attached viruses that have not been repelled, providing a double layer of protection against viruses. This could greatly reduce the number of pathogens transferred from fomites to person, and then from person to person. The improved biocompatibility and lower toxicity of structurally-engineered repellent materials would allow them to be used in a larger range of applications including the highly regulated food[146] and medical industries.[147]

Combining a spectrum of materials with different antimicrobial mechanisms is expected to lead to smart surfaces that attract, bind, and eliminate a multitude of pathogens. Finally, integrating simple and real-time sensing capabilities to these antimicrobial surfaces, in addition to mitigating the risk of transmission, could help in identifying the pathogens present in the environment, and eventually aiding the public health authorities in managing infectious disease outbreaks.

Table 2.3 Emerging technologies with potential to be used as antiviral coatings

Material and Structure	Antimicrobial Testing		Promising Features	Challenges	Ref.
	Virus	**Bacteria**			
Micro/nano Structuring					
Nanostructured Aluminum	Respiratory syncytial virus (RSV) Rhinovirus (RV)	*Pseudomonas aeruginosa* *Staphylococcus aureus*	Dual action of antiviral and antibacterial 3-4 log reduction in viability counts of RV within 2 hours More rapid reduction of RSV than control 92% inactivation of *P. aeruginosa* 87% inactivation of *S. aureus*, respectively within 3 hours. Mechanically durable, viable option for high-touch surfaces	Limited to aluminum surfaces Nanostructures are not controlled during fabrication	[128]
Nanostructured anatase-rutile-carbon (NsARC) coating	N/A	*Escherichia coli*	Photocatalytic activity was shown to present in UV light (4-log reduction in EOP, over 4 hours) and visible light (3-log reduction, and in the dark (2-log reduction). These results broaden the possible applications to everyday environments.	Did not investigate durability; currently only grown on stainless steel surfaces.	[51]
Hierarchical micro and nanostructure based on thin film wrinkling on plastic shrink wraps.	N/A	*Staphylococcus aureus* *Pseudomonas aeruginosa* *Escherichia coli*	Reduces biofouling for bacteria. Flexibility allows them to be used in both medical devices or as medical surfaces	Requires heating to temperatures of 145C to conform around an object/surface.	[2]
Hexadecyltrimethoxysilane (HDTMS) modified cotton fabric	N/A	*Escherichia coli*	Extremely durable, maintained its repellent properties after washing in solvents and hot water. Simple manufacturing method. Inactivation of *E. coli via* inhibition zone started showing after 12 hours and continued up to 24 hours	Does not investigate why the inhibition zone is created by the hydrophobicity, or how the chemical modification would work on other fabrics	[129]

Material and Structure	Antimicrobial Testing		Promising Features	Challenges	Ref.
	Virus	**Bacteria**			
Lubricant-infused surfaces					
Fluorosilane-based omniphobic lubricant- infused coating on permeable membrane	N/A	Planktonic bacteria	Significantly reduced the formation of biofilm growth and formation of a 21-day period	Did not investigate potential antibiofouling effects on pathogenic bacteria.	125
Tethered-liquid perfluorocarbon surface	N/A	*Pseudomonas aeruginosa* *Escherichia coli*	*Pseudomonas aeruginosa* was grown in coated PVC medical tubing for 6.5 weeks and showed an eight-fold reduction in the formation of the biofilm. The surfaces also reduced blood related biofouling	Reduction of biofilm *in vitro* only lasted 24 hours. Lubricant layer can evaporate over time resulting in the loss of performance.	5
PTFE membrane infused with perfluoropolyether	N/A	*Staphylococcus aureus* *Pseudomonas aeruginosa* *Escherichia coli*	The PTEF lubricant-infused substrates showed 99.6% decrease in biofilm formation in a 7-day incubation under flow, for *Staph. aureus*. While showing a 96-97.2% reduction for the other two pathogens in a 2-day period	Lubricant layer can evaporate over time resulting in a loss of performance.	119
Liquid/particle-based material					
GAG mimetic functionalized solid and mesoporous silica nanoparticles (SSN-SO3 and MSN-SO3)	HSV-1 and HSV-2	N/A	The GAG mimetic MSN and SSN act as a viral binding inhibitor that inhibits HSV 1 and 2 from infecting cells within 1 hour	GAG modification is attractive towards viruses, so it should be combined with an antiviral modification	130
poly(N-benzyl-4-vinylpyridinium bromide (BVP) resin	enterovirus, HSV, poliovirus, and HIV coxsackievirus and echovirus human rotavirus, influenza virus, human adenovirus, and Japanese encephalitis virus	N/A	efficient removal of viruses from aqueous solutions based on pyridinium affinity for viruses. 64-fold reduction for HRV, 256 fold reduction for Influenza A, 32-fold reduction Ad-37 and 16 fold reduction in JEV after 30 min.	Toxicity was not discussed and means of use on various surfaces. This method is attractive towards viruses, so it should be combined with an antiviral modification	132

Material and Structure	Antimicrobial Testing		Promising Features	Challenges	Ref.
	Virus	**Bacteria**			
poly(N-benzyl-4-vinylpyridinium chloride)	Bacteriophage T4	N/A	efficient removal of viruses from air based on pyridinium affinity for viruses	A membrane was fabricated, addition of this material to existing membranes was not investigated. This method is attractive towards viruses, so it should be combined with an antiviral modification	133
water-soluble pyridinium-type polyvinylpyrrolidones with different counter anions comprising of 4-Vinylpyridine (4VP) and N-vinyl pyrrolidone (NVP) (Poly(4VP-co-NVP), quaternized with benzyl halides	Influenza virus	*Staphylococcus aureus* and *Escherichia coli*	Adsorption of the polymer onto the virus envelope followed by penetration inactivates the virus at small titers (50 ppm). They also displayed the ability To inactivate *E. coli* within 3 min.	Only showed antiviral effect on enveloped viruses. Potential to add on surfaces was not explored	134
Graphene quantum dots (GQDs) suspension	N/A	*E. coli* and MRSA	90% of both cell species were not viable after 15 min of irradiation with blue light in a 200 µg/mL GQD suspension.	Performed in solution, not tested against virus titers	135
Silver nanoparticles (Ag-NPs) decorated with GQDs	N/A	*P. aeruginosa* and *S. aureus*	Minimum inhibitory concentrations of 50 µg/mL and 25 µg/mL were obtained for the nanoparticle suspensions against *P. aeruginosa* and *S. aureus*, respectively, after incubation with NPs for 24 h.	Performed in solution, not tested against virus titers	136

2.7 Conclusion

Modification of surfaces to confer antiviral capabilities is an area that is ripe for investigation. With the current SARS-CoV-2 pandemic, there has been a rapid surge in the number of studies that focus on quantifying the survival of SARS-CoV-2 on various surfaces.[6,148,149] We anticipate that several of the technologies presented here could be used as surface coatings to reduce the spread of infectious diseases, including COVID-19, *via* surfaces. We petition researchers to apply a more systematic approach to their investigations in studying the antimicrobial properties of surfaces, rigorously testing each category of viruses – enveloped or non-enveloped, DNA-based or RNA-based – prior to making claims of effectiveness. Above all, it is imperative that research claiming antimicrobial capabilities becomes more accurate about effectiveness against viruses, only making these claims when viral studies have been executed. Surfaces capable of immediately repelling and/or inactivating pathogens are urgently needed, and it is now the responsibility of scientists, industry, and governments to work together towards this goal.

2.8 Acknowledgements

TFD acknowledges the financial support provided by NSERC Discovery and CRD grants, Ontario Early Researcher Award grant and McMaster start-up funds to T.F.D.

2.9 Vocabulary

Plaque assay: A method of viral quantification relying on the formation of plaque-forming units of infected (lysed) cells *in vitro* after inoculation with a viral titer. Plaque-forming units are counted manually and given in units of PFU/mL. Alternatively, immunostaining targeting viral antibodies can be used to quantify viral activity, measured in units of focus forming units (FFU/mL). Reactive oxygen species (ROS): Oxygen-containing free radicals produced during photoactivity and a

variety of metabolic processes. In excess quantities, cause oxidative damage to components of the cell, including lipid membranes and genetic material. **Bacteriophage:** A virus that specializes in infecting and replicating inside bacteria. **Photocatalysis:** A process in which chemical reactions are generated in the presence of light. In semiconductors, this can result in the development of electron/hole pairs and reactive oxygen species in the presence of oxygen-containing compounds. **Enveloped virus:** Virus whose outermost layer is an envelope derived from the host cell's plasma membrane and composed of phospholipids, lipoproteins, and glycoproteins. Non-enveloped viruses are instead protected mainly by a shell-like protein capsid. All viruses possess a capsid, but not all are enveloped. **Electrospinning/spraying:** Related fabrication processes by which polymer solutions in an electric field are forced through an opening when electrostatic repulsion between droplets exceeds surface tension. Electrospinning occurs when the droplets form a continuous stream; electrospraying occurs when the droplets separate. **Positive and negative-sense ssRNA:** Viruses that replicate using single stranded RNA may produce a strand complimentary or identical to the genetic material produced in the host cell. Positive-sense strands possess the same nucleotide sequence, and may be directly translated into proteins, while negative-sense strands possess the complimentary sequence.

2.10 References

(1) Llorens, A.; Lloret, E.; Picouet, P. A.; Trbojevich, R.; Fernandez, A. Metallic-Based Micro and Nanocomposites in Food Contact Materials and Active Food Packaging. *Trends in Food Sci. Technol.* **2012**, *24*, 19–29.

(2) Imani, S. M.; Maclachlan, R.; Rachwalski, K.; Chan, Y.; Lee, B.; McInnes, M.; Grandfield, K.; Brown, E. D.; Didar, T. F.; Soleymani, L. Flexible Hierarchical Wraps Repel Drug-Resistant Gram-Negative and Positive Bacteria. *ACS Nano* **2020**, *14*, 454–465.

(3) Nguyen, D. H. K.; Pham, V. T. H.; Truong, V. K.; Sbarski, I.; Wang, J.; Balčytis, A.; Juodkazis, S.; Mainwaring, D. E.; Crawford, R. J.; Ivanova, E. P. Role of Topological Scale in the Differential Fouling of: *Pseudomonas aeruginosa* and *Staphylococcus aureus* Bacterial Cells on Wrinkled Gold-Coated Polystyrene Surfaces. *Nanoscale* **2018**, *10*, 5089–5096.

(4) Crawford, R. J.; Webb, H. K.; Truong, V. K.; Hasan, J.; Ivanova, E. P. Surface Topographical Factors Influencing Bacterial Attachment. *Adv. Colloid Interface Sci.* **2012**, *172–182*, 142–149.

(5) Leslie, D. C.; Waterhouse, A.; Berthet, J. B.; Valentin, T. M.; Watters, A. L.; Jain, A.; Kim, P.; Hatton, B. D.; Nedder, A.; Donovan, K.; Super, E. H.; Howell, C.; Johnson, C. P.; Vu, T. L.; Bolgen, D. E.; Rifai, S.; Hansen, A. R.; Aizenberg, M.; Super, M.; Aizenberg, J. *et al.* A Bioinspired Omniphobic Surface Coating on Medical Devices Prevents Thrombosis and Biofouling. *Nat. Biotechnol.* **2014**, *32*, 1134–1140.

(6) Kampf, G.; Todt, D.; Pfaender, S.; Steinmann, E. Persistence of Coronaviruses on Inanimate Surfaces and Their Inactivation with Biocidal Agents. *J. Hosp. Infect.* **2020**, *104*, 246–251.

(7) Pirtle, E. C.; Beran, G. W. Virus Survival in the Environment. *Rev. Sci. Tech.* **1991**, *10*, 733–748.

(8) Centers for Disease Control. Recommendations for Prevention of HIV Transmission in Health-Care Settings. *MMWR Suppl.* **1987**. *36*, 1-18.

(9) Otter, J. A.; Donskey, C.; Yezli, S.; Douthwaite, S.; Goldenberg, S. D.; Weber, D. J. Transmission of SARS and MERS Coronaviruses and Influenza Virus in Healthcare Settings: The Possible Role of Dry Surface Contamination. *J. Hosp. Infect.*, **2016**, *92*, 235–250.

(10) Weiss, C.; Carriere, M.; Fusco, L.; Fusco, L.; Capua, I.; Regla-Nava, J. A.; Pasquali, M.; Pasquali, M.; Pasquali, M.; Scott, J. A.; Vitale, F.; Vitale, F.; Unal, M. A.; Mattevi, C.; Bedognetti, D.; Merkoçi, A.; Merkoçi, A.; Tasciotti, E.; Tasciotti, E.; Yilmazer, A.; Yilmazer, A.; Gogotsi, Y.; Stellacci, F.; Stellacci, F.; Delogu, L. G. Toward Nanotechnology-Enabled Approaches against the COVID-19 Pandemic. *ACS Nano* **2020**, *14*, 6383–6406.

(11) Sportelli, M. C.; Izzi, M.; Kukushkina, E. A.; Hossain, S. I.; Picca, R. A.; Ditaranto, N.; Cioff, N. Can Nanotechnology and Materials Science Help the Fight against SARS-CoV-2? *Nanomaterials* **2020**, *10*, 802.

(12) Vincent, M.; Duval, R. E.; Hartemann, P.; Engels-Deutsch, M. Contact Killing and Antimicrobial Properties of Copper. *J. Appl. Microbiol.* **2017**, *124*, 1032–1046.

(13) Milanino, R. Copper in Medicine and Personal Care: A Historical Overview. *Copper and the Skin*; Dermatology: Clinical & Basic Science Series; Informa Healthcare USA, Inc.: New York, NY, 2006; 170–182.

(14) Borkow, G. Using Copper to Fight Microorganisms. *Curr. Chem. Biol.* **2012**, *6*, 93–103.

(15) Nan, L.; Liu, Y.; Lü, M.; Yang, K. Study on Antibacterial Mechanism of Copper-Bearing Austenitic Antibacterial Stainless Steel by Atomic Force Microscopy. *J. Mater. Sci. Mater. Med.* **2008**, *19*, 3057–3062.

(16) Karlstrom, A. R.; Levine, R. L. Copper Inhibits the Protease from Human Immunodeficiency Virus 1 by Both Cysteine-Dependent and Cysteine-Independent Mechanisms. *Proc. Natl. Acad. Sci. U. S. A.* **1991**, *88*, 5552–5556.

(17) Sagripanti, J.; Goering, P. L.; Lamanna, A. Interaction of Copper with DNA and Antagonism by Other Metals. *Toxicol. Appl. Pharmacol.* **1991**, *110*, 477-485.

(18) Sunada, K.; Minoshima, M.; Hashimoto, K. Highly Efficient Antiviral and Antibacterial Activities of Solid-State Cuprous Compounds. *J. Hazard. Mater.* **2012**, *235–236*, 265–270.

(19) Warnes, S. L.; Summersgill, E. N.; Keevil, C. W. Inactivation of Murine Norovirus on a Range of Copper Alloy Surfaces is Accompanied by Loss of Capsid Integrity. *Appl. Environ. Microbiol.* **2015**, *81*, 1085–1091.

(20) Warnes, S. L.; Keevil, C. W. Inactivation of Norovirus on Dry Copper Alloy Surfaces. *PLoS One* **2013**, *8*, 75017.

(21) Bleichert, P.; Santo, C. E.; Hanczaruk, M.; Meyer, H.; Grass, G. Inactivation of Bacterial and Viral Biothreat Agents on Metallic Copper Surfaces. *BioMetals* **2014**, *27*, 1179–1189.

(22) Noyce, J. O.; Michels, H.; Keevil, C. W. Inactivation of Influenza A Virus on Copper *versus* Stainless Steel Surfaces. *Appl. Environ. Microbiol.* **2007**, *73*, 2748–2750.

(23) Minoshima, M.; Lu, Y.; Kimura, T.; Nakano, R.; Ishiguro, H.; Kubota, Y.; Hashimoto, K.; Sunada, K. Comparison of the Antiviral Effect of Solid-State Copper and Silver Compounds. *J. Hazard. Mater.* **2016**, *312*, 1–7.

(24) Li, J.; Dennehy, J. J. Differential Bacteriophage Mortality on Exposure to Copper. *Appl. Environ. Microbiol.* **2011**, *77*, 6878–6883.

(25) Warnes, S. L.; Little, Z. R.; Keevil, C. W. Human Coronavirus 229E Remains Infectious on Common Touch Surface Materials. *MBio* **2015**, *6*, e01697-15.

(26) Borkow, G.; Gabbay, J. Putting Copper into Action: Copper-Impregnated Products with Potent Biocidal Activities. *FASEB J.* **2004**, *18*, 1728–1730. .

(27) Borkow, G.; Sidwell, R. W.; Smee, D. F.; Barnard, D. L.; Morrey, J. D.; Lara-Villegas, H. H.; Shemer-Avni, Y.; Gabbay, J. Neutralizing Viruses in Suspensions by Copper Oxide-Based Filters. *Antimicrob. Agents Chemother.* **2007**, *51*, 2605–2607.

(28) Borkow, G.; Zhou, S. S.; Page, T.; Gabbay, J. A Novel Anti-Influenza Copper Oxide Containing Respiratory Face Mask. *PLoS One* **2010**, *5*, e11295.

(29) Imai, K.; Ogawa, H.; Bui, V. N.; Inoue, H.; Fukuda, J.; Ohba, M.; Yamamoto, Y.; Nakamura, K. Inactivation of High and Low Pathogenic Avian Influenza Virus H5 Subtypes by Copper Ions Incorporated in Zeolite-Textile Materials. *Antiviral Res.* **2012**, *93*, 225–233.

(30) Ingle, A. P.; Duran, N.; Rai, M. Bioactivity, Mechanism of Action, and Cytotoxicity of Copper-Based Nanoparticles: A Review. *Appl. Microbiol. Biotechnol*. **2014**, *98*, 1001–1009.

(31) Li, Y.; Pi, Q. M.; You, H. H.; Li, J. Q.; Wang, P. C.; Yang, X.; Wu, Y. A Smart Multi-Functional Coating Based on Anti-Pathogen Micelles Tethered with Copper Nanoparticles *via* a Biosynthesis Method Using L-Vitamin C. *RSC Adv.* **2018**, *8*, 18272–18283.

(32) Dakal, T. C.; Kumar, A.; Majumdar, R. S.; Yadav, V. Mechanistic Basis of Antimicrobial Actions of Silver Nanoparticles. *Front. Microbiol.* **2016**, *7*, 1–17.

(33) Read, S. A.; Obeid, S.; Ahlenstiel, C.; Ahlenstiel, G. The Role of Zinc in Antiviral Immunity. *Adv. Nutr*. **2019**, *10*, 696–710.

(34) Halbus, A. F.; Horozov, T. S.; Paunov, V. N. Colloid Particle Formulations for Antimicrobial Applications. *Adv. Colloid Interface Sci.* **2017**, *249*, 134–148.

(35) Champagne, V.; Sundberg, K.; Helfritch, D. Kinetically Deposited Copper Antimicrobial Surfaces. *Coatings* **2019**, *9*, 1–9.

(36) Rai, M.; Deshmukh, S. D.; Ingle, A. P.; Gupta, I. R.; Galdiero, M.; Galdiero, S. Metal Nanoparticles: The Protective Nanoshield against Virus Infection. *Crit. Rev. Microbiol.* **2016**, *42*, 46–56.

(37) Lara, H. H.; Ayala-Nuñez, N. V; Ixtepan-Turrent, L.; Rodriguez-Padilla, C. Mode of

Antiviral Action of Silver Nanoparticles against HIV-1. *J. Nanobiotechnology* **2010**, *8*, 1.

(38) Castro-Mayorga, J. L.; Randazzo, W.; Fabra, M. J.; Lagaron, J. M.; Aznar, R.; Sánchez, G. Antiviral Properties of Silver Nanoparticles against Norovirus Surrogates and Their Efficacy in Coated Polyhydroxyalkanoates Systems. *LWT - Food Sci. Technol.* **2017**, *79*, 503–510.

(39) Park, S. J.; Park, H. H.; Kim, S. Y.; Kim, S. J.; Woo, K.; Ko, G. P. Antiviral Properties of Silver Nanoparticles on a Magnetic Hybrid Colloid. *Appl. Environ. Microbiol.* **2014**, *80* , 2343–2350.

(40) Stohs, S. J.; Bagchi, D. Oxidative Mechanisms in the Toxicity of Metal Ions. *Free Radical Biol. Med*. **1995**, *18*, 321–336.

(41) AshaRani, P. V; Mun, G. L. K.; Hande, M. P.; Valiyaveettil, S. Cytotoxicity and Genotoxicity of Silver Nanoparticles in Human Cells. *ACS Nano* **2009**, *3*, 279–290.

(42) Hodek, J.; Zajícová, V.; Lovetinská-Šlamborová, I.; Stibor, I.; Müllerová, J.; Weber, J. Protective Hybrid Coating Containing Silver, Copper and Zinc Cations Effective against Human Immunodeficiency Virus and Other Enveloped Viruses. *BMC Microbiol.* **2016**, *16*, 1–12.

(43) Nguyen, V. Q.; Ishihara, M.; Kinoda, J.; Hattori, H.; Nakamura, S.; Ono, T.; Miyahira, Y.; Matsui, T. Development of Antimicrobial Biomaterials Produced from Chitin-Nanofiber Sheet/Silver Nanoparticle Composites. *J. Nanobiotechnology* **2014**, *12*, 49.

(44) Chen, Y. N.; Hsueh, Y. H.; Hsieh, C. Te; Tzou, D. Y.; Chang, P. L. Antiviral Activity of Graphene–Silver Nanocomposites against Non-Enveloped and Enveloped Viruses. *Int. J. Environ. Res. Public Health* **2016**, *13*, 430.

(45) Zodrow, K.; Brunet, L.; Mahendra, S.; Li, D.; Zhang, A.; Li, Q.; Alvarez, P. J. J. Polysulfone

Ultrafiltration Membranes Impregnated with Silver Nanoparticles Show Improved Biofouling Resistance and Virus Removal. *Water Res.* **2009**, *43*, 715–723.

(46) De Gusseme, B.; Hennebel, T.; Christiaens, E.; Saveyn, H.; Verbeken, K.; Fitts, J. P.; Boon, N.; Verstraete, W. Virus Disinfection in Water by Biogenic Silver Immobilized in Polyvinylidene Fluoride Membranes. *Water Res.* **2011**, *45*, 1856–1864.

(47) Martínez-Abad, A.; Ocio, M. J.; Lagarón, J. M.; Sánchez, G. Evaluation of Silver-Infused Polylactide Films for Inactivation of Salmonella and Feline Calicivirus *in Vitro* and on Fresh-Cut Vegetables. *Int. J. Food Microbiol.* **2013**, *162*, 89–94.

(48) Joe, Y. H.; Park, D. H.; Hwang, J. Evaluation of Ag Nanoparticle Coated Air Filter against Aerosolized Virus: Anti-Viral Efficiency with Dust Loading. *J. Hazard. Mater.* **2016**, *301*, 547–553.

(49) Speshock, J. L.; Murdock, R. C.; Braydich-Stolle, L. K.; Schrand, A. M.; Hussain, S. M. Interaction of Silver Nanoparticles with Tacaribe Virus. *J. Nanobiotechnology* **2010**, *8*, 19.

(50) Rogers, J. V; Parkinson, C. V.; Choi, Y. W.; Speshock, J. L.; Hussain, S. M. A Preliminary Assessment of Silver Nanoparticle Inhibition of Monkeypox Virus Plaque Formation. *Nanoscale Res. Lett.* **2008**, *3* 129–133.

(51) Krumdieck, S. P.; Boichot, R.; Gorthy, R.; Land, J. G.; Lay, S.; Gardecka, A. J.; Polson, M. I. J.; Wasa, A.; Aitken, J. E.; Heinemann, J. A.; Renou, G.; Berthomé, G.; Charlot, F.; Encinas, T.; Braccini, M.; Bishop, C. M. Nanostructured TiO_2 Anatase-Rutile-Carbon Solid Coating with Visible Light Antimicrobial Activity. *Sci. Rep.* **2019**, *9*, 1–11.

(52) Ishiguro, H.; Nakano, R.; Yao, Y.; Kajioka, J.; Fujishima, A.; Sunada, K.; Minoshima, M.; Hashimoto, K.; Kubota, Y. Photocatalytic Inactivation of Bacteriophages by TiO2-Coated Glass Plates under Low-Intensity, Long-Wavelength UV Irradiation. *Photochem.*

Photobiol. Sci. **2011**, *10*, 1825–1829.

(53) Korant, B. D.; Kauer, J. C.; Butterworth, B. E. Zinc Ions Inhibit Replication of Rhinoviruses. *Nature* **1974**, *248* , 588–590.

(54) Gupta, P.; Rapp, F. Effect of Zinc Ions on Synthesis of Herpes Simplex Virus Type 2-Induced Polypeptides. *Proc. Soc. Exp. Biol. Med.* **1976**, *152*, 455–458.

(55) Fridlender, B.; Chejanovsky, N.; Becker, Y. Selective Inhibition of Herpes Simplex Virus Type 1 DNA Polymerase by Zinc Ions. *Virology* **1978**, *84*, 551–554.

(56) Arens, M.; Travis, S. Zinc Salts Inactivate Clinical Isolates of Herpes Simplex Virus *in Vitro*. *J. Clin. Microbiol.* **2000**, *38*, 1758–1762.

(57) Williams, M. C.; Gorelick, R. J.; Musier-Forsyth, K. Specific Zinc-Finger Architecture Required for HIV-1 Nucleocapsid Protein's Nucleic Acid Chaperone Function. *Proc. Natl. Acad. Sci. U. S. A.* **2002**, *99*, 8614–8619.

(58) Mishra, Y. K.; Adelung, R.; Röhl, C.; Shukla, D.; Spors, F.; Tiwari, V. Virostatic Potential of Micro-Nano Filopodia-Like ZnO Structures against Herpes Simplex Virus-1. *Antiviral Res.* **2011**, *92*, 305–312.

(59) Qiu, M.; Chen, Y.; Chu, Y.; Song, S.; Yang, N.; Gao, J.; Wu, Z. Zinc Ionophores Pyrithione Inhibits Herpes Simplex Virus Replication through Interfering with Proteasome Function and NF-KB Activation. *Antiviral Res.* **2013**, *100*, 44–53.

(60) Park, G. W.; Cho, M.; Cates, E. L.; Lee, D.; Oh, B. T.; Vinjé, J.; Kim, J. H. Fluorinated TiO_2 as an Ambient Light-Activated Virucidal Surface Coating Material for the Control of Human Norovirus. *J. Photochem. Photobiol. B Biol.* **2014**, *140*, 315–320.

(61) Sohm, B.; Immel, F.; Bauda, P.; Pagnout, C. Insight into the Primary Mode of Action of TiO_2 Nanoparticles on *Escherichia coli* in the Dark. *Proteomics* **2015**, *15*, 98–113.

(62) Moongraksathum, B.; Chien, M.-Y.; Chen, Y.-W. Antiviral and Antibacterial Effects of Silver-Doped TiO_2 Prepared by the Peroxo Sol-Gel Method. *J. Nanosci. Nanotechnol.* **2019**, *19*, 7356-7362.

(63) Shakeri, A.; Yip, D.; Badv, M.; Imani, S.; Sanjari, M.; Didar, T. Self-Cleaning Ceramic Tiles Produced *via* Stable Coating of TiO_2 Nanoparticles. *Materials (Basel).* **2018**, *11*, 1003.

(64) Akhtar, S.; Shahzad, K.; Mushtaq, S.; Ali, I.; Rafe, M. H.; Fazal-Ul-Karim, S. M. Antibacterial and Antiviral Potential of Colloidal Titanium Dioxide (TiO_2) Nanoparticles Suitable for Biological Applications. *Mater. Res. Express* **2019**, *6*, 105409.

(65) Nakano, R.; Hara, M.; Ishiguro, H.; Yao, Y.; Ochiai, T.; Nakata, K.; Murakami, T.; Kajioka, J.; Sunada, K.; Hashimoto, K.; Fujishima, A.; Kubota, Y. Broad Spectrum Microbicidal Activity of Photocatalysis by TiO_2. *Catalysts* **2013**, *3*, 310–323.

(66) Khater, M. S.; Kulkarni, G. R.; Khater, S. S.; Gholap, H.; Patil, R. Study to Elucidate Effect of Titanium Dioxide Nanoparticles on Bacterial Membrane Potential and Membrane Permeability. *Mater. Res. Express* **2020**, *7*, 035005.

(67) Rao, G.; Brastad, K. S.; Zhang, Q.; Robinson, R.; He, Z.; Li, Y. Enhanced Disinfection of *Escherichia coli* and Bacteriophage MS2 in Water Using a Copper and Silver Loaded Titanium Dioxide Nanowire Membrane. *Front. Environ. Sci. Eng.* **2016**, *10*, 11.

(68) Broglie, J. J.; Alston, B.; Yang, C.; Ma, L.; Adcock, A. F.; Chen, W.; Yang, L. Antiviral Activity of Gold/Copper Sulfide Core/Shell Nanoparticles against Human Norovirus Virus-Like Particles. *PLoS One* **2015**, *10*, e0141050.

(69) Kim, J.; Yeom, M.; Lee, T.; Kim, H. O.; Na, W.; Kang, A.; Lim, J. W.; Park, G.; Park, C.; Song, D.; Haam, S. Porous Gold Nanoparticles for Attenuating Infectivity of Influenza A Virus. *J. Nanobiotechnol.* **2020**, *18*, 1–11.

(70) Di Gianvincenzo, P.; Marradi, M.; Martínez-Ávila, O. M.; Bedoya, L. M.; Alcamí, J.; Penadés, S. Gold Nanoparticles Capped with Sulfate-Ended Ligands as Anti-HIV Agents. *Bioorganic Med. Chem. Lett.* **2010**, *20*, 2718–2721.

(71) Cagno, V.; Andreozzi, P.; D'Alicarnasso, M.; Silva, P. J.; Mueller, M.; Galloux, M.; Goffic, R. Le; Jones, S. T.; Vallino, M.; Hodek, J.; Weber, J.; Sen, S.; Janecek, E. R.; Bekdemir, A.; Sanavio, B.; Martinelli, C.; Donalisio, M.; Welti, M. A. R.; Eleouet, J. F.; Han, Y.; *et al.* Broad-Spectrum Non-Toxic Antiviral Nanoparticles with a Virucidal Inhibition Mechanism. *Nat. Mater.* **2018**, *17*, 195–203.

(72) Choi, S. Y.; Cho, B. Extermination of Influenza Virus H1N1 by a New Visible-Light-Induced Photocatalyst under Fluorescent Light. *Virus Res.* **2018**, *248*, 71–73.

(73) Botequim, D.; Maia, J.; Lino, M. M. F.; Lopes, L. M. F.; Simoes, P. N.; Ilharco, L. M.; Ferreira, L. Nanoparticles and Surfaces Presenting Antifungal, Antibacterial and Antiviral Properties. *Langmuir* **2012**, *28*, 7646–7656.

(74) Shi, Z.; Jayatissa, A. H. Perovskites-Based Solar Cells: A Review of Recent Progress, Materials and Processing Methods. *Materials (Basel).* **2018**, *11*, 729.

(75) Weng, D.; Lei, C.; Wu, T. T.; Sun, R.; Shen, M.; Lu, Y. Spontaneous and Continuous Anti-Virus Disinfection from Nonstoichiometric Perovskite-Type Lanthanum Manganese Oxide. *Prog. Nat. Sci. Mater. Int.* **2015**, *25*, 191–196.

(76) Manjunatha, C. R.; Nagabhushana, B. M.; Raghu, M. S.; Pratibha, S.; Dhananjaya, N.; Narayana, A. Perovskite Lanthanum Aluminate Nanoparticles Applications in Antimicrobial Activity, Adsorptive Removal of Direct Blue 53 Dye and Fluoride. *Mater. Sci. Eng., C* **2019**, *101*, 674–685.

(77) Ehi-Eromosele, C. O.; Olugbuyiro, J. A. O.; Adebisi, A. A.; Edobor-Osoh, A.; Ishola, I. M.

The Effect of Silica Coatings on the Structural, Magnetic and Antimicrobial Properties of Silver Doped Manganite Magnetic Nanoparticles for Biomedical Applications. *J. Bionanosci.* **2017**, *11*, 548–553.

(78) Sinclair, T. R.; Patil, A.; Raza, B. G.; Reurink, D.; van den Hengel, S. K.; Rutjes, S. A.; de Roda Husman, A. M.; Roesink, H. D. W.; de Vos, W. M. Cationically Modified Membranes Using Covalent Layer-By-Layer Assembly for Antiviral Applications in Drinking Water. *J. Memb. Sci.* **2019**, *570*, 494–503.

(79) Hsu, B. B.; Wong, S. Y.; Hammond, P. T.; Chen, J.; Klibanov, A. M. Mechanism of Inactivation of Influenza Viruses by Immobilized Hydrophobic Polycations. *Proc. Natl. Acad. Sci.* **2011**, *108*, 61–66.

(80) Klibanov, A. M. Permanently Microbicidal Materials Coatings. *J. Mater. Chem.* **2007**, *17*, 2479–2482.

(81) Larson, A. M.; Hsu, B. B.; Rautaray, D.; Haldar, J.; Chen, J.; Klibanov, A. M. Hydrophobic Polycationic Coatings Disinfect Poliovirus and Rotavirus Solutions. *Biotechnol. Bioeng.* **2011**, *108*, 720–723.

(82) Gelman, F.; Lewis, K.; Klibanov, A. M. Drastically Lowering the Titer of Waterborne Bacteriophage PRD1 by Exposure to Immobilized Hydrophobic Polycations. *Biotechnol. Lett.* **2004**, *26*, 1695–1700.

(83) Haldar, J.; An, D.; De Cienfuegos, L. Á.; Chen, J.; Klibanov, A. M. Polymeric Coatings That Inactivate Both Influenza Virus and Pathogenic Bacteria. *Proc. Natl. Acad. Sci. U. S. A.* **2006**, *103*, 17667–17671.

(84) Dang, H. T. T.; Tarabara, V. V. Virus Deposition onto Polyelectrolyte-Coated Surfaces: A Study with Bacteriophage MS2. *J. Colloid Interface Sci.* **2019**, *540*, 155–166.

(85) Klibanov, A. M. Permanently Microbicidal Materials Coatings. *J. Mater. Chem.* **2007**, *17*, 2479–2482.

(86) Haldar, J.; Weight, A. K.; Klibanov, A. M. Preparation, Application and Testing of Permanent Antibacterial and Antiviral Coatings. *Nat. Protoc.* **2007**, *2*, 2412.

(87) Haldar, J.; Chen, J.; Tumpey, T. M.; Gubareva, L. V; Klibanov, A. M. Hydrophobic Polycationic Coatings Inactivate Wild-Type and Zanamivir-And/Or Oseltamivir-Resistant Human and Avian Influenza Viruses. *Biotechnol. Lett.* **2008**, *30*, 475–479.

(88) Park, D.; Larson, A. M.; Klibanov, A. M.; Wang, Y. Antiviral and Antibacterial Polyurethanes of Various Modalities. *Appl. Biochem. Biotechnol.* **2013**, *169*, 1134–1146.

(89) Liu, H.; Kim, Y.; Mello, K.; Lovaasen, J.; Shah, A.; Rice, N.; Yim, J. H.; Pappas, D.; Klibanov, A. M. Aerosol-Assisted Plasma Deposition of Hydrophobic Polycations Makes Surfaces Highly Antimicrobial. *Appl. Biochem. Biotechnol.* **2014**, *172* 1254–1264.

(90) Tuladhar, E.; de Koning, M. C.; Fundeanu, I.; Beumer, R.; Duizer, E. Different Virucidal Activities of Hyperbranched Quaternary Ammonium Coatings on Poliovirus and Influenza Virus. *Appl. Environ. Microbiol.* **2012**, *78*, 2456–2458.

(91) Liao, P.; Hu, J.; Wang, H.; Li, J.; Zhou, Z. Recent Advances in Surface-Functionalised Photosensitive Antibacterials with Synergistic Effects. *Biosurface and Biotribology*. **2019**, *5*, 97–103.

(92) Aluigi, A.; Sotgiu, G.; Torreggiani, A.; Guerrini, A.; Orlandi, V. T.; Corticelli, F.; Varchi, G. Methylene Blue Doped Films of Wool Keratin with Antimicrobial Photodynamic Activity. *ACS Appl. Mater. Interfaces* **2015**, *7*, 17416–17424.

(93) Costa, L.; Faustino, M. A. F.; Neves, M. G. P. M. S.; Cunha, Â.; Almeida, A. Photodynamic Inactivation of Mammalian Viruses and Bacteriophages. *Viruses* **2012**, *4*, 1034–1074.

(94) Si, Y.; Zhang, Z.; Wu, W.; Fu, Q.; Huang, K.; Nitin, N.; Ding, B.; Sun, G. Daylight-Driven Rechargeable Antibacterial and Antiviral Nanofibrous Membranes for Bioprotective Applications. *Sci. Adv.* **2018**, *4*, eaar5931.

(95) Alvarado, D. R.; Argyropoulos, D. S.; Scholle, F.; Peddinti, B. S. T.; Ghiladi, R. A. A Facile Strategy for Photoactive Nanocellulose-Based Antimicrobial Materials. *Green Chem.* **2019**, *21*, 3424–3435.

(96) Carpenter, B. L.; Scholle, F.; Sadeghifar, H.; Francis, A. J.; Boltersdorf, J.; Weare, W. W.; Argyropoulos, D. S.; Maggard, P. A.; Ghiladi, R. A. Synthesis, Characterization, and Antimicrobial Efficacy of Photomicrobicidal Cellulose Paper. *Biomacromolecules* **2015**, *16*, 2482–2492.

(97) Verhaelen, K.; Bouwknegt, M.; Rutjes, S.; Maria, A.; Husman, R.; Duizer, E. Wipes Coated with a Singlet-Oxygen-Producing Photosensitizer are Effective against Human Influenza Virus but Not Against Norovirus. *Appl. Environ. Microbiol.* **2014**, *80*, 4391-4397.

(98) Kim, J.; Lee, H.; Lee, J.-Y.; Park, K.-H.; Kim, W.; Lee, J. H.; Kang, H.-J.; Hong, S. W.; Park, H.-J.; Lee, S. Photosensitized Production of Singlet Oxygen *via* C_{60} Fullerene Covalently Attached to Functionalized Silica-Coated Stainless-Steel Mesh: Remote Bacterial and Viral Inactivation. *Appl. Catal. B Environ.* **2020**, *270*, 118862.

(99) Lhotáková, Y.; Plíštil, L.; Morávková, A.; Kubát, P.; Lang, K.; Forstová, J.; Mosinger, J. Virucidal Nanofiber Textiles Based on Photosensitized Production of Singlet Oxygen. *PLoS One* **2012**, 7, e49226.

(100) Stanley, S. L.; Scholle, F.; Zhu, J.; Lu, Y.; Zhang, X.; Situ, X.; Ghiladi, R. A. Photosensitizer-Embedded Polyacrylonitrile Nanofibers as Antimicrobial Non-Woven Textile. *Nanomaterials* **2016**, *6*, 77.

(101) Iyigundogdu, Z. U.; Demir, O.; Asutay, A. B.; Sahin, F. Developing Novel Antimicrobial and Antiviral Textile Products. *Appl. Biochem. Biotechnol.* **2017**, *181*, 1155–1166.

(102) Nohynek, G. J.; Lademann, J.; Ribaud, C.; Roberts, M. S. Grey Goo on the Skin? Nanotechnology, Cosmetic and Sunscreen Safety. *Crit. Rev. Toxicol.* **2007**, *37*, 251–277.

(103) Skocaj, M.; Filipic, M.; Petkovic, J.; Novak, S. Titanium Dioxide in Our Everyday Life; Is It Safe? *Radiol. Oncol.* **2011**, *45*, 227–247.

(104) Zhang, X. Q.; Yin, L. H.; Tang, M.; Pu, Y. P. ZnO, TiO_2, SiO_2, and Al_2O_3 Nanoparticles-Induced Toxic Effects on Human Fetal Lung Fibroblasts. *Biomed. Environ. Sci.* **2011**, *24*, 661–669.

(105) de Lima, R.; Seabra, A. B.; Durán, N. Silver Nanoparticles: A Brief Review of Cytotoxicity and Genotoxicity of Chemically and Biogenically Synthesized Nanoparticles. *J. Appl. Toxicol.* **2012**, *32*, 867–879.

(106) Hackenberg, S.; Scherzed, A.; Kessler, M.; Hummel, S.; Technau, A.; Froelich, K.; Ginzkey, C.; Koehler, C.; Hagen, R.; Kleinsasser, N. Silver Nanoparticles: Evaluation of DNA Damage, Toxicity and Functional Impairment in Human Mesenchymal Stem Cells. *Toxicol. Lett.* **2011**, *201*, 27–33.

(107) Shi, Z.; Neoh, K. G.; Zhong, S. P.; Yung, L. Y. L.; Kang, E. T.; Wang, W. *In Vitro* Antibacterial and Cytotoxicity Assay of Multilayered Polyelectrolyte-Functionalized Stainless Steel. *J. Biomed. Mater. Res., Part A* **2006**, *76*, 826–834.

(108) Buchman, J. T.; Hudson-Smith, N. V; Landy, K. M.; Haynes, C. L. Understanding Nanoparticle Toxicity Mechanisms to Inform Redesign Strategies to Reduce Environmental Impact. *Acc. Chem. Res.* **2019**, *52*, 1632–1642.

(109) Umer, A.; Naveed, S.; Ramzan, N.; Rafique, M. S.; Imran, M. A Green Method for the

Synthesis of Copper Nanoparticles Using L-Ascorbic Acid. *Rev. Mater.* **2014**, *19*, 197–203.

(110) El Badawy, A. M.; Silva, R. G.; Morris, B.; Scheckel, K. G.; Suidan, M. T.; Tolaymat, T. M. Surface Charge-Dependent Toxicity of Silver Nanoparticles. *Environ. Sci. Technol.* **2011**, *45*, 283–287.

(111) Wu, F.; Harper, B. J.; Harper, S. L. Differential Dissolution and Toxicity of Surface Functionalized Silver Nanoparticles in Small-Scale Microcosms: Impacts of Community Complexity. *Environ. Sci. Nano* **2017**, *4*, 359–372.

(112) Nie, Z.; Liu, J.; Zhong, C.-J.; Wang, L.-F.; Yang, Y.; Tian, Q.; Liu, Y. Enhanced Radical Scavenging Activity by Antioxidant-Functionalized Gold Nanoparticles: A Novel Inspiration for Development of New Artificial Antioxidants. *Free Radic. Biol. Med.* **2007**. *43*, 1243-1254.

(113) Jokinen, V.; Kankuri, E.; Hoshian, S.; Franssila, S.; Ras, R. H. A. Superhydrophobic Blood-Repellent Surfaces. *Adv. Mater.* **2018**, *30*, 1705104.

(114) Zhang, X.; Wang, L.; Levänen, E. Superhydrophobic Surfaces for the Reduction of Bacterial Adhesion. *RSC Advances*. **2013**, *3*, 12003–12020.

(115) Cheng, Y. T.; Rodak, D. E.; Wong, C. A.; Hayden, C. A. Effects of Micro- and Nano-Structures on the Self-Cleaning Behaviour of Lotus Leaves. *Nanotechnology* **2006**, *17*, 1359–1362.

(116) Hasan, J.; Roy, A.; Chatterjee, K.; Yarlagadda, P. K. D. V. Mimicking Insect Wings: The Roadmap to Bioinspiration. *ACS Biomater. Sci. Eng*. **2019**, *5*, 3139-3190.

(117) Wong, T. S.; Kang, S. H.; Tang, S. K. Y.; Smythe, E. J.; Hatton, B. D.; Grinthal, A.; Aizenberg, J. Bioinspired Self-Repairing Slippery Surfaces with Pressure-Stable Omniphobicity. *Nature* **2011**, *477*, 443–447.

(118) Villegas, M.; Zhang, Y.; Abu Jarad, N.; Soleymani, L.; Didar, T. F. Liquid-Infused Surfaces: A Review of Theory, Design, and Applications. *ACS Nano* **2019**, *13*, 8517–8536.

(119) Epstein, A. K.; Wong, T. S.; Belisle, R. A.; Boggs, E. M.; Aizenberg, J. Liquid-Infused Structured Surfaces with Exceptional Anti-Biofouling Performance. *Proc. Natl. Acad. Sci. U. S. A.* **2012**, *109*, 13182–13187.

(120) Badv, M.; Jaffer, I. H.; Weitz, J. I.; Didar, T. F. An Omniphobic Lubricant-Infused Coating Produced by Chemical Vapor Deposition of Hydrophobic Organosilanes Attenuates Clotting on Catheter Surfaces. *Sci. Rep.* **2017**, *7*, 1–10.

(121) Badv, M.; Weitz, J. I.; Didar, T. F. Lubricant-Infused PET Grafts with Built-In Biofunctional Nanoprobes Attenuate Thrombin Generation and Promote Targeted Binding of Cells. *Small* **2019**, *15*, 1905562.

(122) Badv, M.; Alonso-Cantu, C.; Shakeri, A.; Hosseinidoust, Z.; Weitz, J. I.; Didar, T. F. Biofunctional Lubricant-Infused Vascular Grafts Functionalized with Silanized Bio-Inks Suppress Thrombin Generation and Promote Endothelialization. *ACS Biomater. Sci. Eng.* **2019**, *5*, 6485–6496.

(123) Imani, S. M.; Badv, M.; Shakeri, A.; Yousefi, H.; Yip, D.; Fine, C.; Didar, T. F. Micropatterned Biofunctional Lubricant-Infused Surfaces Promote Selective Localized Cell Adhesion and Patterning. *Lab Chip* **2019**, *19*, 3228–3237.

(124) Hosseini, A.; Villegas, M.; Yang, J.; Badv, M.; Weitz, J. I.; Soleymani, L.; Didar, T. F. Conductive Electrochemically Active Lubricant-Infused Nanostructured Surfaces Attenuate Coagulation and Enable Friction-Less Droplet Manipulation. *Adv. Mater. Interfaces* **2018**, *5*, 1800617.

(125) Osborne, M.; Aryasomayajula, A.; Shakeri, A.; Selvaganapathy, P. R.; Didar, T. F.

Suppression of Biofouling on a Permeable Membrane for Dissolved Oxygen Sensing Using a Lubricant-Infused Coating. *ACS Sensors* **2019**, *4*, 687–693.

(126) Badv, M.; Imani, S. M.; Weitz, J. I.; Didar, T. F. Lubricant-Infused Surfaces with Built-In Functional Biomolecules Exhibit Simultaneous Repellency and Tunable Cell Adhesion. *ACS Nano* **2018**, *12*, 10890–10902.

(127) Wu, R.; Xing, S.; Badv, M.; Didar, T. F.; Lu, Y. Step-Wise Assessment and Optimization of Sample Handling Recovery Yield for Nanoproteomic Analysis of 1000 Mammalian Cells. *Anal. Chem.* **2019**, *91*, 10395–10400.

(128) Hasan, J.; Xu, Y.; Yarlagadda, T.; Schuetz, M.; Spann, K.; Yarlagadda, P. K. Antiviral and Antibacterial Nanostructured Surfaces with Excellent Mechanical Properties for Hospital Applications. *ACS Biomater. Sci. Eng.* **2020**, *6*, 3608–3618.

(129) Chauhan, P.; Kumar, A.; Bhushan, B. Self-Cleaning, Stain-Resistant and Anti-Bacterial Superhydrophobic Cotton Fabric Prepared by Simple Immersion Technique. *J. Colloid Interface Sci.* **2019**, *535*, 66–74.

(130) Lee, E. C.; Davis-Poynter, N.; Nguyen, C. T. H.; Peters, A. A.; Monteith, G. R.; Strounina, E.; Popat, A.; Ross, B. P. GAG Mimetic Functionalised Solid and Mesoporous Silica Nanoparticles as Viral Entry Inhibitors of Herpes Simplex Type 1 and Type 2 Viruses. *Nanoscale* **2016**, *8*, 16192–16196.

(131) Mannelli, I.; Reigada, R.; Suárez, I.; Janner, D.; Carrilero, A.; Mazumder, P.; Sagués, F.; Pruneri, V.; Lakadamyali, M. Functionalized Surfaces with Tailored Wettability Determine Influenza A Infectivity. *ACS Appl. Mater. Interfaces* **2016**, *8*, 15058–15066.

(132) Kawabata, N.; Yamazaki, K.; Otake, T.; Oishi, I.; Minekawa, Y. Removal of Pathogenic Human Viruses by Insoluble Pyridinium-Type Resin. *Epidemiol. Infect.* **1990**, *105*, 633–

642.

(133) Kawabata, N.; Ujino, I. Removal of Virus from Air by Filtration Using a Composite Microporous Membrane Made of Crosslinked Poly (N-Benzyl-4-Vinylpyridinium Chloride). *React. Funct. Polym.* **1998**, *37*, 213–218.

(134) Xue, Y.; Xiao, H. Antibacterial/Antiviral Property and Mechanism of Dual-Functional Quaternized Pyridinium-Type Copolymer. *Polymers (Basel).* **2015**, *7*, 2290–2303.

(135) Ristic, B. Z.; Milenkovic, M. M.; Dakic, I. R.; Todorovic-Markovic, B. M.; Milosavljevic, M. S.; Budimir, M. D.; Paunovic, V. G.; Dramicanin, M. D.; Markovic, Z. M.; Trajkovic, V. S. Photodynamic Antibacterial Effect of Graphene Quantum Dots. *Biomaterials* **2014**, *35*, 4428–4435.

(136) Habiba, K.; Bracho-Rincon, D. P.; Gonzalez-Feliciano, J. A.; Villalobos-Santos, J. C.; Makarov, V. I.; Ortiz, D.; Avalos, J. A.; Gonzalez, C. I.; Weiner, B. R.; Morell, G. Synergistic Antibacterial Activity of PEGylated Silver-Graphene Quantum Dots Nanocomposites. *Appl. Mater. Today* **2015**, *1*, 80–87.

(137) Zhu, S.; Zhang, J.; Qiao, C.; Tang, S.; Li, Y.; Yuan, W.; Li, B.; Tian, L.; Liu, F.; Hu, R.; Gao, H.; Wei, H.; Zhang, H.; Sun, H.; Yang, B. Strongly Green-Photoluminescent Graphene Quantum Dots for Bioimaging Applications. *Chem. Commun.* **2011**, *47*, 6858–6860.

(138) Technology: GermStopSQ – Envision SQ. https://envisionsq.com/technology-germstop/ (accessed Aug 19, 2020).

(139) COVAGUARD^{TM} PLATFORM — Covalon Technologies Ltd. https://www.covalon.com/covaguard-platform (accessed Aug 19, 2020).

(140) Technologies - Bio-Gate AG. https://www.bio-gate.de/en/technologies/ (accessed Aug 19, 2020).

(141) Bio-Fence – Antimicrobial, Antiviral Coatings. https://www.bio-fence.com/ (accessed Aug 19, 2020).

(142) Homepage | Allied BioScience. https://www.alliedbioscience.com/ (accessed Sep 1, 2020).

(143) Glynson, B. C. G.; Yeterian, A. A.; Sigalos, J. L.; Mallow, W. A. Novel Uses of Calcium Hydroxide. CA 2598203, November 4, 2005.

(144) Alistagen Corporation. EPA-Approved Antimicrobial Surface Coating Represents Breakthrough in the Control and Spread of Infectious Diseases, 2020. PR Newswire. https://www.prnewswire.com/news-releases/epa-approved-antimicrobial-surface-coating-represents-breakthrough-in-the-control-and-spread-of-infectious-diseases-301027074.html (accessed Sep 1, 2020).

(145) Ready, T. FDA Clears First Antiviral Surgical Mask, 2011. Medscape. https://www.medscape.com/viewarticle/745801 (accessed Sep 1, 2020).

(146) Møretrø, T.; Langsrud, S. Residential Bacteria on Surfaces in the Food Industry and Their Implications for Food Safety and Quality. *Compr. Rev. Food Sci. Food Saf.* **2017**, *16*, 1022–1041.

(147) Chaoui, L.; Mhand, R.; Mellouki, F.; Rhallabi, N. Contamination of the Surfaces of a Health Care Environment by Multidrug-Resistant (MDR) Bacteria. *Int. J. Microbiol.* **2019**, *2019*, 3236526.

(148) Ong, S. W. X.; Tan, Y. K.; Chia, P. Y.; Lee, T. H.; Ng, O. T.; Wong, M. S. Y.; Marimuthu, K. Air, Surface Environmental, and Personal Protective Equipment Contamination by Severe Acute Respiratory Syndrome Coronavirus 2 (SARS-CoV-2) from a Symptomatic Patient. *JAMA - J. Am. Med. Assoc.* **2020**, *323*, 1610–1612.

(149) Kampf, G. Potential Role of Inanimate Surfaces for the Spread of Coronaviruses and Their

Inactivation with Disinfectant Agents. *Infect. Prev. Pract.* **2020**, *2*, 100044.

3 Producing Fluorine-Free and Lubricant-Free Flexible Pathogen and Blood Repellent Surfaces Using Polysiloxane-Based Hierarchical Structures

Liane Ladouceur[1], Amid Shakeri[2], Shadman Khan[1], Alejandra Rey Rincon[1,3], Jeffrey I. Weitz[1,4,5,6], Leyla Soleymani[1,3], Tohid F Didar[1,2,7]

[1]School of Biomedical Engineering, 1280 Main St W, McMaster University, Hamilton, Ontario, Canada, L8S 4L8

[2]Department of Mechanical Engineering, 1280 Main St W, McMaster University, Hamilton, Ontario, Canada, L8S 4L8

[3]McMaster University, Department of Engineering Physics, 1280 Main Street West, Hamilton, L8S 4L7, Canada

[4]Department of Medicine, 1280 Main St W, McMaster University, Hamilton, Ontario, Canada, L8S 4L8

[5]Department of Biochemistry and Biomedical Sciences, 1280 Main St W, McMaster University, Hamilton, Ontario, Canada, L8S 4L8

[6]Thrombosis & Atherosclerosis Research Institute (TaARI), 237 Barton Street East, Hamilton, Ontario, Canada, L8L 2X2

[7]Institute for Infectious Disease Research (IIDR), 1280 Main St W, McMaster University, Hamilton, Ontario, Canada, L8S 4L8

Author Contributions: LL was involved in the design and execution of all experiments and data analysis. TFD and LS designed the experiments and supervised the project. AS, SK and ARR conducted specific bioassays with samples provided by LL and assisted in data analysis. LL wrote the manuscript with contributions from ARR and TD.

KEYWORDS: Fluorine-free repellent surfaces, lubricant-free repellent surfaces, superhydrophobicity, hierarchical surfaces, polysiloxane nanostructures, pathogen repellent surfaces

3.1 Abstract

High-touch surfaces are known to be a major route for the spread of pathogens in healthcare and public settings. Antimicrobial coatings have therefore garnered significant attention to help mitigate transmission of infectious diseases via the surface route. Among antimicrobial coatings, pathogen repellant surfaces provide unique advantages such as instant repellency, affordability, biocompatibility, and long-term stability. While many advances in the fabrication of biorepellent surfaces have been made over the past two decades, this area of research continues to suffer challenges in scalability, cost, compatibility with high-touch applications and performance for pathogen repellency. These features are critical for high-touch surfaces to be used in public settings. Additionally, the environmental impact of manufacturing repellent surfaces continues to be a challenge, mainly due to the use of fluorinated coatings. Here, we present a flexible hierarchical coating with straightforward manufacturing and cost-effective steps without the use of fluorine or lubricant. Hierarchical surfaces were prepared through growth of polysiloxane nanostructures using n-propyltrichlorosilane (n-PTCS) on activated polyolefin, followed by heat shrinking to induce microscale wrinkles. The developed coatings demonstrated repellency, with contact angles over 153° and sliding angles <1°. When mimicking an actual touch assay, these hierarchical surfaces demonstrated a 97.5% reduction in transmission of *Escherichia coli* (*E.coli*), demonstrating their potential as antimicrobial coatings to mitigate the spread of infectious diseases. Additionally, the developed surfaces displayed a 93% reduction in blood staining after incubation with human whole blood.

3.2 Introduction

Surface contamination plays a major role in spread and transmission of pathogens. Whether in healthcare, food supply chain or in public spaces, the risk for pathogen spread through fomites has been extensively demonstrated.[1] In the healthcare system, a major risk is presented by healthcare-associated infections (HAIs). Centers for Disease Control and Prevention (CDC) reports from 2019 estimate that each day 1 in 31 patients across the U.S. are fighting infections associated with their hospital care. [2] For instance, a serious threat is posed by Carbapenem-resistant Enterobacteriaceae (CRE), a family of pathogens which are resistant to nearly all antibiotics, accounting for 13,100 cases of infection and resulting in an estimated 1,100 deaths in 2017.[3] Transmission of pathogens by healthcare workers through direct contact with infected patients or indirectly by touching contaminated surfaces in patient areas has been estimated to account for 20 to 40% of HAIs.[4] This highlights the importance of designing repellent surfaces that resist contamination or biofouling. While many efforts have been made to tackle this problem, proposed solutions face numerous limitations including cost-prohibitive production methods, environmentally unfriendly materials or incompatibility with high-touch applications.[5]–[7]

To achieve these repellent properties, researchers aim to create superhydrophobic surfaces characterized by contact angles >150 degrees and sliding angles <10 degrees.[8] Strategies for manufacturing are often bioinspired, such as physical modifications to add roughness inspired by the multiscale texture found on lotus leaves and butterfly wings. [9], [10] This increased roughness provides the basis for Cassie-Baxter or Wenzel wetting states.[11], [12] Conventional techniques to accomplish roughness include etching,[13]–[15] electrochemical deposition,[16], [17] templating,[18], [19] spray coatings,[20], [21] application of nanoparticles such as gold or silica,[22], [23] and sol-gel processes. [24] To closely replicate the lotus effect, researchers

commonly employ a series of these modifications to introduce hierarchical structuring. [25]–[27] By implementing multiple-step approaches, both micro- and nano-scale features are established on surfaces, which can be employed for biorepellency. [25], [28], [29] While these techniques have demonstrated success, it is often difficult to produce these surfaces on a large scale due to manufacturing limitations and prohibitive costs of reagents involved.[6]

Alternatively, chemical modification can be employed to decrease the surface free energy (SFE) of manufactured surfaces, using techniques such as chemical vapour deposition (CVD),[30] liquid phase deposition (LPD),[31] plasma,[32] self-assembly[33]–[35] and solution immersion.[36] These approaches frequently utilize silane molecules to form mono- or multilayer coatings that decrease SFE and can be paired with physical modification to demonstrate superhydrophobic properties. The silane molecules employed contain reactive functional groups such as chlorine, which facilitate self-assembled coatings through surface-initiated condensation reactions and allow ease and control of fabrication.[37] Often, fluorocarbons constitute the backbone of these chemicals, such as those included in trichloro(1H, 1H, 2H, 2H-perfluorooctyl) silane (TPFS) and 1H, 1H, 2H, 2H-perfluorodecyltrichlorosilane (PFDTS). However, these chemicals present potentially serious environmental risks. Long-term studies have demonstrated the toxic effects of long-chain (C9-C20) fluorocarbons and their precursors in mammals,[38] as well as the persistence of these and shorter chains in the environment leading to a bioaccumulation in plants, animals, and humans.[38]–[40] Recent research has confirmed the safety of short-chain (≤5 carbon) fluorocarbons, though the long-term impact of the more pervasive 8-carbon chains remains unknown. [41] For this reason, research has turned to more environmentally friendly modification strategies.

Growth of polysiloxane nanostructures to convey superhydrophobicity has offered a more environmentally friendly approach, first investigated in 2006 by Artus et al.[42] By utilizing trichlorosilane molecules with short, one or two carbon chains and without fluorine groups, coatings have been achieved through both CVD and LPD. [43]–[45] These structures demonstrate a promising route for inducing surface roughness, leading to superhydrophobicity and self-cleaning properties, which has more recently been established for three-carbon chain trichlorosilanes as well.[46], [47] Few reports of pathogen repellency for these surfaces exist, likely due to the conflicting results that have been seen. For example, when coated on glass, polysiloxane nanofilaments and rod structures exhibited varying behaviour for static versus dynamic conditions, based on the type of bacteria tested. [48] Effectiveness was also highly dependent on the architecture of the coating, which research has demonstrated depends heavily on humidity level, temperature, and substrate. [49]

To address the challenges with pathogen repellency that polysiloxane structured surfaces experience, our group has recently employed lubricant. When combined with a silicone oil lubricant layer to imitate the slippery properties of the pitcher plant,[50] polysiloxane nanofilaments were shown to prevent bacterial adhesion and supress thrombosis on medical devices such as catheters and splints.[47] Slippery, liquid-infused surfaces (LIS) represent an exceptional alterative surface modification method with self-cleaning properties. Here, lubricants are added to a chemically or structurally modified surface which is designed to trap a lubricant layer. Excellent performance is demonstrated in liquid repellency, with sliding angles <5°. [51] LIS have demonstrated biorepellent properties with many applications in closed spaces or under flow, using bacteria, viruses and complex biofluids.[52]–[54] Limitations to these surfaces exist,

however, as their liquid-infused nature precludes use for high-touch surfaces. Additionally, many of the lubricants employed are quite volatile, making open-air surfaces impractical. [7]

Herein, the nanoscale polysiloxane features created via CVD treatment with n-PTCS have been paired with microscale features created on a thin thermoplastic material, polyolefin (PO). Employing the advantages of facile, low-cost, and environmentally safe production, we produce a flexible, superhydrophobic hierarchical surface that aims to match the performance of lubricated surfaces such that these may be used in high-touch, open-air settings. Through optimization of the coating process under strict humidity conditions, we have found that the polysiloxane nanostructures provide a sufficiently stiff layer to induce microscale wrinkles upon heat treatment, ultimately producing a hierarchically structured surface. The final product is a flexible, superhydrophobic, biorepellent surface with demonstrated capability to repel bacteria and complex biofluids such as human whole blood.

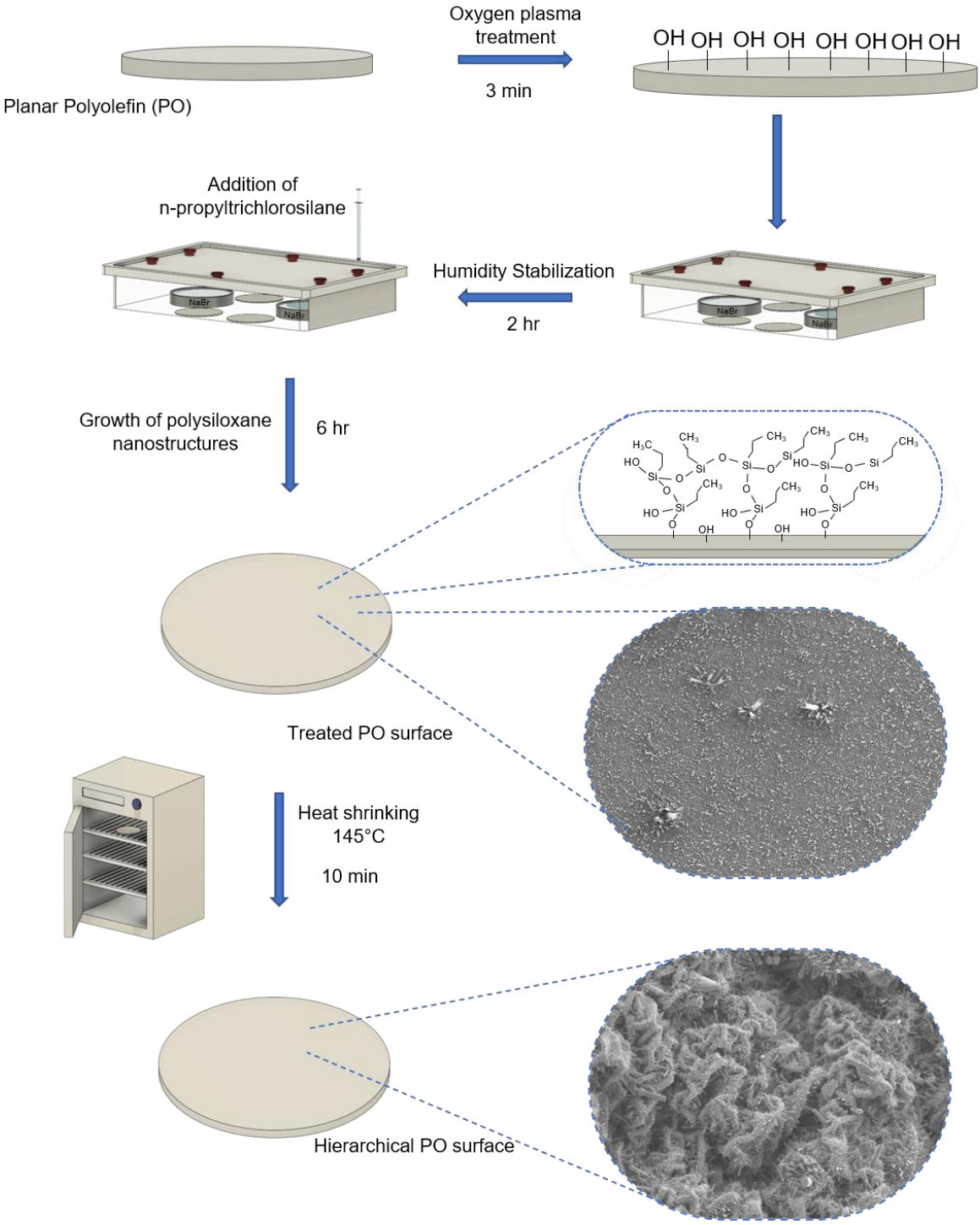

Figure 3.1 Schematic representation of the fabrication process for hierarchical PO surfaces. PO is cut to size then activated using a 3 min oxygen plasma treatment. Immediately following activation, they are placed in a customized humidity chamber for 2 hr to stabilize humidity at ~55%. Addition of n-PTCS is through rubber stoppers to maintain the seal on the chamber. After 6 hr CVD treatment, surfaces are wrinkled using heat treatment at 145°C for 10 min.

3.3 Results and Discussion

Fabrication and Characterization of Polysiloxane Hierarchical Surfaces

We have optimized surface fabrication into a straightforward, three-step method. First, planar PO is activated through oxygen plasma treatment. Next, a custom-made humidity chamber is employed for 6-hr growth of polysiloxane nanostructures on the PO surfaces. Finally, coated surfaces are subjected to heat treatment at 145°C for 10 minutes as further explained in methods (**Figure 3.1**). This procedure to achieve replicable and robust hierarchical surfaces was developed by varying surface activation and substrate incubation time. Bi-directionally strained polyolefin, a widely available polymer, was chosen as the substrate to ensure scalability. To begin, substrates were activated using oxygen plasma treatment. 3-minute and 5-minute activation times were tested, with no significant difference in final surface characteristics (**see Figure 3.S1**). 55% relative humidity (RH) was achieved inside the chamber using an inexpensive supersaturated sodium bromide solution setup. To maintain RH, n-propyltrichlorosilane was introduced to the customized chamber through a sealed rubber stopper. Incubation times were varied to investigate the ideal nanostructure growth for hierarchical surface fabrication, testing 6 hr, 12 hr, 18 hr and 24 hr. Surfaces were tested for contact and sliding angle as a means of quality control. Expected contact angles were above 150° and sliding angles ~1 °. Using a 5 µL drop, water would bounce off or skate across ideal surfaces, a quick measure of satisfactory performance (**Figure 3.2a**). Acceptable surfaces were then subjected to heat treatment at 145°C for 10 minutes to obtain the final hierarchical surface.

Initial characterization of each type of surface included contact and sliding angle measurements (**Figure 3.2b**), as well as visualization using scanning electron microscopy (SEM) (**Figure 3.2c**). Unless otherwise stated, contact angle measurement used a 2 µL droplet while

sliding angle measurements were taken with a 5 µL droplet. Treated surfaces demonstrated water contact angles >150° for both planar and hierarchical conditions, while sliding angles with water varied greatly on planar surfaces but consistently measured <15° on shrunk surfaces. Based on these results, a hierarchical surface after 6-hr incubation was selected as the highest performing surface. Here, the water contact angle was 153.4° and sliding angle was <1° (**Figure 3.2b**). Using SEM, it was possible to confirm the hierarchical structure of the surfaces following shrinking (**Figure 3.2c**). Polysiloxane nanostructures are visible on the surface prior to heat treatment and remain visible on the final wrinkled structures. Based on dimensions of these nanostructures confirmed through side views of the surface (**Figure 3.2d**), both filament and rod structures are visible on the surface, in some cases developing out of volcanos.[49] Through many rounds of fabrication, it was determined that coating density and thickness of surface coating prior to heat treatment can alter the wrinkle structure and lead to crack formation. In cases where the coating became more visible to the naked eye, having an opaque, white colour as seen in **supplementary figure 3.S2(i)**, heat treatment caused cracking in the microstructure of the surface, presumably arising from an increased level of strain experienced in these areas of the surface which is known to alter wrinkle formation. [55] Cracked surfaces presented with a texture visible to the naked eye, which was confirmed with SEM images (**supplementary figure 3.S2(ii-iv)**). To ensure these deformations were not caused by treatment after fabrication, hierarchical surfaces were subjected to a series of washes in ethanol using sonication. Superhydrophobic properties were retained through all washes, as shown in **Figure 3.2e.**

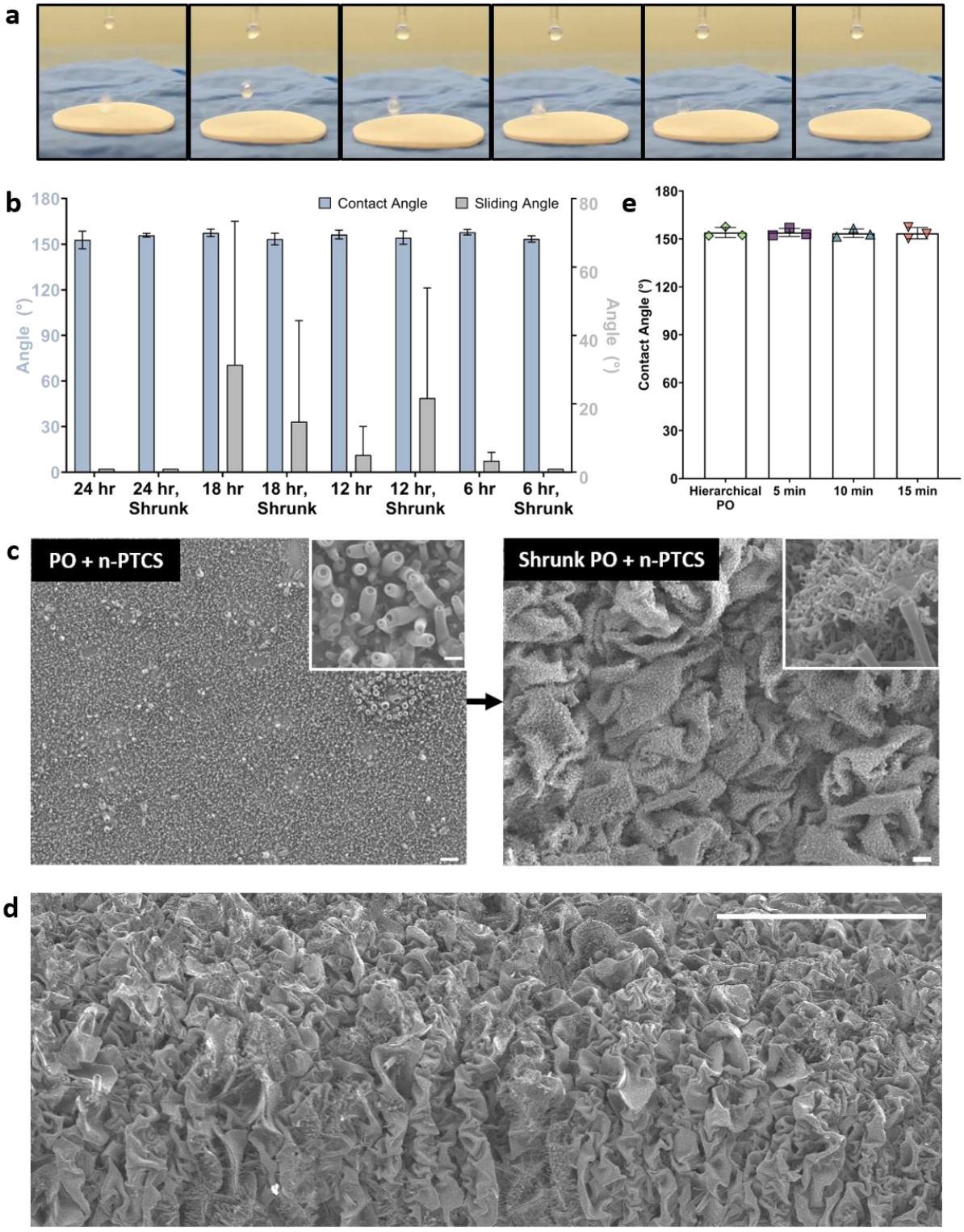

Figure 3.2 a) Frame-by-frame images of water droplet bouncing on hierarchical surface. 5 µL water droplet shows two bounces, with decreasing height when dropped from ~10 mm height. **b) Optimization of the incubation with n-PTCS was characterized using contact and sliding**

angle data. Contact angles remained >150° across all incubations, while sliding angles demonstrated reductions for 24hr and 6hr treatments with significantly less variability seen in these samples. Error bars represent the standard deviation calculated across a minimum of 3 replicate measurements. **c) SEM images of planar and shrunk samples at ideal incubation time.** Scale bar 10 µm, 1 µm for inset. **d) Side view SEM image of 6 hr shrunk surface.** Raw edge of sample was imaged using 45° tilted stub and 45° tilt of stub to produce a side view. Scale bar 100 µm. **e) Sonication in ethanol stability test.** Contact angle data for hierarchical surface subjected to a series of sonication treatments in ethanol.

Addition of Lubricant Layer

Previous research has demonstrated the excellent performance of silicone oil infused nanofilament coatings on glass and various medical devices.[46], [47] To date, this approach has not been tested using a polyolefin substrate. Accordingly, to illustrate a fair comparison of the capability of n-PTCS treated hierarchical surfaces, and thus consider our hierarchical surfaces as a viable replacement for the lubricant-infused approach, it was necessary to create the rival condition. Silicone oil viscosity was varied (10 cSt, 20 cSt, 50 cSt, 100 cSt, 350 cSt, and 1000 cSt) and water contact and sliding angle measurements were taken (**supplementary figure 3.S3**). Contact angles did not demonstrate significant differences across viscosities, however sliding angles decreased with mid-range viscosity. Due to the lower volatility of high viscosity oils, 100 cSt was selected as the ideal case for further experiments, with a 14.1° sliding angle for treated planar surfaces and 5° sliding angle for hierarchical surfaces.

Performance in Complex Biofluids

To evaluate performance of these surfaces in the presence of complex biofluids, preliminary characterization with citrated whole blood was performed (**Figure 3.3a**). Remarkably, after removal of blood droplets for these measurements, hierarchical surfaces showed no staining with the fluid. Prompted by this unexpected characteristic, a droplet staining test was performed by introducing 5 µL droplets of citrated whole blood on samples. Since drying of the droplet

surface was a concern, samples were stored in a humidified petri dish for the duration of the test. Droplets were incubated for 15 min. Hierarchical surfaces demonstrated a full cleaning ability to the naked eye (**Figure 3.3b**). In order to quantify these results, the integrated density of intensity in images of each surface was measured. Intensity measurement trends aligned with visual evaluations, indicating that hierarchical surfaces significantly outperformed control conditions at all time points (**Figure 3.3c**).

Given the success of the droplet study, an additional staining test was run. Surfaces were incubated in citrated whole blood for 20 minutes then gently removed and untreated sides of the sample were wiped clean. Surfaces were then placed in wells filled with DI water and shaken for 30 minutes to remove blood that had adhered to the surface. Measuring the relative absorbance of these wells illustrates once more the resistance to staining of the hierarchical surfaces, with a significant reduction between planar PO and our hierarchical surfaces shown in **Figure 3.3d**.

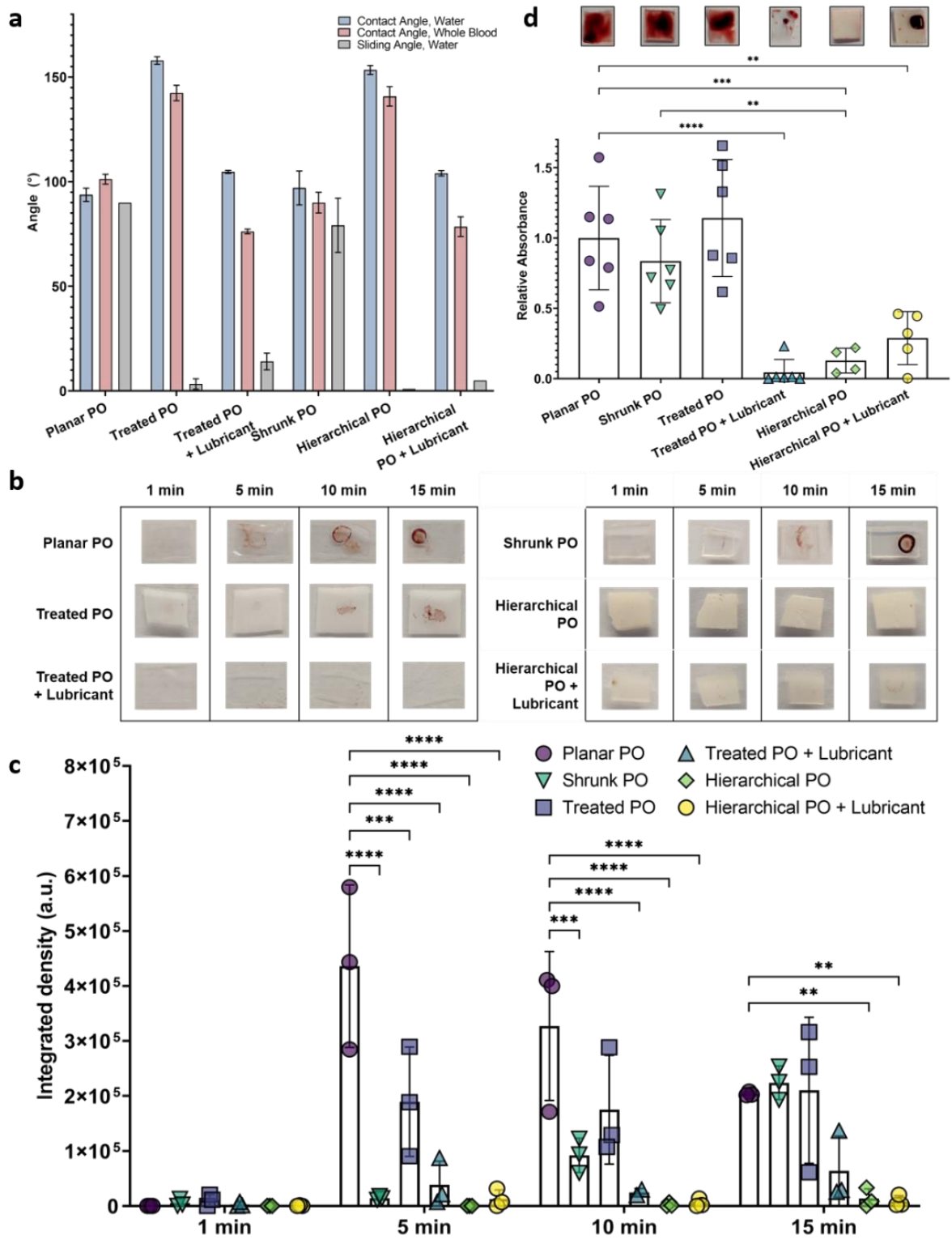

Figure 3.3 a) Comparative summary of contact angle and sliding angle measurements for water and blood. **b) Optical images of residue left by blood droplets.** 5 µL droplets of citrated human

whole blood were introduced to the surface for the time indicated to evaluate staining of surfaces. **c) Quantitative evaluation of blood droplet staining.** Images such as samples in b) were evaluated in ImageJ to obtain integrated density values. Significant reduction was calculated using a two-way ANOVA test and demonstrated across multiple groups, indicated here with ** (P= 0.01), *** (P = 0.001) and **** (P = 0.0001). Error bars represent standard deviation. **d) Relative absorbance values from whole blood staining.** Data is normalized to the control condition, planar PO. Optical images of a sample surfaces are shown below each condition on the plot. Significance was tested with a one-way ANOVA and is indicated here with ** (P = 0.01), ***(P = 0.001) and **** (P = 0.0001)

Preventing Pathogen Transfer to High-Touch Surfaces

We designed an experiment to mimic pathogen transfer to high-touch surfaces. For this purpose, bacterial repellency of the hierarchical surfaces was investigated using *E. coli* K-12 bacteria transfected with green fluorescent protein (GFP). Using agar plugs incubated for 5 minutes with GFP transfected *E. coli* K-12, surfaces were stamped with bacteria. Bacterial adhesion was quantified using fluorescence intensity by imaging surfaces, as seen in **Figure 3.4a**. Hierarchical surfaces demonstrated a 1.6-log (97.5%) reduction in comparison to planar PO, demonstrating the capability of these surfaces to resist the transfer of bacteria (**Figure 3.4b**). Further studies were performed to investigate the colony-forming units (CFU) propagated by these surfaces after the same transmission procedure using agar plugs. In this case, hierarchical surfaces exhibited a 1.2-log reduction (93%) in comparison to the control group, as shown in **Figure 3.4c**. Together, these results indicate a significant resistance to surface contamination using the developed lubricant and fluorine-free hierarchical surfaces. Beyond this, our results also demonstrate no significant differences between the ideal hierarchical surface and a lubricated hierarchical surface. In fact, our hierarchical surface out-performed the planar surface treated with n-PTCS and lubricant (treated PO + lubricant) for this touch assay, as seen in **Figure 3.4b**. This performance is in parallel to previous hierarchical surfaces produced by our group, which demonstrated a 20-fold reduction in fluorescent signal using the same experimental design,

however were manufactured using a fluorosilane coating. [25] Additionally, these surfaces perform consistently with our initial investigations using polysiloxane nanostructures, which demonstrated significant reductions in bacterial adhesion to glass slides coated with n-PTCS and infiltrated with silicone oil lubricant.[47]

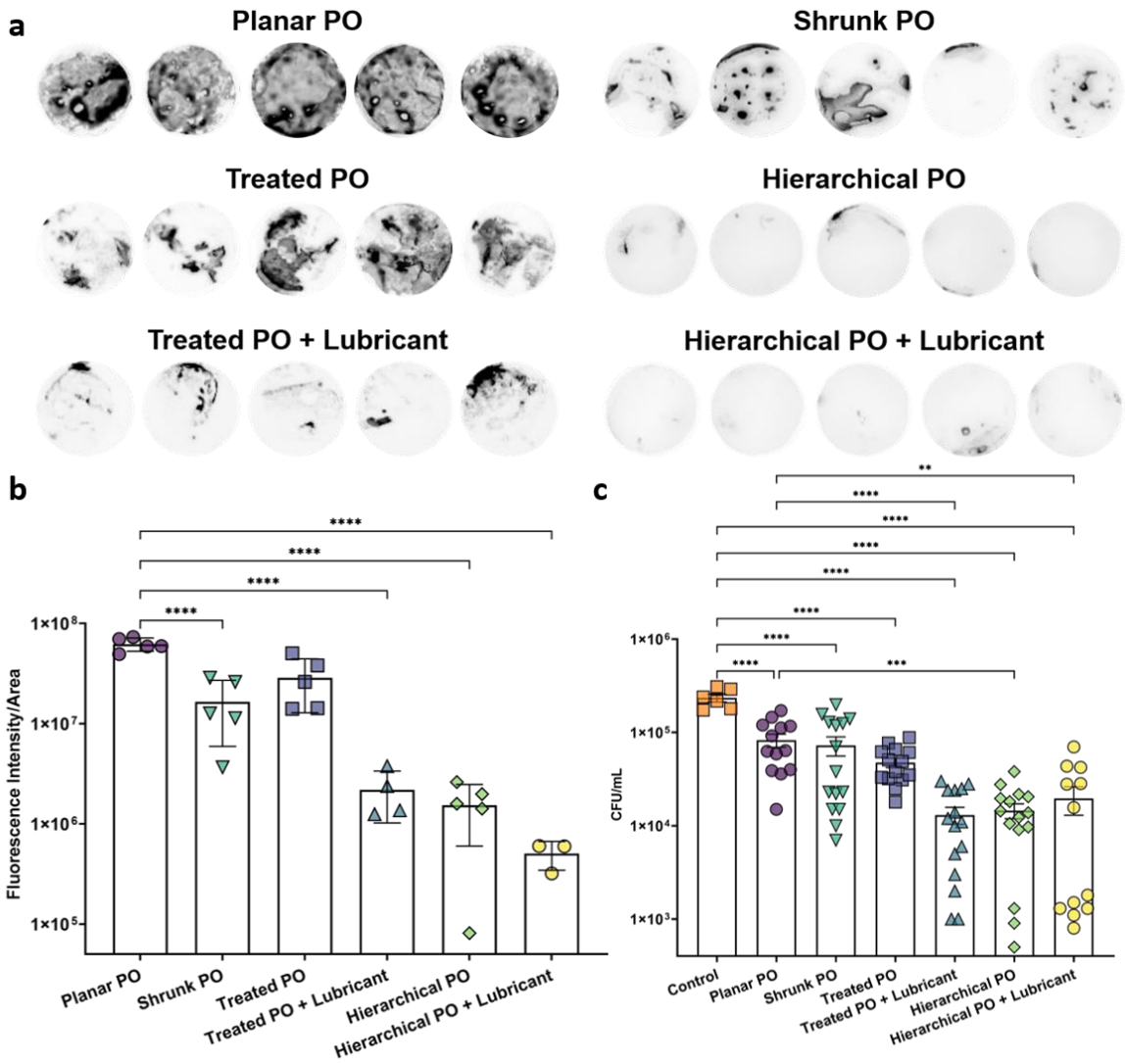

Figure 3.4 a) Fluorescent images of surfaces after bacterial transfer from agar stamps. Surfaces were stamped with GFP tagged *E.coli* K12 and imaged using the Amersham Typhoon imaging system. **b) Quantitative evaluation of fluorescence images using intensity/area.** Values were calculated using ImageJ software. **c) Direct quantification of bacteria transferred from agar stamps.** Samples of bacteria from each condition were plated and incubated overnight to allow growth. Plots use log scale. Error bars represent the standard error of the mean. One-way ANOVA tests were used to evaluate significance, indicated here using *** (P=0.001) and **** (P = 0.0001).

3.4 Conclusion

We have presented here a simple, affordable, and fluorine-free method to manufacture superhydrophobic, biorepellent surfaces with novel topography that achieves performance equivalent to lubricant-infused surfaces. This was achieved by combining established techniques of polysiloxane nanostructuring and wrinkling of thermoplastic polymers to attain a hierarchical, stable surface. By optimizing the n-PTCS coating on polyolefin, a reliable wrinkle structure could be obtained that conveyed superhydrophobic, strongly repellent properties. These surfaces demonstrate obvious applications as high-touch surfaces and further in the healthcare and food industries, based on their repellency to pathogens and stability in cleaning agents such as ethanol. Future efforts will investigate the applications of these surfaces in more long-term biomedical applications such as catheters and implants and as cell-culture platforms.

3.5 Methods

Reagents. n-Propyltrichlorosilane (98%) was purchased from Thermo Fisher Scientific (Whitby, Ontario, Canada). Sodium Bromide (99%) and silicone oils with varying viscosities (10, 20, 50, 100, 350, and 1000 cSt) were purchased from Sigma-Aldrich (Oakville, Ontario, Canada). Ethanol (anhydrous) was purchased from Greenfield (Brampton, Ontario, Canada). Deionized water was used to prepare solutions. *Escherichia coli* K-12 MG1655 transfected with pUA66-GadB GFP was kindly donated by Dr. Eric Brown. LB broth powder was purchased from ThermoFisher Scientific (Whitby, ON). Agar was purchased from Bio-Rad. Kanamycin was purchased from Sigma-Aldrich (Oakville, ON). Venous human whole blood was collected in tubes containing sodium citrate from healthy donors by a licensed phlebotomist. All donors provided a written consent prior to donating blood. All procedures were approved by the McMaster University Research Ethics Board.

Preparation of Substrates. Polyolefin (Cryovac D-955) was cut into desired substrate sizes and shapes. Each substrate was washed with deionized water and ethanol, then dried with nitrogen gas. Three- or five-minute oxygen plasma treatment (Plasma Etch PE-100 Benchtop Plasma Etching System, Carson City, Nevada) was used to activate the surface of each substrate with hydroxyl groups.

Growth of Nanofilaments. Following plasma treatment, substrates were coated with n-PTCS nanofilaments. Samples were first placed inside a sealed chamber for a two-hour humidity stabilization period. Relative humidity was controlled using a super-saturated sodium bromide solution housed at the bottom of the chamber. After the desired RH (around 55%) was obtained, n-PTCS was added to the chamber through sealed rubber stoppers. Surface-initiated polymerization was allowed to proceed for varying times (6 hrs, 12 hrs, 18 hrs and 24hrs) at room temperature.

Hierarchical Surfaces. Subsequent to coating, some samples were further modified using heat treatment. Substrates were placed on a silicon wafer inside an oven preheated to 145°C for 10 minutes to induce wrinkling, resulting in hierarchical surfaces.

Stability Testing. To confirm surface stability through washing with ethanol, hierarchical surfaces were subjected to a series of washes in ethanol using sonication. 7 mL of ethanol was added to a 15 mL falcon tube and a hierarchical surface was submerged. Contact and sliding angle measurements were obtained after sonication for 5, 10, and 15 minute periods.

Lubricated Surfaces. In tests of lubricated conditions, substrates already coated with n-PTCS nanofilaments were further treated with silicone oils of varying viscosities (10, 20, 50, 100, 350 and 100 cSt). Lubricant was added to the substrates for a two-hour incubation, then the substrate

was held vertically for 24 hrs to remove excess oil. Surfaces in this condition were tested immediately following preparation in order minimize additional loss of lubricant.

Sliding and Contact Angle Measurements. Preliminary characteristics of each sample were analyzed using water contact and sliding angle measurements to investigate the wetting properties of the surfaces. Contact angle measurements of samples were obtained using a drop shape analyzer (Kruss DSA30S, Matthews, North Carolina). 2 µL droplets of water were dispensed from the needle and instrument software was used to measure the sessile drop contact angle. Sliding angle measurements were made using a calibrated digital angle level (ROK, Exeter, UK). 5 µL droplets were pipetted onto the sample and the level was tilted slowly until the droplet began to move. For high performing surfaces, droplets often skated across the surface not requiring any tilt to cause movement. These samples were assigned a sliding angle of 1°. In the case that the droplet did not move at 90° or greater, a sliding angle of 90° was assigned. A minimum of three measurements were repeated across the surface for both contact and sliding angle and the average ± standard deviation was reported.

Scanning Electron Microscopy (SEM). In order to visualize the nanostructures formed on the surface, it was necessary to utilize electron microscopy (JEOL JSM-7000F). Samples were prepared as described above and cut to size before mounting to stubs using carbon tape and nickel paste, then coating with 10 nm of platinum using a sputter coater (Polaron model E1500, Polaron Equipment Ltd., Watford, Hertfordshire). SEM images were collected from a top-down view as well as side view for some samples, using 45° tilted stubs.

Whole Blood Droplet Experiment. Small squares (~5 mm x 5 mm) were cut from larger samples and placed in petri dishes humidified using Kimwipes dampened with DI water. A 5 µL droplet of citrated whole blood was placed on the surface of each sample. At timed intervals of 1, 5, 10, and

15 minutes, a Kimwipe was used to gently wick away the droplet from the surface. Care was taken not to smear the fluid across the surface. Optical images were taken of surfaces using consistent lighting and distance from samples. Integrated density of the intensity in these images was quantified using ImageJ software. Images were first cropped to ensure equivalent regions of interest. Background was subtracted from the images, which were then converted to 8-bit and finally the threshold was set as 0-227. Software then calculated integrated density of these images. Standard deviation is reported with the average of these values, calculated from a minimum of 3 replicates for each condition. A two-way ANOVA was performed to determine significance.

Whole Blood Staining Assay. Samples were cut to 1 cm x 1 cm squares and affixed to the bottom of a 24-well plate using double-sided tape. 500 µL of citrated whole blood was pipetted into each well and incubated for 20 minutes. Following incubation, surfaces were carefully removed from the well, ensuring tape was removed and the untreated side of the sample was clear of any blood. Samples were imaged optically then placed in a fresh well plate with wells containing 700 µL of DI water. Wells were shaken at 100 RPM for 30 minutes using a shaker (VWR Incubating Mini Shaker, Troemner, LLC, Thorofare, NJ) to detach any blood that had adhered to the surfaces. Surfaces were then removed and 200 µL of solution was pipetted into a fresh 96-well plate. Absorbance values were read at 450 nm using a plate reader (Synergy Neo2, BioTek, Winooski, Vermont). Relative absorbance values were calculated in reference to the control samples, planar PO. Values were reported as averages with standard deviation, obtained using a minimum of 3 replicates. A one-way ANOVA was used to determine significance.

Bacterial Adhesion Experiments. Surfaces were cut to size (~15mm diameter) and washed with 70% ethanol prior to use. 250 mL of LB broth was combined with 125 µL of Kanamycin to create 50 µg/mL LB-Kan media. A pipette tip was used to pick a single bacteria colony and inoculate the

liquid media, the culture was incubated overnight at 37°C, shaken at 220 RPM. Overnight culture was separated into four 50 mL replicates and centrifuged at 4 × g for 10 minutes. Supernatant was then discarded, and pellets were resuspended in 1 mL of fresh LB-Kan media to create the concentrated cell suspension for experimental use. Agar plugs were prepared by adding 300 mL of water to 9 g of agar, producing a 3% agar mixture, which was autoclaved and poured into polystyrene petri dishes to set. Agar plates were stored at 4°C until use. Prior to beginning experimental procedure, agar plugs were cut to size to match the test surfaces (~15mm diameter). Bacteria was introduced to the plug by adding 20 µL of cell suspension, which was then gently spread across the agar using a pipette tip and allowed to incubate for five minutes. Test surfaces were stamped with these plugs and placed between two glass plates. Surfaces were imaged using the Amersham Typhoon imaging system (GE). Unstamped surfaces were used as controls for background fluorescence. Images were analysed using the ImageJ software, and fluorescence intensity was used to measure bacteria transfer onto the surfaces. Standard error of the mean was calculated for these samples using five replicates for each condition. A one-way ANOVA was used to calculate significance.

To directly quantify the number of bacteria transferred to the surfaces, the protocol above was slightly modified. Bacteria culture grown overnight was diluted to approximately 5.7x10^7 CFU/mL and used instead of the concentrated cell suspension. The surfaces were stamped as explained above and then placed into 5mL of LB-Kan media and mixed. Bacterial transfer onto the surfaces was measured by plating media from each stamped sample at various dilutions. In this case, 20 µL of media from the sample was combined with 180 µL of PBS in a 96-well plate with two replicate wells per sample. Dilutions up to 10^{-5} were created for each sample. 100 µL samples were plated in triplicate using a cell spreader and incubated overnight (37°C). Plates were imaged

using the ChemiDoc MP (BioRad) imaging system with the Blot/UV/Stain-Free Sample Tray and the Fluorescein setting. images were analysed using the cell counter plugin in the ImageJ software. Standard error of the mean was calculated for these samples and a one-way ANOVA was used to determine significance.

3.6 Supplementary

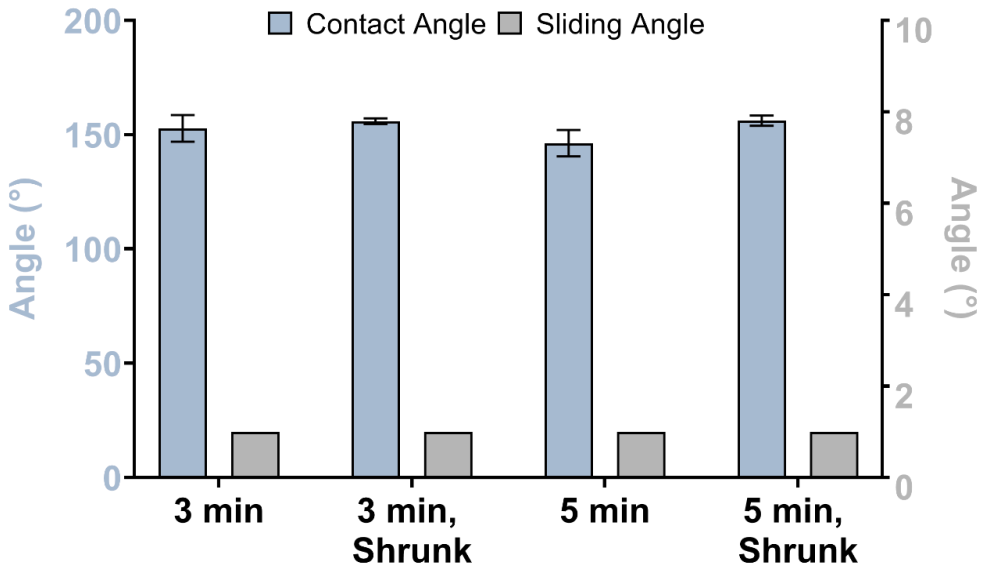

Figure 3.S1 Contact and sliding angle comparison for 3 min and 5 min plasma treatments. Surfaces with both surface activation times and 24 hours incubation with n-PTCS demonstrated contact angles >150° and sliding angles ~1°. Error bars illustrate the standard deviation for contact angles.

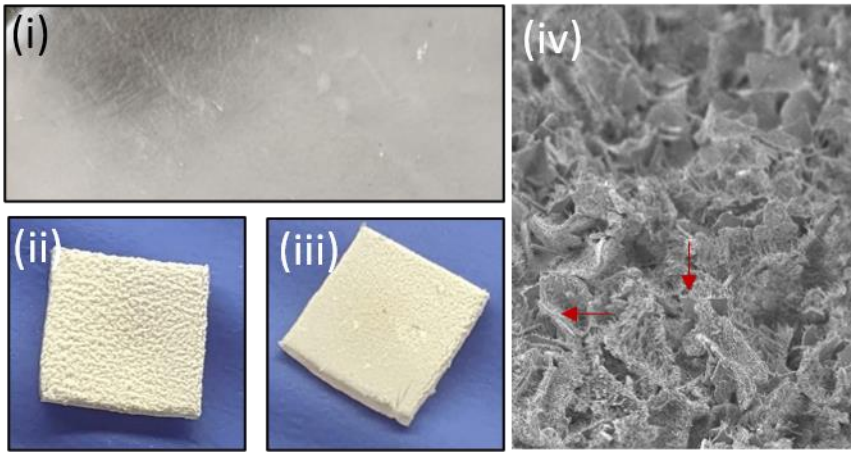

Figure 3.S2 (i) Optical image of planar treated surface with uneven coating. CVD treatment can produce uneven coatings based on arrangement within chamber, leading to poor surface performance. **(ii) Shrunk 6 hr treated sample with uneven coating**. As seen in this optical image, it is immediately visible when a thicker coating has caused cracking on the surface. **(iii) Shrunk 6hr treated sample with even coating.** A smoother surface is presented with proper wrinkle formation allowed due to a less thick, more even treatment with n-PTCS. **(iv) SEM image of shrunk 6hr treated samples with cracks visible.** Red arrows indicate the location of cracks caused by coating thickness.

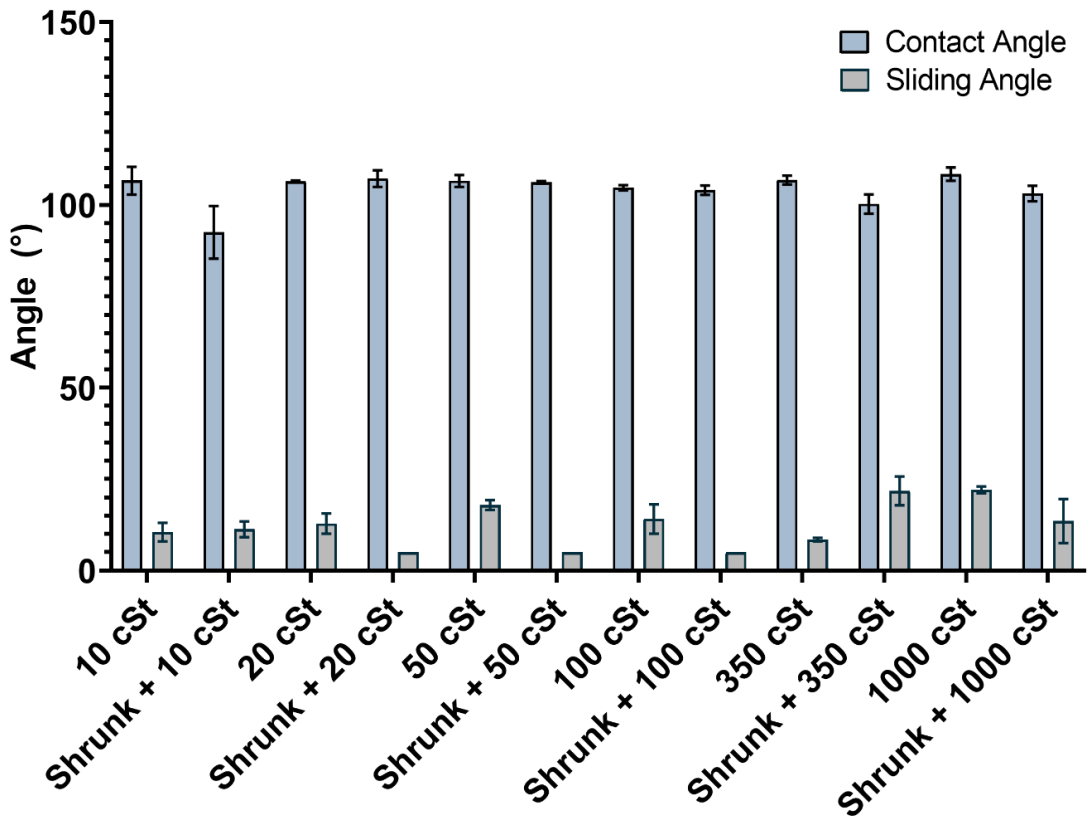

Figure 3.S3 Contact and sliding angle characterization of planar and shrunk samples with silicone oil of varying densities. Evaluation of 10 cSt, 20 cSt, 50 cSt, 100 cSt, 350 cSt and 1000 cSt silicone oil as lubricant for these surfaces was investigated to prepare a proper comparison for hierarchical surfaces. 100 cSt was selected as the ideal viscosity based on sliding angle for both planar and shrunk samples.

3.7 References

[1] B. Stephens, “Microbial exchange via fomites and the implications to human health,” *Springer*, vol. 5, pp. 198–213, 2019.

[2] Center for Disease Control and Prevention, “Current HAI Progress Report,” *CDC*, 2019. https://www.cdc.gov/hai/data/portal/progress-report.html (accessed Apr. 14, 2021).

[3] Center for Disease Control and Prevention, “Carbapenem-resistant Enterobacteriaceae (CRE): An urgent public health threat | A.R. & Patient Safety Portal,” 2020. https://arpsp.cdc.gov/story/cre-urgent-public-health-threat (accessed Apr. 14, 2021).

[4] G. Suleyman, G. Alangaden, and A. C. Bardossy, “The Role of Environmental Contamination in the Transmission of Nosocomial Pathogens and Healthcare-Associated Infections,” *Current Infectious Disease Reports*, vol. 20, no. 6. 2018, doi: 10.1007/s11908-018-0620-2.

[5] K. Manoharan and S. Bhattacharya, “Superhydrophobic surfaces review: Functional application, fabrication techniques and limitations,” *J. Micromanufacturing*, vol. 2, no. 1, pp. 59–78, 2019, doi: 10.1177/2516598419836345.

[6] H. Yildirim Erbil, “Practical Applications of Superhydrophobic Materials and Coatings: Problems and Perspectives,” vol. 29, p. 6, 2020, doi: 10.1021/acs.langmuir.9b03908.

[7] C. Wang and Z. Guo, “A comparison between superhydrophobic surfaces (SHS) and slippery liquid-infused porous surfaces (SLIPS) in application,” *Nanoscale*, vol. 12, no. 44, pp. 22398–22424, 2020, doi: 10.1039/d0nr06009g.

[8] Y. Bai, H. Zhang, Y. Shao, H. Zhang, and J. Zhu, “Recent progresses of superhydrophobic coatings in different application fields: An overview,” *Coatings*, vol. 11, no. 2, pp. 1–30, 2021, doi: 10.3390/coatings11020116.

[9] Y. T. Cheng, D. E. Rodak, C. A. Wong, and C. A. Hayden, "Effects of micro- and nano-structures on the self-cleaning behaviour of lotus leaves," *Nanotechnology*, vol. 17, no. 5, pp. 1359–1362, 2006, doi: 10.1088/0957-4484/17/5/032.

[10] G. Chen, Q. Cong, Y. Feng, and L. Ren, "Study on the wettability and self-cleaning of butterfly wing surfaces," 2004. Accessed: Mar. 26, 2021. [Online]. Available: www.witpress.com,.

[11] A. B. D. Cassie and S. Baxter, "Wettability of porous surfaces," *Trans. Faraday Soc.*, vol. 40, 1944, doi: 10.1039/tf9444000546.

[12] R. N. Wenzel, "Resistance of solid surfaces to wetting by water," *Ind. Eng. Chem.*, vol. 28, no. 8, 1936, doi: 10.1021/ie50320a024.

[13] T. Xiang *et al.*, "A facile method for fabrication of superhydrophobic surface with controllable water adhesion and its applications," *J. Alloys Compd.*, vol. 704, pp. 170–179, 2017, doi: 10.1016/j.jallcom.2017.01.277.

[14] H. Jie, Q. Xu, L. Wei, and Y. L. Min, "Etching and heating treatment combined approach for superhydrophobic surface on brass substrates and the consequent corrosion resistance," *Corros. Sci.*, vol. 102, pp. 251–258, Jan. 2016, doi: 10.1016/j.corsci.2015.10.013.

[15] S. W. Cho, J. H. Kim, H. M. Lee, H. Chae, and C. K. Kim, "Superhydrophobic Si surfaces having microscale rod structures prepared in a plasma etching system," *Surf. Coatings Technol.*, vol. 306, pp. 82–86, Nov. 2016, doi: 10.1016/j.surfcoat.2016.05.009.

[16] D. Seifzadeh and L. Farhoudi, "Electroless Co-P plating on magnesium alloy and its anti-corrosion properties," *Surf. Eng.*, vol. 32, no. 5, pp. 348–355, 2016, doi: 10.1179/1743294415Y.0000000034.

[17] L. Xu, F. Tong, X. Lu, K. Lu, and Q. Lu, "Multifunctional polypyrene/silica hybrid coatings

with stable excimer fluorescence and robust superhydrophobicity derived from electrodeposited polypyrene films," *J. Mater. Chem. C*, vol. 3, no. 9, pp. 2086–2092, Mar. 2015, doi: 10.1039/c4tc02653e.

[18] C. W. Peng *et al.*, "Nano-casting technique to prepare polyaniline surface with biomimetic superhydrophobic structures for anticorrosion application," *Electrochim. Acta*, vol. 95, pp. 192–199, 2013, doi: 10.1016/j.electacta.2013.02.016.

[19] E. Vazirinasab, K. Maghsoudi, R. Jafari, and G. Momen, "A comparative study of the icephobic and self-cleaning properties of Teflon materials having different surface morphologies," *J. Mater. Process. Technol.*, vol. 276, p. 116415, Feb. 2020, doi: 10.1016/j.jmatprotec.2019.116415.

[20] X. Zhang *et al.*, "Robust superhydrophobic epoxy composite coating prepared by dual interfacial enhancement," *Chem. Eng. J.*, vol. 371, pp. 276–285, Sep. 2019, doi: 10.1016/j.cej.2019.04.040.

[21] A. Milionis, J. Languasco, E. Loth, and I. S. Bayer, "Analysis of wear abrasion resistance of superhydrophobic acrylonitrile butadiene styrene rubber (ABS) nanocomposites," *Chem. Eng. J.*, vol. 281, pp. 730–738, Dec. 2015, doi: 10.1016/j.cej.2015.06.086.

[22] X. Chen *et al.*, "Superhydrophobic SERS substrates based on silicon hierarchical nanostructures," *J. Opt. (United Kingdom)*, vol. 20, no. 2, p. 024012, Feb. 2018, doi: 10.1088/2040-8986/aaa100.

[23] S. Zhai and H. Zhao, "Silica-coated metallic nanoparticle-based hierarchical super-hydrophobic surfaces fabricated by spin-coating and inverse nanotransfer printing," *Appl. Phys. Lett.*, vol. 114, no. 23, p. 233702, Jun. 2019, doi: 10.1063/1.5098780.

[24] W. Wei, X. Lü, D. Jiang, Z. Yan, M. Chen, and J. Xie, "A novel route for synthesis of UV-

resistant hydrophobic titania-containing silica aerogels by using potassium titanate as precursor," *Dalt. Trans.*, vol. 43, no. 25, pp. 9456–9467, Jul. 2014, doi: 10.1039/c3dt53389a.

[25] S. M. Imani *et al.*, "Flexible Hierarchical Wraps Repel Drug-Resistant Gram-Negative and Positive Bacteria," *ACS Nano*, vol. 14, no. 1, pp. 454–465, 2020, doi: 10.1021/acsnano.9b06287.

[26] E. Lee and K. H. Lee, "Facile fabrication of superhydrophobic surfaces with hierarchical structures," *Sci. Rep.*, vol. 8, no. 1, p. 4101, Dec. 2018, doi: 10.1038/s41598-018-22501-8.

[27] L. B. Hassan, N. S. Saadi, and T. Karabacak, "Hierarchically rough superhydrophobic copper sheets fabricated by a sandblasting and hot water treatment process," *Int. J. Adv. Manuf. Technol.*, vol. 93, no. 1–4, pp. 1107–1114, Oct. 2017, doi: 10.1007/s00170-017-0584-7.

[28] S. M. Imani, R. Maclachlan, Y. Chan, A. Shakeri, L. Soleymani, and T. F. Didar, "Hierarchical Structures, with Submillimeter Patterns, Micrometer Wrinkles, and Nanoscale Decorations, Suppress Biofouling and Enable Rapid Droplet Digitization," *Small*, vol. 16, no. 50, pp. 1–9, 2020, doi: 10.1002/smll.202004886.

[29] R. Jiang *et al.*, "Lotus-leaf-inspired hierarchical structured surface with non-fouling and mechanical bactericidal performances," *Chem. Eng. J.*, vol. 398, Oct. 2020, doi: 10.1016/j.cej.2020.125609.

[30] L. Wu, L. Li, B. Li, J. Zhang, and A. Wang, "Magnetic, durable, and superhydrophobic polyurethane@Fe3O4@SiO2@fluoropolymer sponges for selective oil absorption and oil/water separation," *ACS Appl. Mater. Interfaces*, vol. 7, no. 8, pp. 4936–4946, Mar. 2015, doi: 10.1021/am5091353.

[31] P. Nbelayim, H. Sakamoto, G. Kawamura, H. Muto, and A. Matsuda, "Preparation of thermally and chemically robust superhydrophobic coating from liquid phase deposition and low voltage reversible electrowetting," *Thin Solid Films*, vol. 636, pp. 273–282, Aug. 2017, doi: 10.1016/j.tsf.2017.06.019.

[32] R. Jafari, S. Asadollahi, and M. Farzaneh, "Applications of plasma technology in development of superhydrophobic surfaces," *Plasma Chem. Plasma Process.*, vol. 33, no. 1, pp. 177–200, Feb. 2013, doi: 10.1007/s11090-012-9413-9.

[33] E. Guzmán, R. G. Rubio, and F. Ortega, "A closer physico-chemical look to the Layer-by-Layer electrostatic self-assembly of polyelectrolyte multilayers," *Advances in Colloid and Interface Science*, vol. 282. Elsevier B.V., Aug. 01, 2020, doi: 10.1016/j.cis.2020.102197.

[34] J. Mao *et al.*, "Constructing multifunctional MOF@rGO hydro-/aerogels by the self-assembly process for customized water remediation," *J. Mater. Chem. A*, vol. 5, no. 23, pp. 11873–11881, Jun. 2017, doi: 10.1039/c7ta01343d.

[35] Q. Shang and Y. Zhou, "Fabrication of transparent superhydrophobic porous silica coating for self-cleaning and anti-fogging," *Ceram. Int.*, vol. 42, no. 7, pp. 8706–8712, May 2016, doi: 10.1016/j.ceramint.2016.02.105.

[36] L. H. Kong, X. H. Chen, L. G. Yu, Z. S. Wu, and P. Y. Zhang, "Superhydrophobic cuprous oxide nanostructures on phosphor-copper meshes and their oil-water separation and oil spill cleanup," *ACS Appl. Mater. Interfaces*, vol. 7, no. 4, pp. 2616–2625, Feb. 2015, doi: 10.1021/am507620s.

[37] P. Murugan, M. Krishnamurthy, S. N. Jaisankar, D. Samanta, and A. B. Mandal, "Controlled decoration of the surface with macromolecules: Polymerization on a self-assembled monolayer (SAM)," *Chem. Soc. Rev.*, vol. 44, no. 10, pp. 3212–3243, May 2015,

doi: 10.1039/c4cs00378k.

[38] C. Lau, K. Anitole, C. Hodes, D. Lai, A. Pfahles-Hutchens, and J. Seed, “Perfluoroalkyl acids: A review of monitoring and toxicological findings,” *Toxicological Sciences*, vol. 99, no. 2. Oxford Academic, pp. 366–394, Oct. 01, 2007, doi: 10.1093/toxsci/kfm128.

[39] J. W. Martin, M. M. Smithwick, B. M. Braune, P. F. Hoekstra, D. C. G. Muir, and S. A. Mabury, “Identification of Long-Chain Perfluorinated Acids in Biota from the Canadian Arctic,” *Environ. Sci. Technol.*, vol. 38, no. 2, pp. 373–380, 2004, doi: 10.1021/es034727+.

[40] Government of Canada, “Perfluorooctanoic Acid (PFOA), its salts, and its precursors - information sheet - Canada.ca,” Feb. 08, 2019. https://www.canada.ca/en/health-canada/services/chemical-substances/fact-sheets/chemicals-glance/perfluorooctanoic-acid-pfoa-salts-precursors-public-summary.html (accessed Apr. 04, 2021).

[41] L. Croce, F. Coperchini, M. Tonacchera, M. Imbriani, M. Rotondi, and L. Chiovato, “Effect of long- and short-chain perfluorinated compounds on cultured thyroid cells viability and response to TSH,” *J. Endocrinol. Invest.*, vol. 42, no. 11, pp. 1329–1335, Nov. 2019, doi: 10.1007/s40618-019-01062-1.

[42] G. R. J. Artus, S. Jung, J. Zimmermann, H. P. Gautschi, K. Marquardt, and S. Seeger, “Silicone nanofilaments and their application as superhydrophobic coatings,” *Adv. Mater.*, vol. 18, no. 20, pp. 2758–2762, 2006, doi: 10.1002/adma.200502030.

[43] M. Jin, S. Li, J. Wang, M. Liao, and Y. Zhao, “Controllable fabrication of organosilane nano-architectured surfaces with tunable wettability,” *Appl. Surf. Sci.*, vol. 258, no. 19, pp. 7552–7555, 2012, doi: 10.1016/j.apsusc.2012.04.084.

[44] A. Stojanovic, S. Olveira, M. Fischer, and S. Seeger, “Polysiloxane nanotubes,” *Chem. Mater.*, vol. 25, no. 14, pp. 2787–2792, 2013, doi: 10.1021/cm400851k.

[45] J. Zimmermann, G. R. J. Artus, and S. Seeger, "Superhydrophobic silicone nanofilament coatings," *J. Adhes. Sci. Technol.*, vol. 22, no. 3–4, pp. 251–263, 2008, doi: 10.1163/156856108X305165.

[46] E. Kasapgil, I. Anac, and H. Y. Erbil, "Transparent, fluorine-free, heat-resistant, water repellent coating by infusing slippery silicone oil on polysiloxane nanofilament layers prepared by gas phase reaction of n-propyltrichlorosilane and methyltrichlorosilane," *Colloids Surfaces A Physicochem. Eng. Asp.*, vol. 560, no. September 2018, pp. 223–232, 2019, doi: 10.1016/j.colsurfa.2018.09.064.

[47] E. Kasapgil *et al.*, "Polysiloxane nanofilaments infused with silicone oil prevent bacterial adhesion and suppress thrombosis on intranasal splints," *ACS Biomater. Sci. Eng.*, vol. 7, no. 2, pp. 541–552, 2021, doi: 10.1021/acsbiomaterials.0c01487.

[48] M. Meier, V. Dubois, and S. Seeger, "Reduced bacterial colonisation on surfaces coated with silicone nanostructures," *Appl. Surf. Sci.*, vol. 459, no. July, pp. 505–511, 2018, doi: 10.1016/j.apsusc.2018.08.003.

[49] G. R. J. Artus, S. Olveira, D. Patra, and S. Seeger, "Directed In Situ Shaping of Complex Nano- and Microstructures during Chemical Synthesis," *Macromol. Rapid Commun.*, vol. 38, no. 4, pp. 1–9, 2017, doi: 10.1002/marc.201600558.

[50] H. F. Bohn and W. Federle, "Insect aquaplaning: Nepenthes pitcher plants capture prey with the peristome, a fully wettable water-lubricated anisotropic surface," *Proc. Natl. Acad. Sci. U. S. A.*, vol. 101, no. 39, pp. 14138–14143, Sep. 2004, doi: 10.1073/pnas.0405885101.

[51] M. Villegas, Y. Zhang, N. Abu Jarad, L. Soleymani, and T. F. Didar, "Liquid-Infused Surfaces: A Review of Theory, Design, and Applications," *ACS Nano*, vol. 13, no. 8, pp. 8517–8536, Aug. 2019, doi: 10.1021/acsnano.9b04129.

[52] M. Osborne, A. Aryasomayajula, A. Shakeri, P. R. Selvaganapathy, and T. F. Didar, "Suppression of Biofouling on a Permeable Membrane for Dissolved Oxygen Sensing Using a Lubricant-Infused Coating," *ACS Sensors*, vol. 4, no. 3, pp. 687–693, Mar. 2019, doi: 10.1021/acssensors.8b01541.

[53] M. Badv, I. H. Jaffer, J. I. Weitz, and T. F. Didar, "An omniphobic lubricant-infused coating produced by chemical vapor deposition of hydrophobic organosilanes attenuates clotting on catheter surfaces," *Sci. Rep.*, vol. 7, no. 1, pp. 1–10, 2017, doi: 10.1038/s41598-017-12149-1.

[54] D. C. Leslie *et al.*, "A bioinspired omniphobic surface coating on medical devices prevents thrombosis and biofouling," *Nat. Biotechnol.*, 2014, doi: 10.1038/nbt.3020.

[55] B. Li, Y. P. Cao, X. Q. Feng, and H. Gao, "Mechanics of morphological instabilities and surface wrinkling in soft materials: A review," *Soft Matter*, vol. 8, no. 21, pp. 5728–5745, 2012, doi: 10.1039/c2sm00011c.

4 Conclusion

This thesis has focused on the modification of surfaces toward biorepellency. In chapter 1, the overview of relevant background for the production of polysiloxane nanostructures was presented. This included consideration of surface wettability, lubricant-infused surfaces, hierarchical surface, previous work specific to polysiloxane nanostructure coatings and the environmental considerations for surface modification research. Chapter 2 presented a literature review of antimicrobial nanomaterials and coatings, with specific focus on viruses. Finally, chapter 3 demonstrated the production of flexible, fluorine- and lubricant-free hierarchical surfaces with promising applications for high-touch surfaces, primarily in healthcare and food industries. Work toward these surfaces included establishment of a sufficient skin layer-thermoplastic pairing to generate wrinkling through application of heat, optimization of a manufacturing process using a customized humidity chamber, and characterization of surfaces with various incubation times to maximize superhydrophobic properties while minimizing production time. After establishing an ideal surface, pathogenic tests and tests in complex fluids were performed. Significant reduction (1.6-log or 97.5% in fluorescence; 1.2-log or 93% in CFU) in surface adhesion of the gram-negative bacteria, E. coli K-12 was demonstrated through stamping assays, and 93% reduction in visual staining with 87.2% reduction in adhesion using complex fluids was demonstrated through investigations with citrated whole blood.

4.1 Future Work

Potential applications for the work presented in chapter 3 stretch beyond the two primary investigations presented. The significant reduction in bacterial transfer warrants further investigation, including tests with additional bacterial strains, particularly gram-positive bacteria, as well as biofilm formation assays. Beyond bacteria, investigation of adhesion of other pathogens

including viruses and molds would be worthwhile. Investigation of additional complex fluids would be pertinent, including milk or other fatty liquids. Additional studies of these surfaces under dynamic flow could also result in promising applications. While the assessment of these surfaces in static clotting and thrombin generation assays remained inconclusive, the flexible nature of these surfaces and their potential formation into tubes could offer advantages not seen on two-dimensional surfaces.

The superhydrophobic properties of these hierarchical surfaces demonstrate potential outside of surface contamination as well. Use as a repellent coating in biosensors, with the paired increase in surface area offered by the nanostructuring could offer great potential for detection of specific proteins in complex fluids. Additionally, patterning of polysiloxane nanostructured surfaces for investigation of surface wettability has been previously investigated, as mentioned above. Given the nature of the nanostructures, it would be interesting to determine whether this same patterning could be applied to investigate cell growth and replication of intestinal villi structures.

Finally, for the potential scale-up of surface production it would be worthwhile to consider alteration of the fabrication chamber setup. As mentioned in chapter 3, inconsistency in the coating application led to cracking rather than wrinkling. For this reason, introduction of mechanical mechanisms to create a more even coating would assist in more large-scale production.